Dissertation zur Erlangung des Doktorgrades der Fakultät für Chemie und Pharmazie der Ludwig-Maximilians-Universität München

Mesenchymal stem cell therapy using theranostic sodium iodide symporter effector gene in glioblastoma

Carolin Gertrud Kitzberger

aus

Bad Mergentheim, Deutschland

2024

Erklärung

Diese Dissertation wurde im Sinne von § 7 der Promotionsordnung vom 28. November 2011 von Frau Professor Dr. Christine Spitzweg betreut und von Herrn Professor Dr. Ernst Wagner von der Fakultät für Chemie und Pharmazie vertreten.

Eidesstattliche Versicherung

Diese Dissertation wurde eigenständig und ohne unerlaubte Hilfe erarbeitet.

München, 24.09.2024

.....

Carolin Kitzberger

Dissertation eingereicht am	24.09.2024
1.Gutachter:	Prof. Dr. Ernst Wagner
2.Gutachterin:	Prof. Dr. Christine Spitzweg
Mündliche Prüfung am	07.11.2024

-meinen Eltern

Die vorliegende Arbeit wurde im Zeitraum von November 2017 bis Dezember 2022 an der Fakultät für Pharmazie und Chemie der Ludwig-Maximilians-Universität München, sowie am LMU Klinikum - Campus Großhadern, Medizinische Klinik und Poliklinik IV, unter der Leitung von Prof. Dr. med. Christine Spitzweg angefertigt.

Table of Contents

1 Introduction

> *“The formation of a tumor is a complex, multi-step process that usually proceeds over a long period. Normal cells evolve into cells with increasingly neoplastic phenotypes through a process termed tumor progression – an uncontrolled process we do not understand in detail. This process takes place at myriad sites throughout the normal human body, advancing further and further as we get older. Rarely does it proceed far enough at any single site to make us aware of its end product, a clinically detectable tumor mass. Tumor progression is driven by a sequence of randomly occurring mutations and epigenetic alterations of DNA that affect the genes controlling cell proliferation, survival, and other traits associated with the malignant cell phenotype. The scope of the problem at hand: How many different sequential changes are actually required in cells and tissues in order to create a human cancer?”*
>
> Prof. Robert Allan Weinberg, tumor biologist, in his lecture on "Mechanisms of Malignant Progression of Carcinoma Cells" in Ulm May 2017 and the second edition of his book “The Biology of Cancer” (1).

Genetic instability and tumor-promoting inflammation are features of cancer that enable cells to survive, proliferate, and disseminate (2). To understand the complexity of cancer development, the following hallmarks have been proposed (2,3) : (i) sustained proliferation, (ii) growth suppressors evasion, (iii) activate invasion and metastasis, (iv) replicative immortality, (v) angiogenesis, (vi) resistance against cell death, (vii) avoidance of immune destruction, (viii) reprogrammed cellular metabolism. In 2022, the hallmark concept was expanded by (ix) unlocking phenotypic plasticity, (x) nonmutational epigenetic reprogramming, (xi) polymorphic microbiomes, and senescent cells were added to the previous cancer conceptualization (4). In this light, elucidating the underlying mechanisms of cancer development and progression helps to develop effective treatment strategies to combat this deadly disease. This thesis focuses on developing targeted tumor therapy for glioblastoma – a tumor desperately needing new treatment options.

This chapter is partially adapted from Kitzberger C, Spellerberg R, Morath V, Schwenk N, Schmohl KA, Schug C, Urnauer S, Tutter M, Eiber M, Schilling F, Weber WA, Ziegler S, Bartenstein P, Wagner E, Nelson PJ, Spitzweg C. The sodium iodide symporter (NIS) as theranostic gene: its emerging role in new imaging modalities and non-viral gene therapy. EJNMMI Res. 2022 May 3;12(1):25

1.1 Glioblastoma

The World Health Organization (WHO) classified Glioblastoma (GBM) as a grade IV glioma. Gliomas summarize brain tumors originating from glial cells, including astrocytes, oligodendrocytes, and ependymal cells. GBM represents the most aggressive and common malignant type of primary brain tumor in adults. It accounts for approximately 15% of all primary brain tumors and other central nervous system (CNS) neoplasms (5).

Histologically, GBM is characterized as an astrocytic tumor with dense cellularity and areas of palisading necrosis with/or microvascular proliferation (6). However, there is evidence that GBM does not exclusively derive from glial cells. Instead, they may also arise from neuroglial progenitor cells with stem-cell-like properties allowing for differentiation into multiple cell types/phenotypes (7).

Despite recent advances in managing GBM patients, the overall prognosis remains remarkably poor and lacks long-term survival. Based on registry data from 2011-2015, the average annual age-adjusted incidence of GBM is 3.2 cases per 100,000 population in the United States, with a slight predominance in men over women (1.58:1). Thereby, the relative overall 5-year survival is 5.6% (5). In Germany, GBM comprised approximately two-thirds of all diagnosed malignant brain tumors, with a relative 5-year survival of 7-8% in 2017-2018 (8).

GBM is divided into primary and secondary glioblastoma. Patients with primary GBM tend to be older aged, with a median age at diagnosis of 64 years, accounting for the majority with approximately 90% of all GBM patients. In secondary GBM, the tumor also originates from the brain and is not seen as a metastatic disease of any other tumor entity. Here, a low-grade glioma slowly develops into a high-grade GBM and preferentially arises in younger patients (9). Symptoms of GBM patients correlate with the location of the tumor rather than the tumor pathology, for example, affection of brain areas that control speech or motion resulting in handicaps in this ability. Common complications include seizures, headache, cognitive dysfunction (e.g., personality changes, memory loss), nausea, and venous thromboembolism (9). In most cases, these symptoms are often unexplained at early stages and not directly associated with GBM hampering the process of early diagnosis and treatment. The

progressive decline in cognitive function devastates patients' quality of life and their social environment, which is more pronounced than in other types of cancer (10).

In general, GBM is characterized by a high intra- and intertumoral heterogeneity on the molecular and cellular level that complicates the design of effective treatment strategies. Thus, expanding the knowledge of genetic and cellular targets found in GBM helps improve the development of new effective, more personalized treatment options (11,12). In addition to the histological appearance, glioblastomas are also classified by molecular features. One such feature is the isocitrate dehydrogenase (IDH) status (wildtype or mutant) (13). The IDH-mutation status is primarily found in patients with secondary GBM as a biomarker, while IDH-wildtype mostly corresponds with primary GBM. The IDH status is often associated with the patient's prognosis predicting better outcomes for IDH-mutant GBM arising in younger patients with secondary GBM (13). In 2008, the Cancer Genome Atlas (TCGA) Research Network stated common molecular alterations or gene expression patterns found in primary GBM like i) TERT promoter mutation, ii) epidermal growth factor receptor (EGFR) overexpression, iii) phosphate and tensin homolog (PTEN) deletion, iv) MGMT (O-6-methylguanine-DNA methyltransferase) promoter methylation and v) loss of chromosome 10q (14). Further, alterations in the three core signaling pathways of tumor protein p53, receptor tyrosine kinase (RTK)/Ras/ phosphatidylinositol 3-kinase (PI3K), and retinoblastoma (RB) are highly abundant (15). In addition, four subtypes of GBM have been identified: classical, pro-neural, neural, and mesenchymal. These subtypes differentiate between the above-mentioned molecular features and their clinical characteristics (16). Tailoring future therapies to target these molecular features and subtypes of GBM may expand therapeutic options and improve therapy response.

Treatment failure, resistance, and recurrence in GBM, in particular, not only result from the above-mentioned extreme inter- and intratumoral heterogeneity on the molecular level. The tumor location and the notoriously infiltrative growth of tumor cells into the normal brain parenchyma limit complete surgical resection. Furthermore, systemic drug delivery is constrained by the blood-brain barrier (BBB) (17). The BBB is a highly restrictive barrier between blood and CNS formed by continuous non-fenestrated blood vessels (18). Endothelial cells (ECs) and surrounding pericytes, vascular smooth muscle cells, and astrocyte endfeets build the main components of the BBB. ECs of the CNS are held together by tight junctions and harbor unique properties compared to those cells found in other body tissues. CNS ECs strictly regulate the influx and efflux of molecules, ions, and cells between blood and CNS. Paracellular flux and transcytosis are minimal, and mainly the transport in and out of the brain occurs only via specific transporters (18,19). However, the BBB is only partly intact in the disease scenario and loses some of its extreme barrier functions necessary for maintaining CNS homeostasis – which allows immune cells, molecules, and ions to enter the CNS (18).

1.2 (Brain) Tumor Microenvironment

The tumor microenvironment (TME) represents a complex network of cancer cells, various types of non-malignant stromal cells, and non-cellular components (Figure 1). The cross-talk between tumor cells and the TME is a dynamic and bidirectional relationship that plays a critical role in tumor growth, invasion, and metastatic dissemination (20). The TME is not 'an innocent bystander' but an essential player in creating a suitable environment for the formation and progression of cancer (21,22). In GBM, glioma stem cells (GSCs) – multipotent cells with self-renewing and high differentiation potential – are thought to build the bulk of malignant tumor cells that promote tumor initiation, progression, and resistance to conventional treatment (23). Cells found in the tumor stroma of many solid tumors include cancer-associated fibroblasts (CAFs), pericytes, endothelial cells, and immune cells like macrophages, microglia, and lymphocytes. Mesenchymal stem cells (MSCs) originating from different tissues in the body are also part of the tumor stroma. Non-cellular components compromise extracellular matrix proteins (ECM), cytokines, chemokines, and growth factors secreted by the cellular components of the TME (3,22).

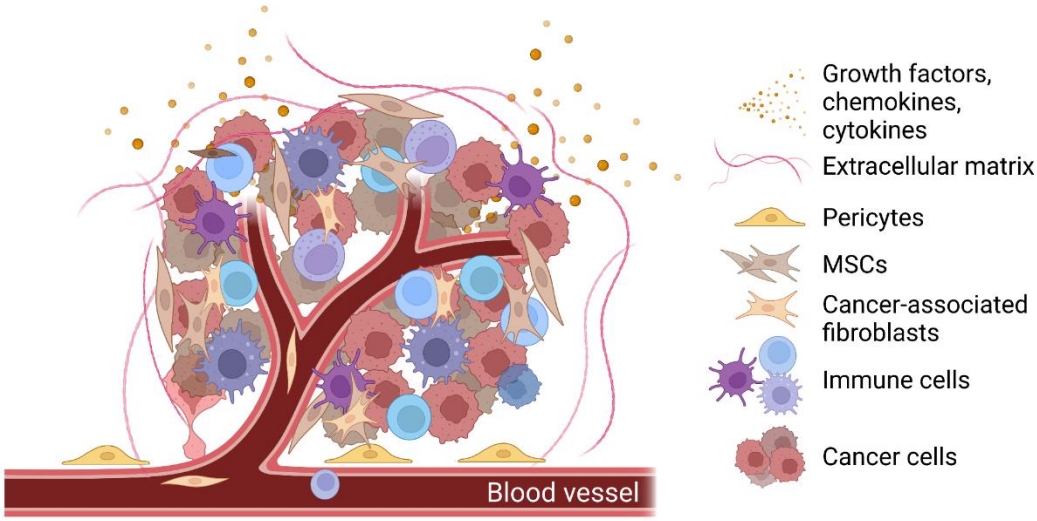

Figure 1: Tumor microenvironment (TME). Solid tumors are composed of cancer cells and the surrounding stroma. The tumor stroma is composed of cellular components such as immune cells, cancer-associated fibroblasts (CAFs), mesenchymal stem cells (MSCs), cancer stem cells, cells that form blood vessels like endothelial cells and pericytes, as well as non-cellular components like the extracellular matrix, growth factors, chemokines, and cytokines. Adapted from Balkwill et al J Cell Sci. 2012 125, 5591-6 (24); Illustration was created with BioRender.com.

Notably, the primary cell types in the GBM stroma are immune cells, such as resident microglia and infiltrating macrophages, representing >30% of the non-malignant cellular components, exerting either promoting or suppressive effects on tumor development (25). Fibroblasts are much less defined in the TME in GBM when compared to other tumor entities (25,26). Cells associated with the structure and function of blood vessels, e.g., endothelial cells or pericytes, are highly abundant in GBM, as is the case for the highly vascularized brain in general (27). Furthermore, a hypoxic and acidic condition is a predominant feature in the GBM TME, leading to neo-vascularization to provide sufficient oxygen and nutrients for rapidly growing GBM tumors (22,23).

Targeting the tumor microenvironment displays an enormous advantage in developing new GBM therapies considering the extreme intra- and intertumoral heterogeneity as it overcomes the requirement of a specific molecular or cellular target of the GBM landscape.

1.3 Glioblastoma Therapy

The first-line treatment of GBM patients after diagnosis is a multimodal approach: It starts with surgical resection followed by radiation therapy, systemic therapy (concomitant/adjuvant chemotherapy and/or targeted therapy), and supportive care (16,28). There is no standard of care for progressive disease, underscoring the need for alternative, more effective treatment strategies to combat GBM (16).

1.3.1 Surgery

The initial intervention for GBM treatment is surgical resection to reduce tumor volume. A greater extent of maximal safe resection may contribute to improved overall survival, progression-free survival, and an increase in the patient's quality of life (9,16). A complete surgical resection of the tumor is often impossible due to its location in areas that do not allow extensive surgical interventions as they control speech, motoric function, and senses. In addition, the infiltrative growth pattern of GBM with distant microsatellites further prevents complete resection of malignant cells, and thus, leading to tumor progression and recurrence (29). The resected material is used for histological diagnosis and genotype profiling, as the basis for tailored treatment decision making (16).

1.3.2 External Radiation therapy (RT) plus Chemotherapy

Standard fractioned external radiation therapy (RT) following surgery has been in use since 1970 (30) and was the postoperative standard treatment until 2005, when it got replaced by the so-called “Stupp regime” (9). Typical ionizing radiation doses of 60 Gray (Gy) in 2.0-Gy fractions showed to be effective. Other dosing regimens with doses higher or lower than 60 Gy or different fractioning were investigated but did not lead to significant changes or benefits of survival (16). According to the “Stupp protocol” radiotherapy is combined with the gold standard chemotherapy temozolomide (TMZ), an oral alkylating agent, followed by six cycles of adjuvant TMZ treatment. This combined chemoradiotherapy significantly improved the 2-year survival of GBM patients (26.5% for RT+TMZ treatment) as compared to radiotherapy alone (10.4% for RT alone) with minimal additional adverse toxicity (28). Epigenetic silencing of the DNA repair gene MGMT by methylation of its promoter increases TMZ treatment effectiveness resulting in increased survival of respective patients. Therefore, the MGMT status of the tumor is not only used as an emerging prognostic marker but further helps select patients that may benefit from TMZ treatment (16). Nevertheless, recurrence after combined radio-and chemotherapy occurs for most patients within six months (16).

1.3.3 Tumor-treating Fields

As a treatment next to adjuvant TMZ after standard therapy, the delivery of locoregionally tumor-treating fields (TTFs, Optune®) received approval from the FDA (US Food and Drug Administration) in 2011 for recurrent and in 2015 as adjuvant treatment for newly diagnosed GBM (31). Low-intensity, intermediate-frequency alternating electrical fields delivered by transducer arrays employed to the scalp result in an antimitotic effect on tumor cells as well as causing apoptosis or cell death (32). An improvement in progression-free survival and overall survival of GBM patients has been reported compared to maintenance TMZ treatment alone (33).

1.3.4 Alternative Therapies

Due to the lack of efficient and successful treatment strategies for GBM with high recurrence, there is a clear need for more innovative treatment options. Extensive research is ongoing and explores novel therapies, including the field of precision oncology targeting relevant molecular signaling pathways driving gliomagenesis as outlined above (see 1.1), immunotherapy, gene therapy (see 1.3.3.1), stem cell–based therapies (see 1.5), and nanotechnology (15). Nevertheless, only one targeted drug, Bevacizumab – a monoclonal antibody inhibiting the

vascular endothelial growth factor (VEGF) to prevent tumor angiogenesis – has been approved by the FDA so far for the treatment of recurrent GBM (34).

1.3.4.1 Gene Therapy

Cancer gene therapy introduces foreign genetic material into the host tumor cell to modify its gene expression product (35,36). Gene substitution or introduction of new genes are possible at certain stages of the multistep gene expression process, e.g., by traditionally used delivery of linear or circular plasmid DNA (pDNA), messenger RNA (mRNA), or more recently established techniques using RNA interference (RNAi) or genome editing system such as CRISPR/Cas9 mRNA (36). Until 2017, about 65% (n=1668) of all clinical trials for gene therapy (approximately n=2600) worldwide have addressed cancer (37). The most widely used gene therapy strategies are immunomodulatory gene therapy, suicide gene therapy, or oncolytic virotherapy. Thus, the most frequent gene types used for gene transfer in cancer therapy are encoding antigens, cytokines, tumor suppressors, and suicide enzymes/proteins (37). Gene vector systems that are currently under investigation for an efficient treatment are cellular vectors (e.g., bacteria, neural stem cells, progenitor cells, and immune cells), other non-viral vectors (e.g., synthetic nanoparticles and cationic liposomes) and viral vectors (non-replicating viruses and replication-competent/oncolytic viruses) (35). Almost two-thirds of all clinical gene therapy trials have used viral vectors (37).

Gene therapy for GBM treatment has gained attention in recent decades and has shown therapeutic efficacy in preclinical animal models. Nevertheless, phase II/III clinical trials have failed and could not confirm the findings from preclinical studies in GBM patients. The limitations of efficient clinical translation may arise due to the host immune system and appropriate preclinical GBM models (38).

1.4 Sodium iodide symporter (NIS)

1.4.1 General Characteristics

The human sodium (Na^+)/iodide (I^-) symporter (NIS) belongs to the protein family of solute carriers 5 A (SCL5A). Its molecular characterization started in 1996 with the isolation of the rat NIS cDNA (39), followed by the human NIS orthologue (40). The human *NIS* gene is located on chromosome 19p12-13.2 and encodes a protein with a length of 643 amino acids. Its secondary structure model contains 13 transmembrane α-helices with three N-linked glycosylation sites, an extracellular N-terminus, and an intracellular C-terminus (Figure 2A, B) (41). Functional NIS protein represents an integral plasma membrane glycoprotein that

mediates the active transport of iodide from the blood into thyroid cells or other NIS-expressing cells. Other extra-thyroidal, endogenously NIS-expressing tissues are, among others, the salivary glands, gastric mucosa, lactating breast, intestine, and choroid plexus (42,43).

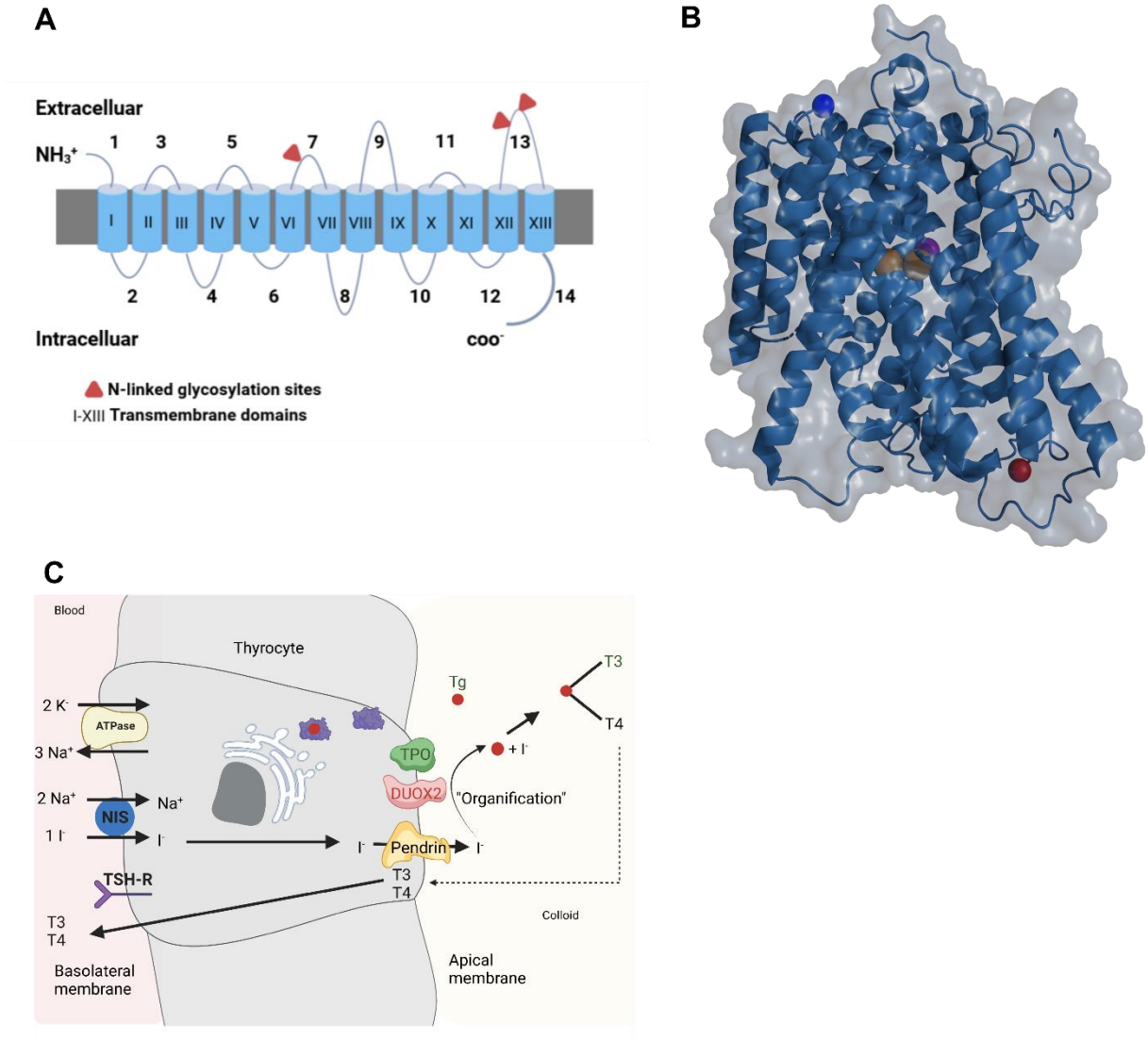

Figure 2 Schematic illustration of the sodium iodide symporter (NIS) protein structure. (**A)** The human NIS consists of 643 amino acids (aa) with an extracellular NH_2-terminus and an intracellular COOH-terminus. NIS is a hydrophobic protein with 13 transmembrane domains (α-helices are shown as cylinders) and three glycosylation sites at aa residue 225, 485, and 495 (indicated by red triangles). Adapted from Spitzweg et al J. Clin. Endocrinol. Metab 2001 86, 3327–35. (**B)** 3D structure of rat NIS that shares 89% sequence identity with human NIS and has similar transport properties. I^- in purple and two Na^+ ions in orange, transmembrane domains in blue (PDB Id: 7UV0; Ravera et al. Nature 2022 618, 795-801 (43)). PyMOL software was used for visualization. (**C)** Iodide uptake and I^- processing of thyroid follicular cells. Adapted from Hingorani et al. Curr Cancer Drug Targets 2010 10, 242-67 (44). DUOX2: Dual oxidase 2; TSH-R: Thyroid stimulation hormone receptor; TPO: Thyroperoxidase; T3, T4: Thyroid hormones.

As a symporter, NIS co-transports two Na^+ ions along with one I^- ion (2:1 Na^+/I^- stoichiometry) using the transmembrane Na^+ gradient as the driving force that is generated by the Na^+/K^+ ATPase pump. In the thyroid, NIS-mediated iodide uptake is a crucial step in thyroid hormone biosynthesis (Figure 2C): NIS actively transports iodide across the basolateral membrane of thyroid follicular cells. Subsequently, the process called 'iodide organification' takes place in the follicular lumen, where thyroperoxidase (TPO) catalyzes the oxidation and covalent conjugation of iodide on tyrosine residues within the thyroglobulin (Tg) backbone, followed by oxidative coupling of iodinated tyrosines to ultimately generate the thyroid hormones T3, T4 (44). Transcriptional and post-transcriptional modification of NIS in the thyroid is primarily regulated by thyroid stimulation hormone (TSH). NIS expression of non-thyroidal tissue is TSH-independent and lacks the process of iodide organification (44). The NIS-mediated iodide uptake of the thyroid or non-thyroidal tissue can be reduced by the potent competitive inhibitors perchlorate and thiocyanate or the Na^+/K^+ ATPase inhibitor ouabain (45).

1.4.2 *NIS* as Theranostic Gene

The management of differentiated thyroid cancer using the dual ability of *NIS* to accumulate diagnostic and therapeutic radioisotopes has been used since 1946, constituting the first theranostic application (46,47). Further, endogenous NIS expression in breast cancer and its metastases has been reported, raising the opportunity to use its theranostic properties also to the management of breast cancer (Figure 3A) (44,48). In addition to iodide, NIS also transports different substrates that enable its use as a reporter gene by applying non-invasive standard nuclear medicine imaging techniques. Radioimaging allows for dosimetry that helps estimate the appropriate absorbed tumor and other body organ doses for a more personalized treatment approach. Thereby, off-target toxicity due to excessive radiation exposure can be reduced, and the therapeutic effect in the tumor can be optimized. Functional NIS expression can be detected by positron emission tomography (PET) using the radiotracers ^{124}I or ^{18}F-Tetrafluoroborate (TFB) or by single-photon emission computed tomography (SPECT) and scintigraphy using ^{123}I, ^{125}I and ^{99m}Tc (Technetium) (49,50). Therapeutic radionuclides such as ^{131}I, ^{188}Re (Rhenium), or ^{211}At (Astatine) are transported by NIS and can be used to kill NIS-expressing cells and neighboring cells by radiotoxicity caused by β^-- or α-radiation. Cytotoxicity is obtained through bystander effects that result from the crossfire effect of the applied radioisotope (e.g. maximum pathlength of 2.4 mm of ^{131}I in tissue) and the radiation-induced biological bystander effect (49).

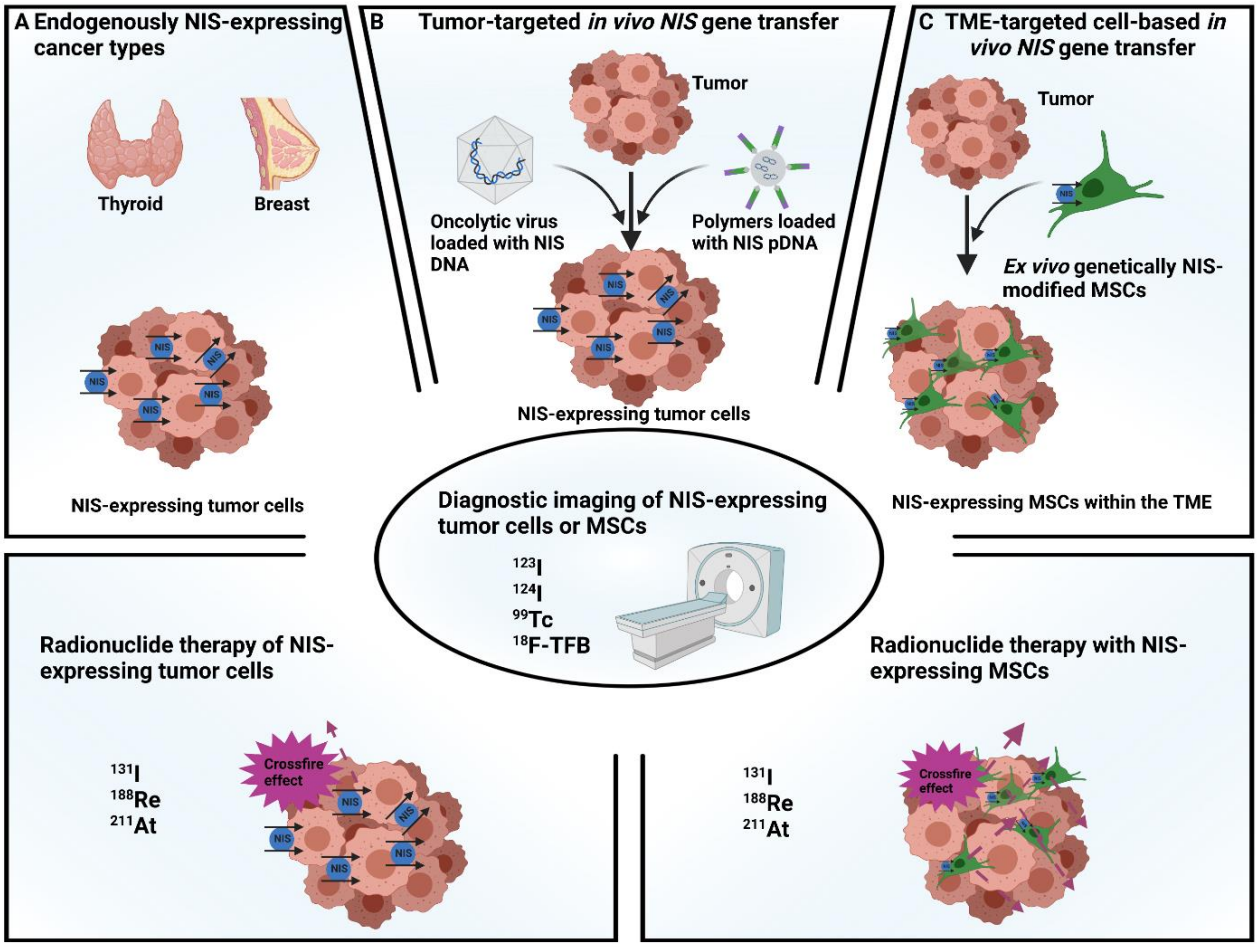

Figure 3: The role of *NIS* as theranostic gene. (A) The conventional theranostic function of *NIS* is used in the management and treatment of NIS-expressing cancer entities in particular differentiated thyroid cancer and its metastases. Tumor cells endogenously express *NIS* and can be monitored by diagnostic imaging such as scintigraphy, SPECT or high-resolution PET imaging after application of appropriate radionuclides (e.g. ^{123}I, ^{124}I, ^{99}Tc, ^{18}F-TFB). Absorbed doses of organs can be calculated and personalized based on the imaging for more effective treatment. As a next step, an internal radiotherapy can be performed by applying radionuclides like ^{131}I, ^{188}Re or ^{211}At to treat NIS-expressing cells as well as neighboring cells through bystander effects of the radiation-emitting particles. **(B)** To target non-NIS-expressing tumors by the beneficial dual role of *NIS* as reporter and therapy gene, the most common technique for *NIS* gene transfer to tumors are viral vectors or synthetic polymers that are inspired by the viral biology including their delivery action but circumvent typical concerns raised using viral systems. These *NIS* gene delivery vectors result in NIS-expressing tumor cells through distinct mechanisms and follow the same molecular principle for NIS-mediated diagnosis and therapy as seen by endogenously NIS-expressing tumors in A. **(C)** Another delivery platform for targeted *NIS* gene transfer is a cell-based approach with mesenchymal stem cells (MSCs) that can be easily obtained and genetically engineered to express *NIS*. This approach targets the tumor microenvironment (TME) and not the tumor cells directly. After selective tumor homing, NIS-expressing MSCs enable imaging of the tumor after radionuclide application. Further, accumulation of therapeutically active radionuclides in the TME through selective homing of NIS-expressing MSCs allows for treatment of tumors using bystander effects. Created with BioRender.com.

1.4.3 *NIS* Gene Therapy

The cloning of NIS cDNA in 1996 paved the way for its use as a theranostic gene in non-thyroidal malignancies after targeted *NIS* gene transfer. Different gene delivery platforms are used in the context of *NIS* gene therapy. The main categories are viral or non-viral delivery systems (Figure 3B, C). Common viral vectors used for *NIS* gene therapy in clinical trials are vaccinia virus, vesicular stomatitis virus, adenovirus, and measles virus (Source: Clinicaltrials.gov). Ongoing and completed clinical trials for tumor-specific NIS transduction in various tumor types including head and neck squamous cell carcinoma, multiple myeloma, endometrial, ovarian, breast, and prostate cancer used engineered viral vectors (e.g., NCT03120624, NCT02068794, NCT00788307, NCT00450814, NCT01503177, NCT01846091, NCT02192775, NCT02364713, NCT03017820, NCT03647163, NCT00408590). In GBM monitoring and therapy, viral-based approaches have also been used for *NIS* gene delivery in preclinical rat and mouse models (51-54). Problems encountered when using viral vectors include their immunogenicity, the requirement of high doses, cost-extensive manufacturing processes, small payload capacity, and control of transgene expression (55).

Nucleic acid carrier systems that mimic viral biology but circumvent issues raised when using viral vectors, include synthetic polyplexes (36). Previous studies performed by our group in close collaboration with Prof. Ernst Wagner from Pharmaceutical Biology, Department of Pharmacy at the LMU Munich have used several generations of synthetic nanocarriers aimed at more efficient, specific, and safe delivery of *NIS* to the tumor site after systemic injection (56-59). The major obstacles to the systemic delivery of genetic information are the particle's charge and size, which prevent them from overcoming various extracellular and intracellular barriers. The newest generation of polymers use nanosized, sequence-defined cationic lipo-oligo amides (OAAs) that complex with plasmid DNA through electrostatic interactions and are generated by precise solid-phase supported synthesis (55). In addition, click chemistry – awarded the Nobel Prize for Chemistry in 2022 – can be applied, where the OAAs are azido-functionalized, thus, enabling easy post-modification of their surface, for example, with a targeting moiety. Via copper-free click reaction, the azido group of the pDNA-loaded OAA can react, for instance, with a DBCO (dibenzocyclooctyne)-linked ligand that specifically binds to extracellular structures for targeted DNA delivery (60). To enhance blood circulation of polyplexes and avoid undesired immune responses and non-specific aggregation (e.g., with biomolecules in the bloodstream or self-aggregation), the ligands are PEGylated to lower the surface charge (61). In this context, the newest approach has used the epidermal growth factor receptor (EGFR) as a target for *NIS* gene-based therapy in GBM by functionalizing NIS polymers with the EGFR-binding ligand GE11 (61). Highly sensitive ^{124}I PET imaging enabled

in vivo monitoring of the so-called monoDBCO-PEG24-GE11/NIS polyplexes and their selective delivery to brain tumors after systemic application in a xenograft U87 mouse model. Subsequent ^{131}I therapy led to a significant decrease in GBM tumor volume and an extension of survival of GBM-bearing mice. To improve this approach, a parallel targeting approach with two different ligands that can be click-conjugated to NIS pDNA-loaded OAAs was investigated. For this purpose, the GE11-ligand and a second ligand targeting the transferrin receptor (TfR) were used for functionalization. The TfR is highly expressed in endothelial cells of the BBB and, thus, is expected to allow synthetic polymers to cross the BBB. This dual-targeted approach resulted in a superior therapeutic outcome as compared to mono-targeted GE11- or TfR-functionalized NIS polymers (62).

Cell-based vectors represent an alternative delivery platform for the transfer of therapeutic *NIS* gene to solid tumors (63-69). The application of CAR-T cell therapy for the treatment of solid tumors is subject of intense current research (68). Chimeric antigen receptor (CAR) T cell therapy is based on genetically modified T-cells isolated from a patient to express artificial receptors that target cancer cells and induce cytotoxic effects. To date, clinical implementation of CAR-T cell therapy has been successful for several hematologic malignancies but lacks satisfactory application for solid tumors. Some of the pitfalls of CAR-T cell therapy in the treatment of solid tumors include limitations of quantitative CAR-T-cell trafficking, CAR-T cell exhaustion, and severe toxicity (69). In this regard, *NIS* has been successfully used as a reporter gene for *in vivo* tracking of CAR-T cell fate and to diagnose potential toxicities associated with CAR-T cell treatment by PET imaging in preclinical studies (68,69).

Another cell-based approach for *NIS* gene tumor therapy is the use of mesenchymal stem cells (MSCs), representing the focus of this thesis and is described in more detail in the following section.

1.5 Mesenchymal stem cells

1.5.1 General Characteristics

Mesenchymal stem cells (MSCs) are multipotent progenitor cells with self-renewal capabilities that have the capacity for differentiation towards various cell lineages (e.g., muscle, bone, fat, and cartilage lineages) (70) and can be easily isolated from different tissue sources such as umbilical cord, adipose tissue and bone marrow (71,72). MSCs are non-hematopoietic and non-endothelial cells that lack expression of CD14, CD19, CD34, and CD45, that adhere to plastic, and express markers such as CD73, CD90, and CD105 (73). Several characteristics

of MSCs are favorable for their application in tumor therapy (or tissue repair): MSCs allow for allogenic as well as autologous transplantation due to the lack of MHC (major histocompatibility complex) expression, ease of cell propagation, the possibility to genetically modify them *ex vivo* and fewer ethical concerns in comparison to stem cells, e.g., originating from human embryos (74).

1.5.2 MSCs as Gene Delivery Vehicles for Tumor Therapy

Mesenchymal stem cells have been widely used in the field of regenerative medicine, whereas their use to treat solid tumors is currently being explored in several early-phase clinical trials, including GBM (Trial ID: NTC04657315; NTC03896568). Their application in solid tumors is based on their inherent tropism to sites of injury and has been widely demonstrated in various preclinical tumor models such as breast, liver, pancreatic, lung, and cervical cancer (63,66,74-78). Tumors can be thought of as 'chronic injuries' or 'never healing wounds' that lead to mobilization and engraftment of MSCs to the tumor bed (79). The exact underlying mechanism driving MSCs recruitment is not fully elucidated, but is thought to mirror that seen in leukocyte recruitment and is driven by chemokines, cytokines, and growth factors released by the tumor cells and the stromal compartment (80). MSCs represent promising delivery vehicles for anti-tumor cargo as they can overcome several obstacles in GBM treatment. They (i) are able to cross the BBB after systemic application, (ii) interact with a highly heterogenous TME without the need for a specific tumor target, (iii) have a high tumor selectivity while minimizing toxicity to healthy brain tissue, (iv) migrate towards the bulk tumor mass and more critical to distant infiltrative microsatellites, (v) finally can be used as monotherapy or adjuvant treatment that may boost the general therapeutic efficacy. Major hurdles encountered when using MSCs in cancer treatment include poor persistence and retention time within tumor settings and their controversially discussed pro- or anti-tumorigenic potential (81). Many of the potential drawbacks of using MSCs in tumor therapy can be avoided when using *NIS* as a theranostic transgene. For example, the accumulation of β^-- or α-emitting isotopes by NIS-expressing MSCs eliminates the MSC vector as well as the surrounding (tumor) cells through the crossfire and bystander effect.

MSCs can be easily modified *ex vivo* and thus used to deliver various distinct anti-tumor cargos such as miRNAs, proteins, suicide genes, immunostimulants, oncolytic viruses, or nanoparticles (82-88). Engineered versions of MSCs used for *NIS* transgene delivery into the tumor stroma have been established in collaboration between Christine Spitzweg's and Peter Nelson's laboratories at the Ludwig-Maximilians-University of Munich (Figure 4). Previous work has demonstrated the successful, tumor-selective delivery of constitutively active NIS-

expressing, bone marrow-derived mouse and human MSCs (CMV-NIS-MSCs) in diverse tumor settings including hepatocellular carcinoma (HCC) xenografts (63) and pancreatic ductal adenocarcinoma (PDAC) (66). Adverse effects may occur in off-target organs such as skin or spleen due to normal MSC homing to these sites and NIS expression within these organs (76). To better restrict anti-tumor effects to tumor microenvironments and thus spare healthy tissue, *NIS* transgene expression can be controlled by the use of tissue-specific promoters that are activated in response to tumor stroma-associated signaling pathways (Figure 4). Various inducible gene promoters have been investigated for their suitability to drive transgene expression of the *NIS* gene in MSCs, by making use of proinflammatory signals that can activate RANTES (Regulated on Activation, normal T-cell Expressed and presumably Secreted)/CCL5 gene promoter (75,89) or a synthetic version of a transforming growth factor-β (TGF-β)-responsive Smad promoter (65,90). In addition, a synthetic hypoxia-inducible factor-1 (HIF-1) promoter (64) or vascular endothelial growth factor (VEGF) promoter (91) were found to efficiently target MSC-NIS expression within the hypoxic regions and abundant vascularization seen in most solid tumors.

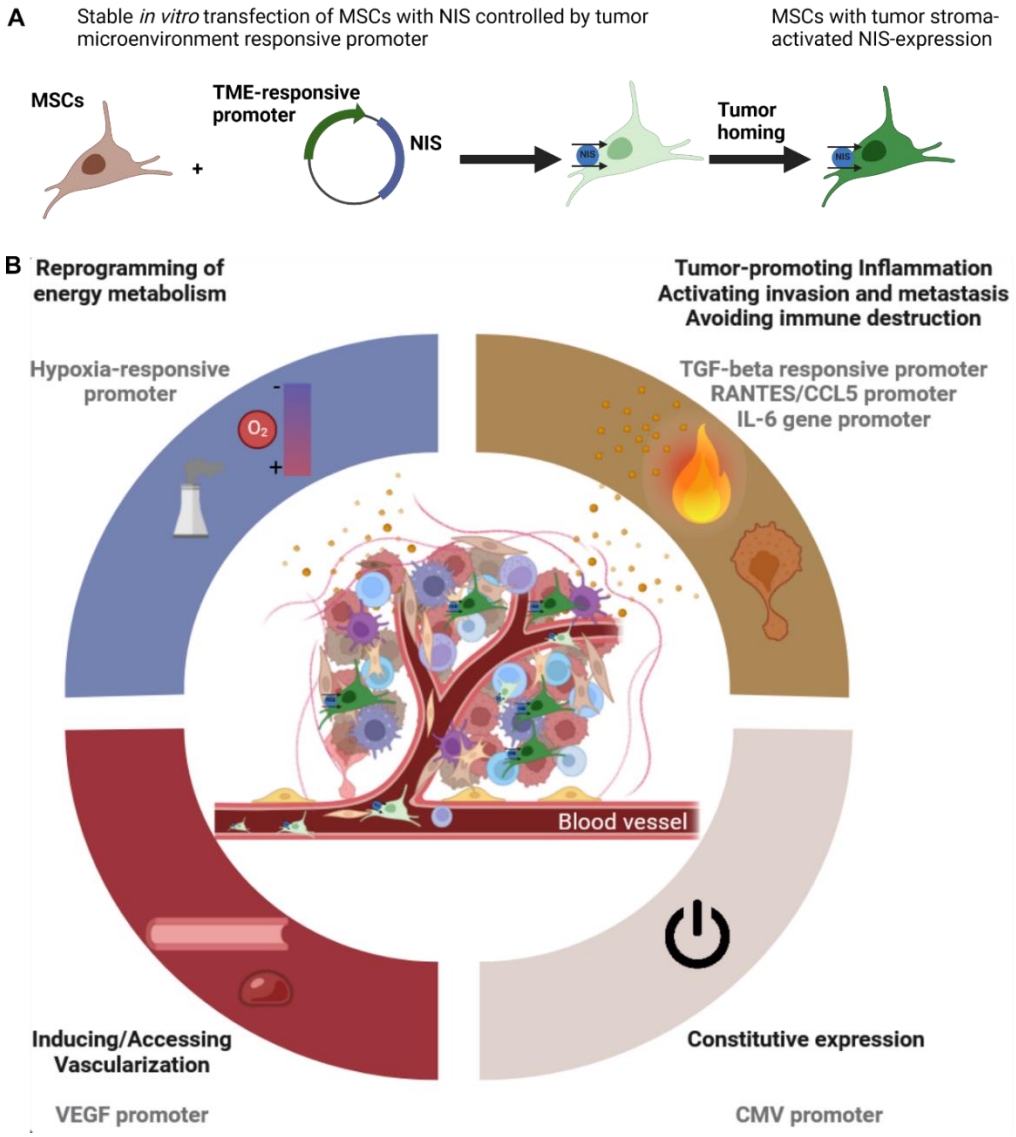

Figure 4: MSCs engineered to drive NIS expression controlled by various tumor stroma-responsive gene promoters. (A) Principle of *ex vivo* stable transfection of immortalized, bone marrow-derived mesenchymal stem cells (MSCs) with plasmids driving NIS expression under the control of gene promoters responsive to signaling pathways highly abundant in tumor environments (light green indicates NIS-transfected MSCs) that become activated after migration and homing to the tumor site (dark green indicates activated NIS-expressing MSCs). TME = tumor microenvironment. **(B)** After systemic application, engineered MSCs follow the same principle as endogenous MSCs and lymphocytes within the body and are actively recruited to the tumor. MSCs were engineered to control NIS expression through different promoters that target several hallmarks of cancer like inducing/accessing vascularization or changes in energy metabolism (VEGF-promoter, HIF-1α promoter), tumor-promoting inflammation, activation of invasion and escape from immune recognition (TGF-β responsive Smad-promoter, RANTES/CCL5 promoter, IL-6 promoter) described by Hanahan and Weinberg in 2000 & 2011 (2,3), latest updated by Hanahan in 2022 (4). For constitutive *NIS* transgene expression, CMV-NIS-MSCs were generated, where NIS expression is independent of activation in the TME. Created with BioRender.com.

1.5.2.1 Potential of the combination of the MSC-mediated *NIS* gene therapy concept with conventional treatment strategies

Different strategies can be pursued to increase the therapeutic efficacy of the MSC-mediated *NIS* gene therapy concept. NIS offers the possibility to transport various radionuclides. Depending on the tumor burden or grade of invasiveness, the therapeutic radioisotope transported by NIS can be selected and, thus, adjusted highly flexible to the patient's need: ^{131}I or ^{188}Re as β^-- emitters might be more suitable for larger tumors based on an enhanced crossfire effect that results from the deposition of their energy over several millimeters in tissue (^{131}I mean path length of 0.8 mm and ^{188}Re mean path length of 3.5 mm). The α-emitter ^{211}At has higher dose rates based on its shorter half-life and higher energy as compared to ^{131}I or ^{188}Re (^{131}I: physical half-life of 8 d, average β-energy of 0.192 MeV, ^{188}Re: physical half-life of 16.7 h, average beta-energy = 0.764 MeV; ^{211}At: physical half-life of 7.2 h, average α-energy = 6.8 MeV, mean path length of 65 nm) as well as shorter range in tissue. The properties of α-particles are more favorable for eradicating single tumor cells like minimal residual disease and micrometastases (49,92). A combination of the different radionuclides during different stages of the therapy could improve the precision of the employed doses, survival, and well-being of patients.

Furthermore, the MSC-mediated approach allows for the combination with conventional standard-of-care treatments or other targeted therapies as adjuvant or concomitant treatment, and potentially, might be a more realistic prospect for clinical translation. As stated above, the current standard treatment at diagnosis and in progressive disease are multimodal options incorporating surgery, radiotherapy, systemic therapy (chemotherapy or targeted therapy), supportive and palliative care for GBM and other cancer types (16). In the context of GBM, its infiltrative growth often results in tumor extension into the adjacent brain parenchyma and the formation of distant tumor microsatellites that preclude complete surgical resection, potentially promoting tumor recurrence. It has been reported in an experimental rat glioma model that intratumorally injected MSCs were able to migrate within glioma remnants during partial resection (93). Building upon this knowledge, either systemic application during surgical excision or direct implantation of NIS-MSCs in the surgical cavity followed by systemic administration of radionuclides transported by NIS may be beneficial to prevent postsurgical relapse (12).

Another viable approach that builds upon the inherent features of MSC is their combination with radiotherapy. Several preclinical studies have investigated the synergistic effects of irradiation as pre-treatment and MSC-mediated cancer treatment (90,94-98). The radiation-induced enhancement of the inflammatory response, including increased secretion of growth

factors, chemokines, and cytokines released by the tumor microenvironment, might facilitate MSC recruitment to the tumor after intravascular administration (96). In a previous study, we showed that external beam radiotherapy (EBRT) enhanced recruitment of systemically applied NIS-expressing MSCs into hepatocellular carcinoma. Further, the combination of EBRT and MSC-mediated *NIS* gene therapy using ^{131}I led to a dramatically enhanced therapeutic efficacy assessed by prolonged survival and delayed tumor growth (99). In addition, radiation has been shown to enhance vascular permeability, which could help MSCs to cross the endothelial cell barrier and potentiate the therapeutic efficacy in GBM, as one of the most vascularized cancers, due to enhancement of the maximal quantity and wider parenchymal distribution of MSCs localized in the tumor (27,96,100). The use of tumor stroma-specific promoters driving *NIS* gene expression in combination with conventional radiotherapy could ultimately yield a tremendous increase in the therapeutic efficacy of the *NIS* gene therapy concept (90,98). Schug *et al.* described a possible 'self-energizing effect': An enhancement of the inflammatory response and vascular permeability due to both external and/or internal radiotherapy of the tumor may increase MSCs recruited to the tumor environment. In the case of MSCs engineered with tumor-stroma responsive promoters driving NIS expression, the enhanced tumor signaling by irradiation additionally stimulates promoter activation.

In addition to external beam radiation therapy treatment, locoregional hyperthermia employed to the tumor strongly enhanced MSC recruitment to tumors following the enhanced release of proinflammatory cytokines, chemokines, and growth factors in response to treatment (90,101).

1.6 Aim of the Thesis

The main focus of this doctoral thesis was to expand the gene therapy concept based on mesenchymal stem cells armed with the theranostic sodium iodide symporter to glioblastoma (GBM) using clinically relevant imaging modalities (scintigraphy, PET, CT, MRT). Major challenges associated with the treatment of GBM were addressed through this approach, including non-invasive and efficient delivery of anticancer treatment across the blood-brain barrier. We hypothesized that the MSC-mediated *NIS* gene therapy concept represents an effective therapy option for GBM patients and might help improve state-of-the-art GBM therapy approaches by using the sodium iodide symporter as reporter and effector gene.

To provide a detailed characterization of MSC tracking using *NIS* as reporter gene – a prerequisite for planning and monitoring of gene therapy trials using engineered versions of MSCs – PET imaging offers the highest sensitivity and resolution as compared to SPECT or scintigraphy. As an initial study, PET-radiotracers transported by NIS, ^{124}I and ^{18}F-TFB, into constitutively NIS-expressing brain tumors were compared by small animal PET imaging to define their detection limit in this low-volume disease. In this regard, an in-house synthesis protocol ^{18}F-TFB was developed allowing more precise tumor localization for quantification.

In a following proof-of-concept study, subcutaneous and orthotopic GBM models were used to examine the homing of constitutively NIS-expressing MSCs (CMV-NIS-MSCs) to GBM after systemic administration by applying different dosing regimens. The constitutive expression of NIS allows for efficient assessment of *in vivo* distribution of eMSCs using NIS-based PET imaging. Based on the pre-therapy imaging study and dosimetry, the effect of therapeutic doses of ^{131}I following CMV-NIS-MSC administration was investigated in a syngeneic orthotopic GBM model.

Next, we aimed to enhance tumor selectivity of NIS expression in MSCs by using tissue-specific gene promoters that are activated in the GBM environment to drive NIS transgene expression, thereby limiting off-target toxicity and maximize safety. Based on the role of IL-6 pathway signaling that is highly abundant in the tumor environment and a prognostic marker for a poor prognosis in GBM patients, a MSC line was established that expresses NIS driven by an IL-6 promoter (IL-6-NIS-MSCs). IL-6-NIS-MSCs were investigated in analogy to the previous study and compared to CMV-NIS-MSC after systemic application in the same syngeneic orthotopic GBM mouse model.

Taken together, these investigations are important to evaluate the efficacy of MSC-mediated NIS gene therapy in experimental GBM preclinically as an essential basis for potential clinical translation.

2 Chapter 1: NIS as theranostic gene: its emerging role in new imaging modalities and non-viral gene therapy

This chapter is a pre-copy-edited version of a peer-reviewed article published in *EJNMMI Res.* 2022 May 3;12(1):25 and assigned the DOI doi: 10.1186/s13550-022-00888-w.

The sodium iodide symporter (NIS) as theranostic gene: its emerging role in new imaging modalities and non-viral gene therapy

Carolin Kitzberger[1], Rebekka Spellerberg[1], Volker Morath[2], Nathalie Schwenk[1], Kathrin A Schmohl[1], Christina Schug[1], Sarah Urnauer[1], Mariella Tutter[1], Matthias Eiber[2], Franz Schilling[2], Wolfgang A Weber[2], Sibylle Ziegler[3], Peter Bartenstein[3], Ernst Wagner[4], Peter J Nelson[1], Christine Spitzweg[1,5,#]

[1]*Department of Internal Medicine IV, University Hospital, LMU Munich, Munich, Germany*
[2]*Department of Nuclear Medicine, School of Medicine, Klinikum rechts der Isar, Technical University of Munich, Munich, Germany*

[3]*Department of Nuclear Medicine, University Hospital, LMU Munich, Munich, Germany*

[4]*Pharmaceutical Biotechnology, Department of Pharmacy, Centre for System-Based Drug Research and Centre for Nanoscience, LMU Munich, Munich, Germany*

[5]*Division of Endocrinology, Diabetes, Metabolism and Nutrition, Mayo Clinic, Rochester, Minnesota, USA*

Key words: Sodium iodide symporter, [^{18}F]tetrafluoroborate,^{124}I, PET, glioblastoma, gene therapy

2.1 Abstract

Cloning of the sodium iodide symporter (NIS) in 1996 has provided an opportunity to use *NIS* as a powerful theranostic transgene. Novel gene therapy strategies rely on image-guided selective *NIS* gene transfer in non-thyroidal tumors followed by application of therapeutic

radionuclides. This review highlights the remarkable progress during the last two decades in the development of the *NIS* gene therapy concept using selective non-viral gene delivery vehicles including synthetic polyplexes and genetically engineered mesenchymal stem cells. In addition, *NIS* is a sensitive reporter gene and can be monitored by high resolution PET imaging using the radiotracers sodium [^{124}I]iodide ([^{124}I]NaI) or [^{18}F]tetrafluoroborate ([^{18}F]TFB). We performed a small preclinical PET imaging study comparing sodium [^{124}I]iodide and in-house synthesized [^{18}F]TFB in an orthotopic NIS-expressing glioblastoma model. The results demonstrated an improved image quality using [^{18}F]TFB. Building upon these results, we will be able to expand the *NIS* gene therapy approach using non-viral gene delivery vehicles to target orthotopic tumor models with low volume disease, such as glioblastoma.

2.2 Introduction

The sodium iodide symporter (NIS) is a plasma membrane glycoprotein localized at the basolateral membrane of thyroid follicular cells mediating the active transport of iodide into the thyroid gland as an important prerequisite for the biosynthesis of thyroid hormones (Fig. 1) (44,102). NIS-mediated iodide transport can be inhibited by the competitive inhibitors thiocyanate and perchlorate, as well as by the Na^+Ka^+-ATPase inhibitor ouabain (45). Functional NIS expression provides the basis for the diagnostic and therapeutic application of radioiodide that has been widely used in the treatment of differentiated thyroid cancer for 80 years (103). The cytoreductive effect of targeted NIS-mediated radioisotope therapy is associated with the so called “crossfire effect”, which is the impact of radiation of accumulated radioisotopes in NIS-expressing cells on neighboring non-expressing cells through particle decay (49). In addition to radioiodide, alternative radionuclides, such as the beta-emitter ^{188}Re or the alpha-emitter ^{211}At, that are also transported by NIS offer the possibility of higher energy deposition in a shorter time period due to their higher energy and shorter half-life (^{188}Re: physical half-life 16.7 h, E = 0.764 MeV, path length 23-32 mm, ^{211}At: physical half-life 7.2 h,

high linear energy transfer 97 KeV/µm) as compared to ^{131}I (physical half-life 8d, E = 0.134 MeV, therapeutic range 2.6-5 mm), resulting in an enhanced crossfire effect (104-106).

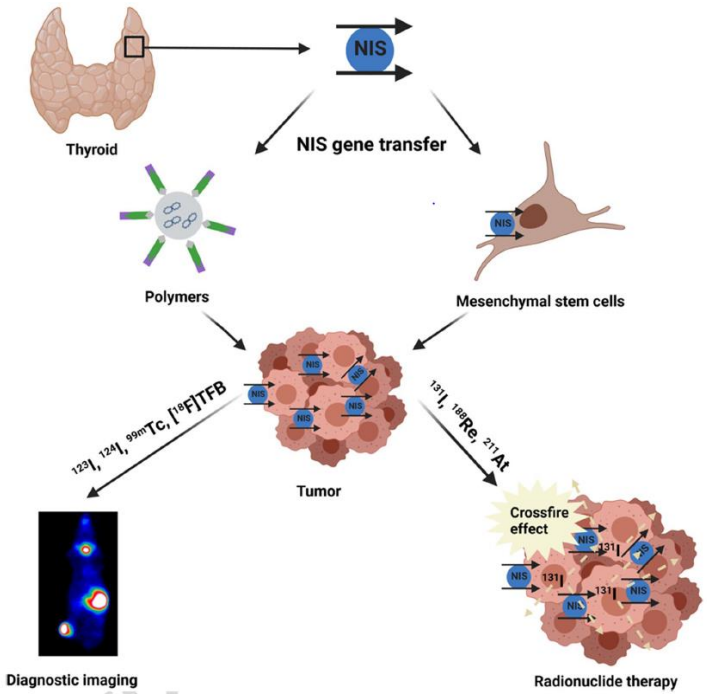

Fig. 1 Schematic illustration of NIS and its role in gene therapy. NIS is a powerful theranostic tool for diagnostic imaging and the application of therapeutic radionuclides. The transport of various radiotracers allows non-invasive monitoring of the *in vivo* biodistribution of functional NIS expression by whole body scintigraphy, SPECT or PET imaging and the application of therapeutic active radionuclides enables cytoreductive effects.

In 1996, N. Carrasco and her team succeeded in cloning of NIS cDNA and thereby provided a new and well-proven dual function tool allowing the establishment of image-guided selective *NIS* gene transfer into non-thyroidal tumors followed by the application of therapeutically effective radionuclides (Fig. 1) – work that was started by the pioneer study by Shimura *et al.* that showed successful restoration of radioiodide accumulation *in vitro* as well as *in vivo* after stable transfection of transformed rat thyroid cells (FRTL-Tc) with rat NIS cDNA (39,107).

2.3 Main text

Non-viral systemic *NIS* gene delivery

An important step in the clinical translation of *NIS* gene therapy of extrathyroidal tumors is the development of effective and safe gene delivery vehicles that allow sufficient and tumor selective NIS expression levels, ideally after systemic vector application. In addition to the option of monitoring and targeting primary tumors, some of these approaches provide options

to treat metastases by enhanced targeted delivery of the *NIS* transgene. Non-viral vector systems for targeted *NIS* gene transfer into non-thyroidal tumors are currently under investigation by our group in collaboration with E. Wagner and P. Nelson at the Ludwig-Maximilians-University in Munich and are summarized in this review. Synthetic polyplexes and mesenchymal stem cells can deliver anti-cancer therapies after systemic administration by different targeting strategies. Both systems represent promising platforms with a potential for clinical success.

Targeted polyplex-mediated and tumor-selective *NIS* gene delivery

Polyplexes are chemically defined carrier systems inspired by viral biology and developed for targeted nucleic acid delivery. These synthetic carriers are designed to overcome some of the current limitations of virus-mediated gene delivery such as immunogenicity, limited nucleic acid binding capacity and difficulty in synthesis and upscaling (36). Linear polyethylenimine (LPEI) represents the current 'gold standard' for synthetic gene delivery systems and is based on polycationic polymers that complex vector DNA through electrostatic interactions. LPEI-targeting and efficiency is refined by the incorporation of polyethylenglycol (PEG) and targeting ligands (58). PEG shielding lowers the positive surface charge to reduce self-aggregation or aggregation with other biological macromolecules. Furthermore, it protects from immune recognition and provides longer blood circulation (55). Targeting ligands are for example synthetic peptides that mimic ligands for cell surface receptors overexpressed on cancer cells. Their use can greatly improve the tumor selectivity of gene delivery. The epidermal growth factor receptor (EGFR) is a well-characterized receptor tyrosine kinase upregulated on diverse tumors. The peptide GE11 is a specific allosteric ligand for this receptor (108).

Polyplexes based on LPEI, shielded by PEG and coupled to GE11 (LPEI-PEG-GE11) were employed for systemic *NIS* gene delivery in subcutaneous (s.c.) EGFR overexpressing anaplastic thyroid carcinomas (ATC). ATC is the most aggressive form of thyroid cancer unresponsive to radioiodide therapy. After *in vitro* characterization of different ATC cell lines,

SW1736 with a high EGFR expression level and Hth74 with an intermediate level of EGFR expression were chosen for subsequent *in vivo* imaging studies. Tumoral ^{123}I uptake after systemic LPEI-PEG-GE11 administration was found to be 5.6-7.8% ID/g in SW1736 and 4.5-5.8% ID/g in Hth74 tumors (56). For ^{131}I, this translates to a tumor-absorbed dose of 35.1 mGy/MBq in the SW1736 model and 25.0 mGy/MBq in the Hth74 model (56). High transduction efficiency and EGFR-specificity of the LPEI-PEG-GE11 polyplex were demonstrated. ^{131}I therapy performed in the s.c. SW1736 tumor model showed significant delay in tumor growth and a longer median survival time (42 days) of the therapy group (LPEI-PEG-GE11/NIS + ^{131}I) compared to the control groups (28 days for LPEI-PEG-GE11/antisenseNIS + ^{131}I and NaCl + NaCl or 18 days for LPEI-PEG-GE11/NIS + NaCl). The data opened the exciting prospect of NIS-mediated radionuclide imaging and therapy of ATC after non-viral reintroduction of the *NIS* gene (56).

The EGFR-targeting approach was then evaluated in an advanced genetically engineered spontaneous mouse model of pancreatic ductal adenocarcinoma (Ptf1a$^{+/Cre}$; Kras$^{+/LSL-G12D}$; Tp53$^{lox/loxP}$ [Kras;p53]). Efficient tumor targeting was demonstrated by [^{123}I]NaI-scintigraphy (tumoral iodide uptake: 14.2 ± 1.4% ID/g) and confirmed using three-dimensional high resolution [^{124}I]NaI-PET imaging. Following application of [^{131}I]NaI, a tumor absorbed dose of 96.5 mGy/MBq was determined. Three cycles of LPEI-PEG-GE11/NIS followed by [^{131}I]NaI 48 h later resulted in a significantly reduced tumor growth in this aggressive tumor model (59).

A further evaluation of the EGFR-targeted LPEI-PEG-GE11 polymers was conducted in a mouse model of disseminated colon cancer liver metastases, established by intrasplenic injection of LS174T human colon cancer cells. High levels of NIS-mediated tumoral [^{18}F]TFB (tetrafluoroborate) uptake (4.8 ± 0.6% ID) were subsequently measured in mice treated with LPEI-PEG-GE11 (2.2 ± 0.6% ID) as compared to mice injected with untargeted polyplexes (LPEI-PEG-Cys). After administration of [^{131}I]NaI, the therapy group showed a significant reduction in hepatic metastases load resulting in extended survival of these mice (15 days post

therapy start compared to 8 days for the NaCl + NaCl group or 13 days for the LPEI-PEG-GE11/NIS + NaCl group) (57).

As a next step in the development of polyplex-based *NIS* gene shuttle systems additional sequence-defined polymer backbones containing integrated functional groups were developed, including: cationic oligoethano amide cores for enhanced nucleic acid binding and protonable amino acids with buffer function for a higher rate of endosomal escape (109). In addition, selective targeting using a second important tyrosine kinase receptor was explored. The cMET binding peptide cMBP2 targets the cMET/hepatocyte growth factor receptor (HGFR) that is overexpressed in a majority of cancers (110). New polymers making use of this biology were evaluated in a s.c. hepatocellular carcinoma (HuH7) xenograft mouse model. High transduction efficiency of cMBP2-PEG-Stp/NIS polyplexes were demonstrated using [^{123}I]NaI-scintigraphy: Mice treated with cMBP2-PEG-Stp/NIS polyplexes revealed a significantly higher tumoral iodide accumulation of 6.6 ± 1.6% ID/g as compared to mice injected with untargeted polyplexes (Ala-PEG-Stp/NIS). These results were confirmed in an *ex vivo* biodistribution study: a perchlorate-sensitive tumoral radioiodide uptake of 3% ID in NIS-tranduced HuH7 xenografts was seen while almost no iodide uptake was measured in tumors of control mice. A tumor-absorbed dose of 41 mGy/MBq for ^{131}I was calculated based on the results of the imaging study. A significant delay in tumor growth and prolonged survival was seen in a therapy study after three cycles of polyplex/[^{131}I]NaI application (111).

Inter- and intratumoral heterogeneity represent major issues for efficient tumor therapy. To help address this, a dual-targeted polymer was established based on the LPEI-PEG-backbone coupled to both GE11 (EGFR-targeting) and cMBP2 (cMET-targeting). Enhanced tumor targeting of the dual-targeted polyplexes was found as compared to single-targeted polyplexes in an orthotopic HuH7 xenograft mouse model by [^{124}I]NaI-PET imaging (112).

Mesenchymal stem cells as *NIS* gene delivery vehicles

The use of mesenchymal stem cells (MSC) as tumor therapy vehicles is based on their intrinsic tumor-homing capacity (74,113). Tumors show an enhanced production of inflammatory cytokines, growth factors and chemokines and thereby drive the active recruitment of MSCs into the tumor microenvironment, where they contribute to the genesis of the tumor stroma (114,115). MSCs are well-suited for clinical purposes as they can be easily harvested, amplified and transplanted across the allogenic barrier (116). Genetically engineered MSCs are promising vehicles for the delivery of therapeutic genes such as *NIS*. The use of engineered versions of MSCs for the treatment of solid tumors are currently being explored in early-phase human clinical trials. One study determining toxicity and efficacy after i.p. administration of engineered MSCs infected with oncolytic measles virus encoding *NIS* as treatment for patients with recurrent ovarian cancer (Clinical trial ID NCT02068794) is being conducted at the MayoClinic (Rochester, MN). A second phase I/II trial was conducted at the University Hospital of the LMU built upon our previous studies using autologous MSCs engineered to express the suicide gene thymidine kinase within tumor environments (117).

A series of preclinical studies have demonstrated the potential of CMV (cytomegalovirus) promoter driven MSC-mediated *NIS* gene delivery in xenograft tumor mouse models that have shown successful selective NIS expression in tumors and metastases plus a robust therapeutic response after [^{131}I]NaI application (63,75,89).

These proof-of-concept studies were expanded to an immunocompetent advanced genetically engineered pancreatic ductal adenocarcinoma mouse model described above. Tumoral ^{123}I uptake was assessed by [^{123}I]NaI-scintigraphy after intravenous MSC application resulting in an impressive level of NIS-mediated iodide accumulation (16.2 ± 2.9% ID) and a tumor absorbed dose of 136.9 mGy/MBq for ^{131}I. The tumor selective radionuclide uptake was confirmed by [^{124}I]NaI-PET imaging. A significant reduction in tumor growth was seen in the subsequent ^{131}I therapy study (66).

A potential side effect of MSC-directed tumor gene therapy is represented by potential MSC homing to normal tissues as part of normal tissue homeostasis that could lead to potential off-target tissue damage. A series of different gene promoters that become activated in response to signaling pathways within tumor microenvironments were evaluated to better control *NIS* transgene expression and enhance the tumor specificity of MSC-based tumor targeting. Hypoxia-inducible factor (HIF) -1 is a key mediator of the cellular response to hypoxia. Hypoxic regions in cancer are more resistant to conventional chemo- or radiotherapy and therefore efficient targeting of those is an important issue in cancer therapy. MSCs engineered with a synthetic HIF-responsive promoter (HIF-NIS-MSC) showed effective transgene induction *in vitro* under hypoxic conditions using tumor cell spheroid models. In *in vivo* studies, *NIS* transgene expression was compared between an orthotopic intrahepatic HuH7 mouse model and s.c. HuH7 flank tumors. The maximum ^{124}I uptake in the orthotopic tumors was elevated (6.9 ± 0.9% ID/g with a tumor-absorbed dose of 46.8 mGy/MBq ^{131}I) as compared to the maximum ^{123}I uptake in s.c. tumors (3.9 ± 0.4% ID/g with a tumor-absorbed dose of 26.5 mGy/MBq for ^{131}I). These results were confirmed in *ex vivo* biodistribution studies. The higher tumoral iodide accumulation in the intrahepatic tumors was based on more efficient MSC recruitment due to a more physiologic tumor microenvironment and resulted in a successful ^{131}I therapy study. The delay in tumor growth seen in the therapy group (HIF-NIS-MSC + ^{131}I) was associated with a reduced tumor perfusion as assessed by contrast-enhanced ultrasound (64).

Activation of the tumor growth factor (TGF-) β/Smad signaling pathway is strongly linked to tumor biology. The use of a synthetic SMAD-based TGF-β-responsive gene promoter to drive *NIS* transgene expression in engineered MSCs (SMAD-NIS-MSC) was evaluated in a series of experimental tumor settings. SMAD-NIS-MSCs induced an ^{123}I uptake of 6.8 ± 0.8% ID/g as visualized by [^{123}I]NaI-scintigraphy and a tumor-absorbed dose of 28.2 mGy/MBq for ^{131}I in a s.c. HuH7 xenograft mouse model. The MSCs were effective in tumor homing and showed a robust TGF-β-induced NIS expression. While the tumor-absorbed dose was lower than that

seen in previous studies, the ^{131}I therapy study resulted in a stronger therapeutic effect including a significant delay in tumor growth and prolonged survival (65).

New strategies to enhance the tumor-homing properties of MSCs were developed making use of additive effects of combining MSC-mediated *NIS* gene therapy with other treatment options. Potential additive effects could help optimize the therapeutic effectiveness of cancer treatment and overcome tumor resistance. External beam radiation therapy (EBRT) when used in cancer therapy causes extensive tissue damage. EBRT-treated tumor tissues release inflammatory chemokines and growth factors known to be linked to MSC migration (96). After irradiation of HuH7 cells *in vitro*, a strong dose-dependent increase in steady state mRNA levels of CXCL8, CXCL12, FGF2, PDGFβ, thrombospondin-1, VEGF and TGF-β1 was found and validated by ELISA. A live cell tracking migration assay monitored by time-lapse microscopy showed that MSCs migrate preferably to supernatant of EBRT-treated HuH7 cells as compared to supernatant from untreated HuH7 cells. MSC migration after EBRT pre-treatment was examined *in vivo* using *NIS* as a reporter gene. A significant dose-dependent accumulation of radioiodide after i.v. injection of CMV-NIS-MSCs was shown by [^{123}I]NaI-scintigraphy. Subcutaneous HuH7 tumors irradiated with 5 Gy revealed the highest ^{123}I uptake (9.2 ± 1.5% ID/g) as compared to 2 Gy (7.9 ± 1.4% ID/g) and non-irradiated tumors (5.3 ± 0.8% ID/g). These results demonstrated enhanced tumor homing of MSCs after EBRT treatment of the tumor (94).

The increased TGF-β1 seen after tumor irradiation raised the prospect of applying EBRT prior to injection of SMAD-NIS-MSCS to better control and focus *NIS* transgene expression within the tumor. EBRT enhances the migratory behavior of MSCs, and may also act to amplify SMAD-based promoter activation due to enhanced release of TGF-β1. The combination of focused EBRT (5 Gy) with MSC-mediated systemic *NIS* gene delivery under control of the synthetic TGF-β1-inducible SMAD-responsive promoter was evaluated. [^{123}I]NaI-scintigraphy was performed followed by an ^{131}I therapy in s.c. HuH7 xenograft mouse models. Non-irradiated tumors revealed an iodide accumulation of 7.0% ID/g with a tumor-absorbed dose

of 52.37 mGy/MBq for ^{131}I, while tumors pre-treated with a radiation dose of 5 Gy 24 h before MSC application showed an iodide uptake of 9.8% ID/g and a tumor-absorbed dose of 56.72 mGy/MBq for ^{131}I. In the therapy study, the therapy group (5 Gy + SMAD-NIS-MSC ^{131}I) showed a pronounced reduction in tumor growth leading to a complete tumor remission in a subset of mice and a dramatically prolonged survival of animals as compared to 5 Gy + CMV-NIS-MSC + ^{131}I treated mice or untreated controls. We believe this robust therapeutic effect can be linked to a series of relevant issues: The tissue damage caused by EBRT leads to increased cytokines that enhance recruitment of MSCs. The enhanced levels of TGF-β1 further activate *NIS* transgene expression. NIS-based radioiodide treatment causes further tissue damage leading to higher TGF-β1 levels. Thus, a self-energizing cycle may be responsible for the pronounced therapeutic effect seen in this study. The SMAD-responsive promoter may represent a powerful indirect radiation-responsive promoter (90).

Another approach evaluated the combination of regional hyperthermia and MSCs to increase MSC recruitment to the tumor stroma. Hyperthermia is an adjuvant tool in multimodal treatment approaches and is used to enhance therapeutic efficacy. Pleiotropic effects on malignant cells, such as reduction of DNA repair, heat shock protein (HSP) production and modulation of inflammatory cytokines are thought to help trigger an antitumor immune response. This biology also suggested a potential basis for combining MSC based *NIS* gene therapy with local hyperthermia. Hyperthermia of HuH7 cells *in vitro* resulted in an increased production of immunomodulatory factors and in a live cell tracking migration assay MSCs showed directed chemotaxis towards the supernatant of heat-treated cells as compared to non-treated HuH7 cells. The enhanced migration of CMV-NIS-MSCs *in vivo* to heat-treated s.c. HuH7 tumors was demonstrated by [^{123}I]NaI-scintigraphy (8.9 ± 1.1% ID/g for tumors heated at 41 °C as compared to 5.4 ± 0.5% ID/g for 37 °C). A ^{131}I therapy study resulted in significantly enhanced efficacy by combining CMV-NIS-MSC-based *NIS* gene delivery with regional heat treatment 24 h later and an [^{131}I]NaI injection 48 h later (101).

In a subsequent series of experiments, MSCs were engineered with a heat-inducible HSP70B promoter allowing tumor-specific, time- and temperature-dependent NIS expression. Optimal promoter activation was evaluated using [^{123}I]NaI gamma imaging. Iodide application 12 h after 41 °C heat treatment revealed the highest tumoral uptake (9.7 ± 2.3% ID/g as compared to 6.8 ± 1.9% ID/g in 37 °C controls). This most optimal application regime was then evaluated in an ^{131}I therapy study where the therapy group showed a reduction in tumor growth and an extension in survival length (67).

The role of NIS in advanced imaging modalities

As demonstrated in the previous sections, *NIS* is a powerful theranostic gene that allows the efficient monitoring of molecular therapies after application of radionuclides (39). *NIS* also has many features of a well-suited reporter gene: It is a naturally occurring protein originating from thyroid follicular cells and is non-immunogenic and non-toxic to cells (118). As iodide accumulation only occurs in living cells, functional NIS activity is associated with cell viability (118). The active transport of substrates leads to an accumulation of radiolabeled substrates and concentrates the signal. Thus, the detection sensitivity is higher as compared to a reporter that simply binds its substrate stoichiometrically (48). NIS translocates various substrates and thereby makes various standard nuclear medicine imaging modalities suitable for localizing NIS-positive cells. The active transport of ^{123}I, ^{125}I, ^{131}I, ^{99m}Tc and ^{188}Re facilitates gamma scintigraphy and single-photon emission computed tomography (SPECT). Additionally, ^{131}I and ^{188}Re are therapeutically effective radionuclides through their beta decay. Planar scintigraphy or SPECT have been used as the core technologies of molecular imaging of NIS in the clinic. However, the imaging of functional NIS expression by PET allows the prospect of improved resolution, sensitivity and effective quantitative analysis (119). As positron emitter, ^{124}I is the best known and most often applied tracer for NIS-mediated PET imaging in the preclinical and clinical setting. However, ^{124}I has several disadvantages for the routine diagnostic clinical use: It has a relatively long half-life of 4.2 days, a low positron yield (23%), high positron energy

and additional high energy gamma emissions (>500 keV) that result in high radiation exposure and image quality degradation (120). Further, the complexity of its production leads to high costs and limited availability.^{124}I is currently commercially available from only a few sites in Europe. The situation is compounded by the fact that Perkin Elmer stopped its distribution in 2019 and only very few reliable ^{124}I source such as DSD-Pharma remain. Through organification of iodide in the thyroid, the tracer is made less available for non-thyroidal targeted cells due to this “thyroid-sink” effect. To reduce this impact and to avoid toxic thyroidal off-target effects, patients may be pre-treated with L-thyroxine to downregulate the TSH-dependent thyroidal NIS expression and thus lower iodide uptake in the thyroid (121). A novel tracer for NIS-based PET imaging was recently established. ^{18}F-Tetrafluoroborate (TFB) has been introduced as a potential alternative to ^{124}I showing several advantages for routine diagnostic use based on the radiochemical and physical properties of ^{18}F (119). [^{18}F]TFB possesses advantages over ^{124}I due to its shorter half-life (110 min vs. 100 h), branching ratio (97 vs. 23%) and especially the lower positron energy (E_{max}; 0.634 vs. 2.14 MeV) resulting in a clearer and less ‘blurred’ PET image (119,120,122,123). TFB is a fluorine-containing ion that is structurally comparable to pertechnetate, a substrate of NIS as shown by electrochemical studies (123). [^{18}F]TFB is trapped, but as is seen with [^{99m}Tc]pertechnetate, it is not organified by the thyroid. As a nonorganified NIS tracer, it shows a biodistribution similar to that seen with [^{99m}Tc]pertechnetate with a physiological tracer accumulation in the thyroid, stomach, salivary glands, with mainly renal secretion, and is pharmacologically and radiobiologically safe in humans (120,124,125). [^{18}F]TFB is a very promising iodide analogue as shown in a series of preclinical animal models and in the clinical setting in healthy individuals as well as thyroid cancer patients (120,122,124-128). In a preclinical study a higher absolute [^{18}F]TFB uptake was observed in non-thyroidal NIS-expressing tissues as compared to iodide due to the lack of metabolic entrapment of [^{18}F]TFB in the thyroid resulting in a higher availability of [^{18}F]TFB to extrathyroidal NIS-expressing organs (129). In addition, [^{18}F]TFB can deliver excellent target-to-background ratios in contrast to the image quality of ^{124}I. It shows a high signal-to-

noise ratio within ~1 h post injection, allows more optimal imaging times for patients and has less radiation exposure for the patient (122). In a preclinical comparative imaging study using a NIS-expressing orthotopic xenograft breast cancer mouse model, the pharmacokinetic differences between the PET tracer [^{18}F]TFB and the SPECT tracer [^{123}I]iodide were evaluated, which play a crucial role for imaging performance regarding the imaging sensitivity (129). The authors found a faster and more complete clearance of [^{18}F]TFB from the blood paired with faster tumoral uptake which led to higher target-to-blood ratios as compared to ^{123}I and importantly allowed imaging of small NIS-expressing metastases, which were not detectable with routine metabolic [^{18}F]FDG-PET. The clinical implementation of [^{18}F]TFB has lagged, despite its superiority over ^{124}I. To date only a small cohort of individuals have been imaged with [^{18}F]TFB (8 healthy individuals and 39 patients with differentiated thyroid cancer) (130). In addition, the short half-life and especially the different pharmacokinetics of [^{18}F]TFB compared to iodine do not allow reliable radiation dosimetry extrapolation using [^{18}F]TFB for radioiodine treatment. Due to improved image quality, [^{18}F]TFB-PET imaging allows expansion of gene therapies that employ *NIS* as reporter gene in low volume tumor models, such as metastatic disease or glioblastomas. Additionally, the potential overlap of the signal seen in these low volume tumors with the organs that physiologically express NIS can be circumvented by improved delineation of signals.

The role of NIS-imaging in glioblastoma

Glioblastoma (GBM) is the most common primary brain tumor with a poor prognosis and mainly palliative therapy concepts (13). As a highly complex tumor that exploits several mechanisms to evade therapy, novel treatment strategies for GBM are urgently needed (13). One reason of restrictions in the effective treatment and detection of GBM is the blood-brain-barrier (BBB) that can block radiotracers and gene vectors. NIS-mediated radionuclide imaging and therapy does not require complex radiolabeling procedures and the small sized radionuclides used are able to penetrate the BBB and diffuse into the tumor (53).

Several preclinical studies have demonstrated the potential application of NIS for glioma imaging and therapy. A study by Cho *et al.* used a rat model with intracerebral F98 gliomas that had been retrovirally transduced with human NIS. The authors showed the possibility of non-invasive glioma imaging by [^{99m}Tc]pertechnetate- and [^{123}I]NaI-scintigraphy followed by an increased survival time of rats after ^{131}I therapy (52). Guo *et al.* published imaging and therapy experiments with ^{188}Re and ^{131}I in mice bearing xenografted tumors after injection of the human glioma cell line U87 that was transfected with a recombinant lentiviral vector containing human NIS into the right armpit (53). *In vivo* imaging results showed ^{188}Re/^{131}I accumulation in the NIS-containing tumors as assessed by gamma camera imaging and an effective decrease in tumor volume was achieved in mice receiving ^{188}Re or ^{131}I as compared to untreated control mice. In another study, using one of the most extensively explored oncolytic viruses for *NIS* gene transfer, Opyrchal *et al.* reported effective [^{123}I]NaI or [^{99m}Tc]pertechnetate gamma camera or microSPECT/CT imaging of s.c. and orthotopic murine glioblastoma xenografts after intratumoral infection with measles virus encoding NIS (MV-NIS) to induce NIS expression in brain tumor tissue. Combined radiovirotherapy with MV-NIS and ^{131}I resulted in an improved antitumor activity and survival as compared to virotherapy alone in both glioma settings (54).

The advantages of PET, in contrast to scintigraphy or SPECT, is the potential detection of low volume GBM lesions with relatively low NIS expression levels when systemic gene transfer approaches are used (48). Preclinical imaging studies with [^{18}F]TFB as a PET tracer were performed in athymic mice bearing human NIS-expressing C6 glioma s.c. xenografted tumors yielding an avid NIS-mediated tumoral [^{18}F]TFB uptake (127). Recently, a small imaging series by our group was performed using the human U87 glioma cell line stably transfected with a NIS expressing plasmid (CMV-NIS-pcDNA3) (U87-NIS) to track the tumoral NIS expression of s.c. and orthotopic brain tumors by a direct comparison of ^{124}I and [^{18}F]TFB as radiotracers for small animal PET imaging. The localization of NIS protein on the cell membrane of the U87-NIS cells and its active transport of iodide was confirmed by immunocytochemistry and [^{125}I]iodide uptake assays *in vitro* (Supplemental Fig. 1). The U87-NIS cells were used in a s.c.

model. Stably NIS expressing U87 tumors revealed a pronounced iodide accumulation (Fig. 2a) and endogenous NIS-mediated ^{123}I uptake was observed in stomach, thyroid and salivary glands as well as in the urinary bladder due to renal excretion.

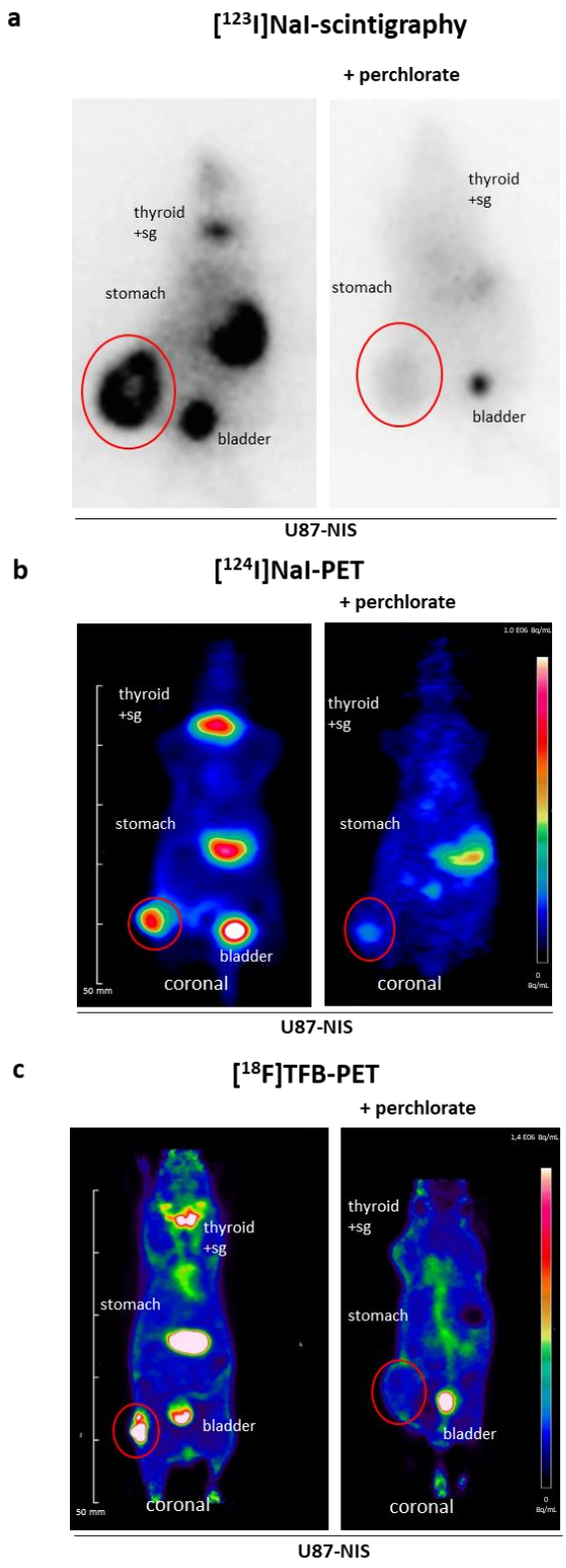

Fig. 2 NIS-mediated *in vivo* imaging of mice bearing subcutaneous U87-NIS tumors. (a) Planar gamma camera imaging showed NIS-specific tumoral ^{123}I uptake of 9.4% ID/g tumor (n=2; + $NaClO_4$ n=1) 1h after intraperitoneal application of 18.5 MBq [^{123}I]NaI. (b) PET scans revealed 4.8 ± 1.1% ID/mL ^{124}I accumulation in the tumor (n=5; +$NaClO_4$ n=3). (c) [^{18}F]TFB-PET scans resulted in a maximum tumoral [^{18}F]TFB accumulation of 7.1% ID/mL (n=1, + $NaClO_4$ n=1). Presented PET images show sectional planes (coronal orientation) 1 h after i.v. tracer injection of 10 MBq. Tracer uptake of the tumors was blocked upon treatment with the NIS-specific inhibitor perchlorate. Tumors circled in red; sg, salivary glands.

In a second group of mice, NIS-based radionuclide biodistribution was investigated using three-dimensional preclinical PET scanners after intravenous injection of [^{124}I]NaI or [^{18}F]TFB. The results showed a high accumulation of the NIS PET tracers in U87-NIS tumors (Fig. 2b, c). With a simple and effective in-house synthesis of [^{18}F]TFB based on the protocol of Phil Blower's group from the King's College in London, we were able to achieve a radiochemical yield of 15% (starting activity of 5 GBq) and a purity of over 97.5% as assessed by radio-thin-layer chromatography (124). To demonstrate that the radiotracer uptake in U87-NIS tumors was NIS-mediated, mice were additionally treated with the competitive NIS-specific inhibitor perchlorate. In these animals the physiological signal of endogenously NIS-expressing organs (thyroid, mammary glands, salivary glands, stomach) as well as tumoral uptake was effectively blocked.

To our knowledge no study has reported PET imaging to monitor *NIS* gene expression in brain tumors. The application of the clinically more relevant orthotopic model was then addressed by our group. Nude mice bearing orthotopic U87-NIS brain tumors received [^{124}I]NaI or [^{18}F]TFB for PET imaging. Both radiopharmaceuticals resulted in NIS-mediated radionuclide accumulation in brain tumors, which was comparable for ^{124}I and [^{18}F]TFB (Fig. 3a, c). Serial scanning was performed and showed a trend towards an inverse pattern of the accumulated tracers (Fig. 3b, d): Tumoral radioiodide efflux was observed over the scanning time in contrast to the [^{18}F]TFB uptake, which showed increasing levels of radionuclide accumulation from the first to the last scan in both settings (s.c. and orthotopic). This increase in [^{18}F]TFB uptake over time was also shown in a biodistribution study (dynamic and whole-body static PET/CT scans over 4 h post injection) of healthy participants by evaluation of 15 organs of the human body as well as in the aforementioned hNIS-expressing C6 glioma flank tumor model (126,127).

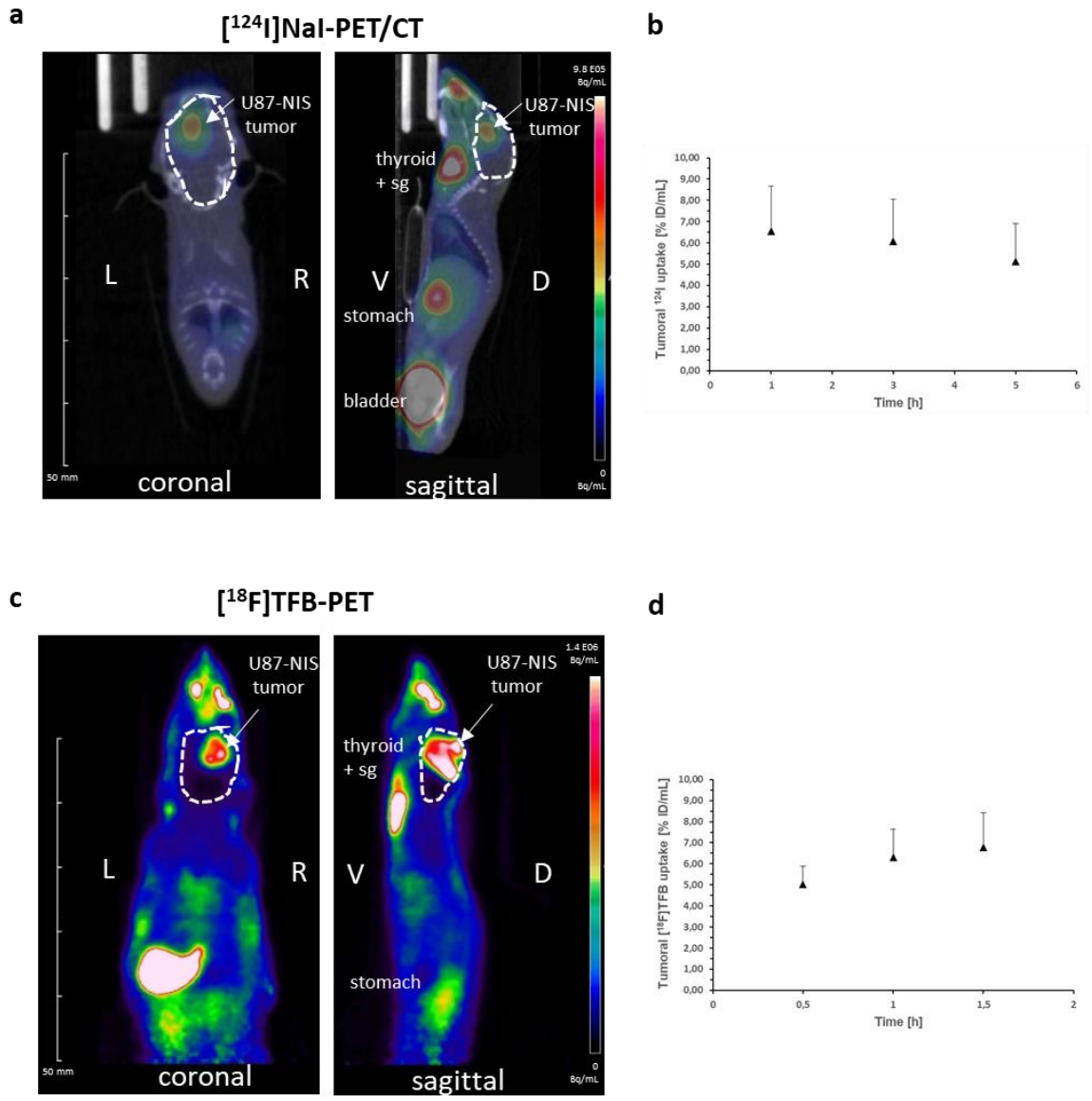

Fig. 3 NIS-mediated *in vivo* small-animal PET imaging of U87-NIS brain tumors. Comparison of U87-NIS brain tumor detection by [^{124}I]NaI- and [^{18}F]TFB-PET. (a, c) Sagittal and coronal planes of [^{18}F]TFB-PET and [^{124}I]NaI-PET/CT scans are displayed. The brain areas are circled in white and tumoral tracer uptake was seen for both radionuclides (arrows). (b, d) Quantification of serial PET imaging representing the efflux of tumoral ^{124}I and a positive change of [^{18}F]TFB in the tumor (n=5 each). (c) Low level of bone accumulation indicate a minimal level of residual free fluoride. Representative pictures show sectional planes of the 1 h time point after i.v. tracer injection (10 MBq). Results are expressed as mean ± SEM.

Ex vivo analysis of both models, s.c. and orthotopic U87-NIS tumors, showed prominent NIS protein expression localized at the cellular membrane (green, Fig. 4a, c) in dissected tumors,

which underlines the NIS-mediated *in vivo* radionuclide uptake in the tumors with 2D and 3D-imaging devices.

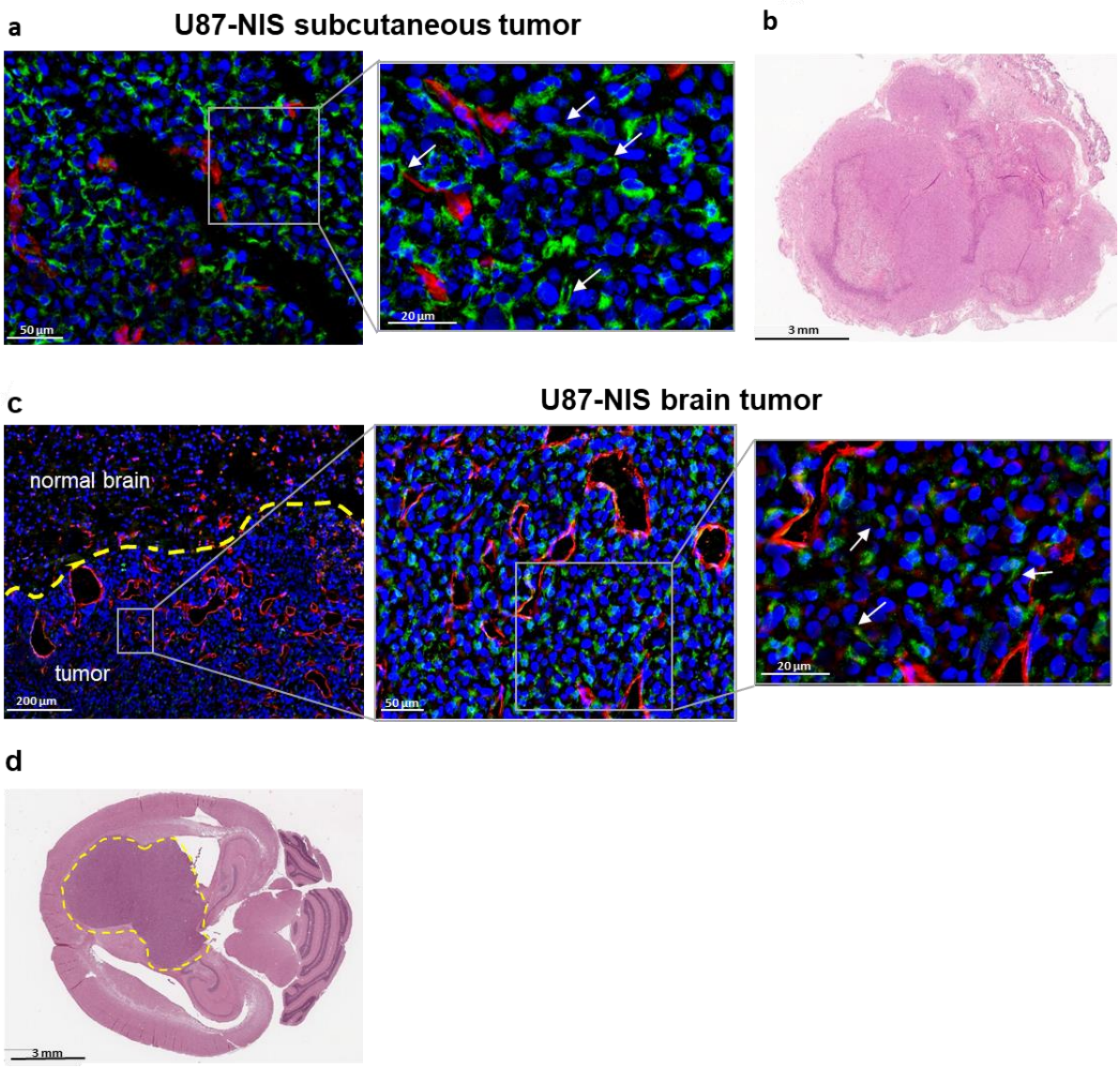

Fig. 4 *Ex vivo* analysis of U87-NIS tumors. (a, c) NIS (green) and CD31 (red, labeling tumor vascularization) immunofluorescence staining of cryosections of U87-NIS flank and brain tumors. Nuclei is stained in blue. NIS protein expression is shown at the cellular membrane (white arrows) of the tumor cells. An increased pattern of vascularization of brain tumors is detected compared to normal brain tissue as well as in contrast to the s.c. model. Section thickness 5 µm (s.c. tumors) and 10 µm (brain section). (b, d) H&E of s.c. U87-NIS xenograft tumor and horizontal section of the brain for visualization of the tumor mass. The area of implantation in the right caudate putamen of orthotopic xenografts is shown and the tumor is circled in yellow.

The current data strongly suggest the potential of *NIS* as reporter gene to image brain tumor lesions using PET. Superior imaging by utilization of [^{124}I]NaI or [^{18}F]TFB as radiotracers allows a detailed/accurate analysis of NIS-mediated radionuclide accumulation in the brain and effectively sets the stage for therapeutic application of [^{131}I]NaI. Finally, the image quality of [^{18}F]TFB easily produced by most nuclear medicine departments is preferable due to a high signal-to-noise ratio in contrast to lower signal-to-background ratios of [^{124}I]NaI-PET. While in these proof-of-principle experimental set-ups *ex vivo* NIS-transfected glioma cell lines were used, as a next step towards clinical application, we sought to apply and improve upon previously validated methods of systemic non-viral *NIS* gene delivery using [^{124}I]NaI or [^{18}F]TFB-PET imaging for monitoring of efficacy and tumor selectivity, which will be addressed in the next section.

Future Perspectives: Non-viral systemic *NIS* gene delivery to glioblastoma

The potential of *NIS* as a theranostic gene and the improvement of novel gene delivery systems has expanded the opportunity to use the *NIS* gene therapy concept in extrathyroidal tumors (49,121). Based on the gene therapy approaches summarized above, the preclinical development of the *NIS* gene therapy approach will be expanded to other aggressive non-thyroid tumor diseases, such as glioblastoma with the main aim of a clinical phase I/II trial. In ongoing studies we are currently addressing the efficacy of non-viral systemic *NIS* gene delivery systems based on mesenchymal stem cells or synthetic polyplexes to target glioblastoma (Fig. 5) and taking advantage of advanced small animal [^{124}I]NaI and [^{18}F]TFB-PET imaging (61).

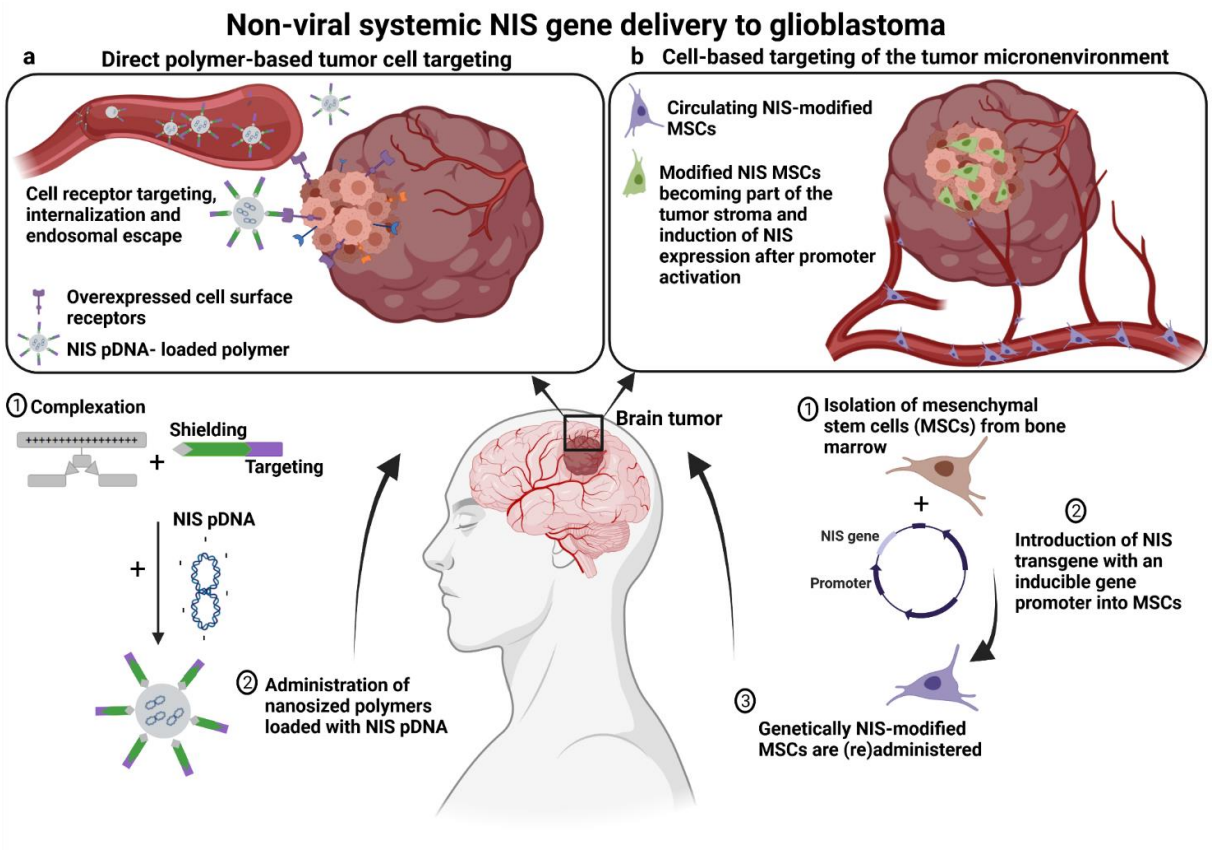

Fig. 5 Non-viral systemic *NIS* gene delivery strategies to glioblastoma (GBM). (a, left panel) Potential approach to use synthetic polymers to deliver the theranostic *NIS* gene directly to GBM cells. (1) The polymer backbone is functionalized with ligands (targeting domain) that have a high affinity to cell surface receptors that are overexpressed in GBM cells. Polymers are loaded with NIS pDNA. (2) Following systemic administration of polymers, the pDNA is released to the GBM cells after binding of the polymer to the cell receptor. (b, right panel) Mesenchymal stem cell (MSC)-based delivery of *NIS* targeting the tumor mircoenvironment of GBM. (1) MSCs can be easily isolated from patients from different tissue sources (e.g. bone marrow or adipose tissue) and (2) genetically modified with the *NIS* gene under the control of tumor-stroma specific gene promoters. (3) Engineered MSCs can be amplified in the laboratory and systemically administered back to the patient or over the allogenic barrier. Tumor-secreted factors (e.g. inflammatory cytokines) promote direct migration and extravasation of MSCs to GBM where they become part of the tumor stroma. NIS expression is induced after promoter activation. Following successful *NIS* gene transfer using both delivery platforms, diagnostic and therapeutic application of radioactive NIS substrates can be applied. pDNA; plasmid DNA

2.4 Conclusion

The application of NIS for radionuclide-based gene therapy of non-thyroidal tumors is a rapidly developing theranostic approach. Non-viral systemic *NIS* transgene transfer systems, such as the use of mesenchymal stem cells or synthetic polymers, have been extensively explored in several preclinical studies, as summarized in this review. These studies have demonstrated the potential of *NIS* as sensitive reporter gene allowing spatial and temporal monitoring of *NIS* transgene expression following therapeutic radionuclide application in non-thyroid cancer settings. The lack of iodide organification in non-thyroid cancer resulting in limited tumoral iodide retention has been raised as an argument against effective *NIS* gene therapy. However, extensive preclinical studies including our own work have convincingly demonstrated that the level of radionuclide accumulation (radioiodide or alternative radionuclides such as ^{188}Re and ^{211}At) achieved in the tumor, the duration of radionuclide retention, and the distribution of *NIS* transgene expression was sufficient to reach a tumor dose within the range considered sufficient for a therapeutic response in thyroid cancer (131,132). More importantly, these levels have been sufficient to elicit a significant therapeutic effect of ^{131}I or alternative radionuclides in a variety of tumor models, including clinically highly aggressive tumor models (56,57,59,65-67,89,90,94,101,111,112). For a more detailed discussion of this aspect, we refer to a recently published review paper (49). The tumor micromilieu might also play a role in regulation of NIS function and/or NIS membrane targeting thereby affecting the efficacy of *NIS* gene therapy approaches, which however has not been explored so far after *in vivo NIS* gene delivery in clinically relevant preclinical tumor models (133). Based on the extensive data from advanced cancer models including our own data, the *NIS* gene therapy concept should be expandable to disseminated, low volume diseases such as glioblastoma. Low volume disease can be associated with relatively low *NIS* transgene expression. In this instance the high resolution and sensitivity of new imaging modalities should hold much promise for optimizing therapy regimens. Among standard nuclear medicine imaging modalities such as scintigraphy or SPECT, PET offers the highest resolution, sensitivity and allows quantitative measures. The

development of [^{18}F]TFB as an alternative PET tracer for monitoring NIS biodistribution overcomes many of the issues encountered when using ^{124}I. ^{18}F-labelled TFB is an excellent iodide analogue with improved imaging quality and availability. In a direct comparison of ^{124}I and [^{18}F]TFB in a preclinical imaging study – to our knowledge, we were the first to show improved imaging – in an orthotopic hNIS expressing brain tumor model. The results suggest that [^{18}F]TFB may serve as promising tracer in the context of NIS-based brain tumor imaging. As a next step, the theranostic features of the *NIS* transgene will be expanded by development of next generation cellular carriers or synthetic polymers to better target the tumor microenvironment of non-NIS-expressing glioblastoma. In this setting, the advantage of [^{18}F]TFB for NIS-tracking will facilitate future clinical translation.

2.5 Statement of ethics approval

Animal experiments were approved by the District Government of Upper Bavaria and were conducted in accordance with institutional guidelines of the Klinikum rechts der Isar of the Technical University of Munich.

2.6 Additional files

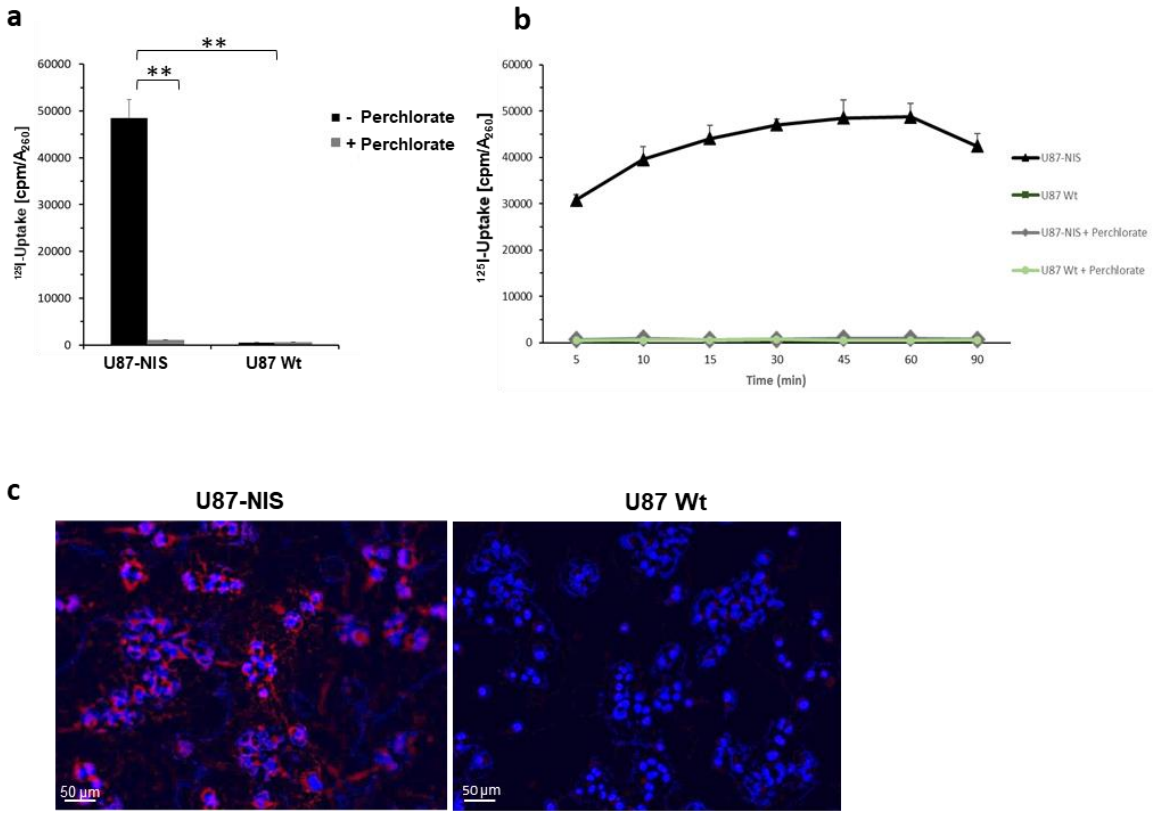

Supplemental Fig. 1 *In vitro* analysis of U87 cells constitutively expressing the sodium iodide symporter (U87-NIS). (a) Radioiodide uptake was measured in U87-NIS cells and compared to U87 Wt cells at steady-state conditions. U87-NIS cells revealed a 52-fold higher iodide accumulation compared to U87-NIS cells treated with perchlorate for the blockage of NIS-mediated iodide uptake of the cells. In addition, radioiodide uptake of U87-NIS cells was 102-fold increased in comparison to U87 Wt cells. No iodide uptake above background level was shown in U87 Wt cells. (b) Time course of ^{125}I uptake in U87-NIS and U87 Wt cells. Half-maximal levels of perchlorate-sensitive ^{125}I accumulation in U87-NIS cells was reached within 5 min and saturation at 45-60 min. (c) NIS-specific immunofluorescence staining of U87-NIS and U87 Wt cells (NIS in red, nuclei in blue). All data are reported as mean ± SEM. (**P<0.01)

2.7 Abbreviations

ATC	anaplastic thyroid carcinoma
BBB	blood brain barrier

CMV	cytomegalovirus
EBRT	external beam radiation therapy
EGFR	epidermal growth factor receptor
GBM	glioblastoma
H&E	hematoxylin and eosin
HGFR	hepatocyte growth factor receptor
HIF	hypoxia inducible factor
HSP	heat shock protein
ID	injected dose
i.v.	intravenous
i.p.	intraperitoneal
LPEI	linear polyethylenimine
MSC	mesenchymal stem cell
NIS	sodium iodide symporter
pDNA	plasmid DNA
PEG	polyethylenglycol
PET	positron emission tomography
s.c.	subcutaneous
sg	salivary glands
SPECT	single-photon emission tomography
TFB	tetrafluoroborate
TfR	transferrin receptor
TGF	transforming growth factor
TSH	thyroid stimulating hormone

2.8 Competing interests

The authors have declared no conflict of interest.

2.9 Availability of data and material

The datasets used and/or analyzed during the current study are available from the corresponding author on reasonable request.

2.10 Authors' contribution

Conception: C.K., R.S., E.W., P.J.N, C.S.

Design: C.K., R.S., V.M., C.S.

Acquisition and analysis: C.K., R.S., N.S., V.M., F.S., C.S., M.T., S.U.

Interpretation of data: C.K.; C.S., W.A.W., M.E.

Writing manuscript: C.K., R.S.

Writing – review & editing: K.A.S, M.E., E.W., P.J.N., S.Z., P.B., W.A.W., V.M., C.S.

The manuscript was drafted by C.K., R.S. and C.S. and edited by all authors. All authors have carefully read and improved the manuscript. All authors have approved the final manuscript.

2.11 Funding

The research from our laboratory cited in this review was funded by grants from the Deutsche Forschungsgemeinschaft within the Collaborative Research Center SFB 824 to C.S. (project C8), SFB 1032 to E.W. (project B4), as well as within the Priority Program SPP1629 to C.S. and P.J.N. and by a grant from the Wilhelm-Sander-Stiftung to C.S. and P.J.N. (2014.129.1).

2.12 Acknowledgements

We owe special thanks to Sybille Reder, Markus Mittelhäuser, Hannes Rolbieski, Martin Grashei and Sandra Sühnel (Department of Nuclear Medicine, School of Medicine, Klinikum rechts der Isar, Technical University of Munich, Munich, Germany) for their valuable assistance in performing the imaging studies. We are grateful to PD Dr. Katja Steiger, Olga Seelbach and

the CeP-team (Institute of Pathology, School of Medicine, Technical University of Munich, Munich, Germany) for preparation of paraffin embedded slides and the H&E staining. We appreciate the help from Prof. Dr. Gabriele Multhoff and Dr. Stefan Stangl (Center for Translational Cancer Research, Klinikum rechts der Isar, Technical University of Munich, Munich, Germany) for establishing the orthotopic glioblastoma mouse model. Furthermore, we thank Prof. Dr. Julia Mayerle, Dr. Ivonne Regel and Dr. Ujjwal Mahajan for allowing us to use their lab equipment. The original data included in this review were performed as partial fulfillment of the doctoral thesis of C.K. and R.S. at the Faculty for Chemistry and Pharmacy of the LMU Munich.

3 Chapter 2: Image-guided, MSC-mediated NIS Gene Therapy of GBM

This chapter is a pre-copy-edited version of a peer-reviewed article published in *Clinical Cancer Research*. 2023 Mar 1;29(5):930-942 and assigned the DOI doi: 10.1158/1078-0432.CCR-22-1433.

Mesenchymal Stem Cell-mediated Image-guided Sodium Iodide Symporter (NIS) Gene Therapy Improves Survival of Glioblastoma-bearing Mice

Kitzberger C [1], Spellerberg R [1], Han Y [1], Schmohl KA [1], Stauss C [1], Zach C [2], Kälin RE [3,4], Multhoff G [5,6], Eiber M [7], Schilling F [7], Glass R [3,4,8], Weber WA [7], Wagner E [9], Nelson PJ [1], Spitzweg C [1,10].

[1]Department of Internal Medicine IV, University Hospital, LMU Munich, Munich, Germany

[2]Department of Nuclear Medicine, University Hospital, LMU Munich, Munich, Germany

[3]Neurosurgical Research, Department of Neurosurgery, University Hospital, LMU Munich, Munich, Germany

[4]Walter Brendel Center of Experimental Medicine, Faculty of Medicine, LMU Munich, Munich, Germany

[5]Center for Translational Cancer Research (TranslaTUM), School of Medicine, Klinikum rechts der Isar, Technical University of Munich, Radiation Immuno-Oncology group, Munich, Germany

[6]Department of Radiation Oncology, School of Medicine, Klinikum rechts der Isar, Technical University of Munich, Munich Germany

[7]Department of Nuclear Medicine, School of Medicine, Klinikum rechts der Isar, Technical University of Munich, Munich, Germany

[8]German Cancer Consortium (DKTK), partner site Munich, Munich and German Cancer Research Center (DKFZ), Heidelberg, Germany

[9]Pharmaceutical Biotechnology, Department of Pharmacy, Centre for System-Based Drug Research and Centre for Nanoscience, LMU Munich, Germany

[10]Division Endocrinology, Diabetes, Metabolism and Nutrition, Mayo Clinic, Rochester, MN, USA

Running Title: Image-guided, MSC-mediated *NIS* Gene Therapy of GBM

Keywords: Glioblastoma; gene therapy; mesenchymal stem cells; NIS; PET imaging

3.1 Translational Relevance

Glioblastoma (GBM) is the most common malignant type of primary brain tumor with poor prognosis and very limited therapy options. Main challenges in the treatment of GBM include limitations of drug delivery due to the blood-brain-barrier, intra- and intertumoral heterogeneity and infiltration into the normal brain parenchyma. Mesenchymal stem cells (MSCs) have gained attention as a new treatment platform for the delivery of anti-cancer cargo, such as therapeutic genes, based on their intrinsic tumor homing capacity targeting the tumor microenvironment of many solid tumors including GBM. Gene therapy based on the biology of the theranostic sodium iodide symporter (NIS) allows radioiodide application for effective tumor imaging and treatment. A MSC-mediated NIS-based radioiodide therapy approach was performed in a preclinical GBM mouse model demonstrating effective MSC recruitment along with functional NIS expression. A reduced tumor growth and significantly prolonged survival was shown after systemic administration of engineered MSCs and radioiodide application.

3.2 Abstract

Mesenchymal stem cells (MSCs) have emerged as cellular-based vehicles for the delivery of therapeutic genes in cancer therapy based on their inherent tumor homing capability. As theranostic gene, the sodium iodide symporter (*NIS)* represents a successful target for non-invasive radionuclide-based imaging and therapy. In this study, we applied genetically engineered MSCs for tumor-targeted *NIS* gene transfer in experimental glioblastoma (GBM) – a tumor with an extremely poor prognosis.

A syngeneic, immunocompetent GL261 GBM mouse model was established by subcutaneous and orthotopic implantation. Further, a subcutaneous xenograft U87 model was used. Bone marrow-derived MSCs were stably transfected with a NIS-expressing plasmid driven by the

constitutively active CMV-promoter (NIS-MSCs). After multiple or single intravenous injection of NIS-MSCs, tumoral iodide uptake was monitored *in vivo* using ^{123}I-scintigraphy or ^{124}I-PET. Following validation of functional NIS expression, a therapy trial with ^{131}I was performed based on the most optimal application regime as seen by ^{124}I-PET imaging in the orthotopic approach.

A robust tumoral NIS-specific radionuclide accumulation was observed after NIS-MSC and radioiodide application by NIS-mediated *in vivo* imaging. NIS immunofluorescence staining of GBM and non-target tissues showed tumor-selective MSC homing along with NIS expression. Application of therapeutically effective ^{131}I led to significantly delayed tumor growth and prolonged median survival after NIS-MSC treatment as compared to controls.

A strong tumor-selective recruitment of systemically applied MSCs into GBM was found using *NIS* as reporter gene followed by successful therapeutic application of radioiodide demonstrating the potential use of *NIS*-based MSCs as therapy vehicles as a new GBM therapy approach.

3.3 Introduction

Glioblastoma (GBM, grade IV) is the most common and malignant type of primary brain tumor in adults with an extremely poor prognosis (14). The current standard of care includes surgical resection followed by radiochemotherapy with temozolomide and by further adjuvant temozolomide (134). Despite recent advances in characterizing new targets for novel therapies, long-term survival is rare due to a very high recurrence rate (135). The development of more efficacious therapeutic strategies is urgently needed to improve the outcome of GBM patients.

The major problems that are encountered during the treatment of GBM include the strong therapy resistance of these highly heterogeneous tumors that are notorious for their infiltrative growth pattern (17). An additional important issue is the limitation of most systemically delivered drugs in overcoming the blood-brain-barrier (BBB), a structural and functional barrier that separates the peripheral blood from the brain (136). This barrier is partly maintained in GBM (137). Finally, the brain tumor microenvironment is characterized by extensive intra- and intertumoral heterogeneity at the cellular and molecular level rendering the process of designing effective targeted, individualized therapies even more complex (138,139).

A promising treatment approach for GBM is the use of cell-based therapies that can in theory target multiple independent parameters in tumor microenvironments (140). Different types of adult stem cells including neural stem cells (NSCs) and mesenchymal stem cells (MSCs) have been previously shown to have an inherent ability to specifically migrate into malignant gliomas

by overcoming the BBB and have shown the ability to even target single infiltrating tumor cells (93,98,141-144).

In their pioneering work, Aboody and colleagues demonstrated that murine NSCs were able to migrate to brain tumors using different routes of implantation: NSC implantation directly into the tumor bed, implantation at an intracranial site distant from the tumor bed in the same or contralateral hemisphere or intravenous (i.v.) implantation led to selective targeting of the brain tumor mass (143). Since the use of NSCs is challenging for clinical application due to the need for high numbers of NSCs needed to meet sufficient dose requirements for human trials, MSCs may represent a more promising alternative source (145). However, to date relatively few early phase I/II clinical trials (e.g. NCT03896568; NCT04758533) have been conducted using MSCs as delivery vehicles for the treatment of GBM.

MSCs are multipotent progenitor cells with self-renewing capabilities and a high differentiation potential (72). They are well suited for clinical purposes, because they can be easily obtained from different tissue sources (e.g. adipose tissue, umbilical cord, bone-marrow), rapidly propagated and relatively easily genetically modified *in vitro*. In addition, their low immunogenicity allows allogenic cells to be used (144).

The mechanisms underlying the recruitment of MSCs to tumor sites is still not well understood, but is thought to be driven by the inflammatory micromilieu of the tumor. In this regard, malignant tumors are often described as a chronic injury or “never healing wound” (79). In the course of injury or during chronic inflammation, MSCs are actively recruited to these sites to contribute to tissue remodeling (146).

Current treatment limitations for GBM are often associated with the BBB. MSCs possess leukocyte-like abilities allowing them to transmigrate across the BBB. In addition, the decreased vessel tightness observed in the tumor neo-vasculature may support diffusion into the tumor parenchyma and lead to passive MSC entrapment in the brain (147).

The therapeutic use of MSCs in cancer is based on their intrinsic tumor-homing capacity that can be exploited for delivery of an anti-tumor cargo. A number of basic and preclinical studies have used MSCs as cell-based vectors to deliver anti-tumor proteins, anti-tumor microRNAs (miRNAs), suicide genes, immunostimulants and oncolytic viruses (82-87). Recently, research on MSCs has focused more on their use in tumor-targeted gene therapy (148).

Over the past two decades, the sodium iodide symporter (*NIS*) has emerged as a powerful theranostic gene for the management and treatment of cancer. NIS is a naturally occurring transmembrane glycoprotein usually localized at the basolateral membrane of thyrocytes. It is responsible for the active transport of iodide from the blood into the thyroid as an important

prerequisite for thyroid hormone synthesis (44). The dual function of *NIS*, as reporter and therapy gene, has been widely used in the treatment of differentiated thyroid cancer for 80 years allowing the application of radioiodide as a diagnostic and therapeutic agent (103). Various isotopes can be efficiently transported by NIS that are used for diagnostic purposes (e.g. ^{123}I, ^{124}I, ^{125}I, ^{99m}Tc, ^{18}F-tetrafluoroborate) using scintigraphy, SPECT (single-photon emission computed tomography) or PET (positron emission tomography) imaging. In addition, the system is ideal for the therapeutic application of radionuclides (^{131}I, ^{188}Re, ^{211}At). Therapeutic efficacy is enhanced through a bystander effect based on the crossfire effects of the β-emitters ^{131}I and ^{188}Re or the α-emitter ^{211}At that act on NIS-transduced cells as well as neighboring cells (49). Several studies including work by our group have shown the great potential of *NIS* gene-based therapy using MSCs as delivery vectors for the treatment of distinct non-thyroidal tumors (63,66,67,75,89,98). In addition to successful MSC delivery to GBM, there are also reports from several preclinical and clinical studies describing the delivery of iodide or alternative isotopes transported by NIS to the brain (52,54,61,98,149,150).

In the present study we sought to expand the *NIS* gene therapy strategy to GBM using a genetically modified murine MSC line, syngeneic to both tumor and host tissue, constitutively expressing *NIS* driven by a CMV (cytomegalovirus) -promoter, using both a subcutaneous and an orthotopic GBM mouse model. The orthotopic GL261 model used in this study has been extensively applied in a series of other experimental studies and shown to recapitulate important histopathological features of human GBM such as invasive growth and pro-angiogenic characteristics, and mimics closely the tumor microenvironment as the host immune system is intact (151). In addition, proof-of-concept was further evaluated in a second subcutaneous U87 xenograft model. We investigated the potential use of *NIS* as reporter gene to track adoptively applied MSCs in GBM *in vivo* and *ex vivo* after systemic delivery followed by therapeutic application using ^{131}I. To this end, *in vivo* biodistribution of NIS-MSCs was monitored by highly sensitive ^{124}I-PET imaging or ^{123}I-scintigraphy. Finally, ^{131}I application in NIS-MSC treated GBM mice lead to a significant increase in survival and reduced tumor growth monitored by magnetic resonance imaging (MRI).

3.4 Material and Methods

Cell culture

The murine glioma cell line GL261 was purchased from the National Cancer Institute (NCI, Frederick, MD, USA) and the human glioma cell line U87 (CLS 300367) was purchased from

Cell Line GmbH (Eppelheim, Germany). Both cell lines were cultured in DMEM low glucose (Sigma-Aldrich, St. Louis, Missouri, USA) supplemented with 10% (v/v) fetal bovine serum (FBS Superior, Sigma-Aldrich), 1% (v/v) MEM non-essential amino acid solution (Thermo Fisher Scientific, Waltham, MA, USA) and 1% (v/v) penicillin/streptomycin (Sigma-Aldrich).

Murine and human MSCs were isolated from the bone marrow (in the following referred to as wildtype MSCs (Wt-MSCs)) and are characterized as previously described (63,66,76). NIS-expressing MSCs (NIS-MSCs) were produced by stable transfection of Wt-MSCs with the expression vector CMV-NIS-pcDNA3, containing the constitutively active CMV-promoter coupled to full-length *NIS* cDNA. NIS functionality, assessed by iodide uptake ability, and tumor-tropic migratory capacity of these NIS-MSCs has been shown by our group previously (63,66). MSCs were cultured in RPMI (Sigma-Aldrich) containing 10% (v/v) FBS and 1% (v/v) penicillin/streptomycin and selection of murine NIS-MSCs was maintained with 100 µg/ml G418 (Sigma-Aldrich) and 500 µg/ml G418 for human MSCs. Preparation of MSCs for injection into mice was performed as described (152).

All cells were maintained in an incubator at 37 °C in a humidified atmosphere of 95% and 5% CO_2. The cell lines were examined for mycoplasma and viruses according to the FELASA (Federation of European Laboratory Animal Science Associations) guidelines by Charles River Research Animal Diagnostic Services (CR RADS, Wilmington, MA, USA; Mouse essential panel) prior to *in vivo* transplantation.

Animals

Female C57Bl/6 mice were purchased from Charles River (Sulzfeld, Germany) and used for subcutaneous (s.c.) (6-week-old) or orthotopic (8-week-old) GL261 cell implantation. For s.c. U87 cell injection (6-week-old) female CD-1 nu/nu mice were purchased from Charles River. Mice were kept under specific pathogen-free conditions with access to chow and water *ad libitum.* Tumor harboring mice were treated with drinking water supplemented with 5 mg/ml levothyroxine (L-T4, Sigma-Aldrich) in 0.01% (v/v) bovine serum albumin (BSA, Sigma Aldrich) to suppress intrinsic thyroidal tracer uptake, in addition to iodide-deficient diet (ssniff Spezialdiäten GmbH, Soest, Germany) 10 days prior to the imaging experiments and during ^{131}I therapy experiments.

All animal experiments were approved by the local governmental commission for animals (Government of Upper Bavaria/Regierung von Oberbayern) and were conducted in accordance with institutional guidelines of animal welfare of the Klinikum rechts der Isar, Technical University of Munich. Mice were sacrificed at defined presymptomatic time points or

at defined humane endpoints (significant weight loss; neurological symptoms; changes in drinking, eating or cleaning behavior; signs of pain).

Establishment of subcutaneous and orthotopic syngeneic GBM mouse models

Subcutaneous (s.c.) syngeneic GL261 and xenograft U87 tumors were generated by s.c. injection of $1x10^6$ cells into the right flank. Tumors were regularly measured using a caliper and the tumor volumes were estimated using the equation volume=length x width x height x 0.52.

For orthotopic brain tumor implantation, mice were anesthetized with ketamine and xylazine and immobilized in a stereotactic frame (David Kopf Instruments, Tujunga, CA, Canada) in a flat-skull position. A middle line skin incision was made on the top of the skull and a hole was carefully drilled into the skull with a 21G needle 1 mm anterior and 1.5 mm to the right of the *bregma*. A blunt Hamilton syringe (22G, Hamilton, Reno, Nevada, USA) was stereotactically inserted 4 mm deep and retracted 1 mm. GL261 cells were implanted ($1x10^5$ cells/µL PBS) into the brain in a total volume of 1 µL within 2 min. The syringe was removed slowly in 1 mm/minute steps and the skin was sutured. Mice were pre- and postoperatively treated with Meloxicam (0.5 mg/kg; Boehringer Ingelheim Vetmedica GmbH, Ingelheim/Rhein, Germany).

Radioiodide biodistribution studies *in vivo* in subcutaneous GBM tumors using ^{123}I-scintigraphy

Once s.c. GL261 and U87 tumors had reached a volume of approximately 500 mm³, mice received three applications of MSCs in 2-day intervals, followed by intraperitoneal (i.p.) injection of 18.5 MBq (0.5 mCi) ^{123}I (GE Healthcare, Braunschweig, Germany) 72 h later. Serial scanning 1 h to 8 h after tracer application was performed on a gamma camera using a low energy high resolution collimator (ecam, Siemens, Munich, Germany). As a control for NIS-specific radioiodide accumulation in the tumor, perchlorate ($NaClO_4$; 2 mg per mouse), a competitive inhibitor for NIS-mediated iodide transport, was injected i.p. 30 min before ^{123}I administration. Regions of interest (ROI) were drawn with HERMES Gold software (HERMES Medical solutions, Stockholm, Sweden) and tumoral iodide uptake was determined and calculated as percentage of the injected radionuclide dose per gram tumor (% ID/g). Tumor weight was assessed after removal of the tumors at the end of the imaging study. Dosimetry for ^{131}I was calculated with a RADAR dose factor (www.doseinfo-radar.com) using the Medical Internal Radiation DOSE (MIRD) concept.

Radioiodide biodistribution studies *in vivo* in orthotopic GBM tumors using ^{124}I-PET/CT imaging

Three-dimensional serial PET imaging was performed in syngeneic orthotopic GL261 tumor bearing mice. NIS- or Wt-MSCs were systemically applied via the tail vein: three MSC applications were given in 2-day intervals 1.5–2 weeks after intracranial (i.c.) tumor cell inoculation, followed by ^{124}I-PET imaging 72 h after the last MSC administration. In addition, shortened application regimes using a single MSC application 2–2.5 weeks after i.c. tumor cell implantation, followed by radioiodide PET 48 h or 72 h later, were applied. Mice received 10 MBq of ^{124}I (Perkin Elmer, Waltham, Massachusetts, USA or DSD Pharma GmbH, Vienna, Austria) intravenously and serial acquisition was performed 1 h, 3 h and 5 h after ^{124}I application using a preclinical small-animal Inveon P120 PET/CT scanner (Siemens). PET images were reconstructed with Inveon Acquisition Workplace (Siemens) and volumes of interest (VOIs) of the whole tumor were drawn using Inveon Research Workplace software (Siemens) and stated as fraction of the whole injected ^{124}I dose per tumor volume (% ID/ml). Tumor volumes determined *ex vivo* (see below) were used. Dosimetry for ^{131}I was calculated with a RADAR dose factor (www.doseinfo-radar.com) using the Medical Internal Radiation DOSE (MIRD) concept.

Mouse brain tissue preparation

After sacrifice, mice were transcardially perfused using PBS (Sigma-Aldrich) followed by 4% formaldehyde solution (Pharmacy, University Hospital LMU Munich, Munich, Germany). Brains were dissected, incubated in 4% formaldehyde for 24 h at room temperature and then transferred into 30% sucrose solution at 4 °C until the brain sank to the bottom of the tube. After brains were embedded in Tissue-Tek® OCT™ compound (Sakura Finetek, Torrance, CA, USA), whole brains were sliced in 10 µm thick horizontal sections using a cryotome. Sections were stored at -20 °C before further processing.

Ex vivo tumor size determination

For tumor size analysis, Hematoxylin and Eosin (H&E) staining was performed on horizontal sections of the brain with defined stereotactic coordinates (at 0.72 to 5.52 mm from the dural surface) according to the mouse brain atlas (153). Stained H&E slides were scanned and the tumor area within each brain section determined using Aperio ImageScope software (Leica biosystems, Wetzlar, Germany). The tumor volume quantification was done as previously described by Zhao *et al.* (154).

Immunofluorescence analysis of NIS and CD31

Frozen sections of brain tumors and sections of control organs (liver, lung, kidney, spleen) were subjected to immunofluorescence staining using rabbit anti-NIS (EUD4101, Origene, Rockville, MD, USA; 1:1000) and rat anti-CD31 (blood vessel density; BD Pharmingen, Heidelberg, Germany; 1:100) primary antibodies. A secondary anti-rabbit Alexa488-conjugated antibody (Jackson ImmunoResearch, West Groove, Pennsylvania, USA) for NIS staining, Cy3-conjugated anti-rat (Jackson ImmunoResearch) for CD31 staining and Hoechst bisbenzimide (5 µg/ml) to counterstain nuclei were used. Finally, sections were mounted with fluorescence mounting medium (Dako, Hamburg, Germany).

All slides were digitalized by whole-slide scanning in a Panoramic MIDI II slide scanner and images were taken with the aid of the software CaseViewer (Version 2.4, 3DHISTECH Ltd., Budapest, Hungary). Quantification of NIS-positive cells (percentage of NIS-positive cells in the tumor) was obtained by evaluation of 6 visual fields (20x magnification) per tumor using ImageJ software (NIH, Bethesda, MD).

Ex vivo mRNA analysis by quantitative RT-PCR

Total RNA of frozen brain tumor sections and non-target organs (liver, lung, kidney and spleen) derived from ^{124}I-PET imaging experiments was extracted using Trizol Reagent (Invitrogen Inc., Carlsbad, CA, USA) according to the manufacturer's instructions. Single stranded cDNA was generated using LunaScript RT SuperMix Kit (New England Biolabs, Ipswich, MA, USA). Quantitative real-time PCR (RT-PCR) was conducted on a Lightcycler 96 System (Roche, Basel, Switzerland) using SybrGreen PCR master mix (Qiagen, Hilden, Germany). The following primers were used: human *NIS* forward *5´-TGCGGGACTTTGCAGTACATT-3´* and reverse 5´-TGCAGATAATTCCGGTGGACA-3´, *Neomycin* (selection cassette detecting NIS-MSCs) forward 5′-ATGCCCGACGGCGAGGATCT-3′ and reverse 5′-ATACCGTAAAGCACGAGGAAGCG-3′, and as internal controls human *18S* forward 5′-*CAGCCACCCGAGATTGAGCA*-3′ and reverse 5′-TAGTAGCGACGGGCGGTGTG-3′ and mouse *ACTB* forward 5′-AAGAGCTATGAGCTGCCTGA-3′ and reverse 5′-TACGGATGTCAACGTCACAC-3′. The mRNA expression level of the target genes were normalized to the internal controls and relative expression was calculated using the ΔΔCt method.

Radioiodide therapy studies *in vivo*

A therapy trial of orthotopic GL261 tumors was started 5–6 days after i.c. tumor implantation. Tumor growth was assessed using a preclinical small animal 7T-MRI scanner (Agilent&GE Healthcare MR Discovery 901 with Bruker AVANCE III HD electronics) using a volume resonator together with a dedicated two-channel brain coil (RAPID Biomedical, Rimpar, Germany). Mice were included in the therapy and randomly distributed to all groups as soon as the inclusion criterion was met (tumor volume of 0.6–2.1 mm^3) (day 0). Tumor growth was then monitored twice a week by MR imaging and *in vivo* tumor volume determined as previously described (61).

Based on imaging results, an application regime with one MSC application followed by i.p. injection of 55.5 MBq ^{131}I (GE Healthcare or Rotop Pharmaka GmbH, Dresden, Germany) 48 h later was employed. This therapy cycle was repeated three times, with two days between each cycle. Four treatment cohorts were used: The therapy group received NIS-MSCs + ^{131}I (n=5) and controls received either Wt-MSCs + ^{131}I (n=5), NIS-MSCs + saline (NaCl) (n=6) or NaCl only (n=5).

Indirect immunofluorescence analysis of CD31/Ki67

After ^{131}I therapy, mice were transcardially perfused and brain tissue was processed as described above. Frozen brain tumor sections were subjected to immunofluorescence staining using rabbit anti-Ki67 (proliferation fraction; ab16667, abcam, Cambridge, UK; 1:200) and rat anti-CD31 (blood vessel density; BD Pharmingen; 1:100) antibodies. Secondary anti-rabbit Alexa488-conjugated antibody (Jackson ImmunoResearch) for Ki67 staining, Cy3-conjugated anti-rat (Jackson ImmunoResearch) for CD31 staining and Hoechst bisbenzimide (5 µg/ml) to counterstain nuclei were used. Finally, sections were mounted with fluorescence mounting medium (Dako).

All slides were scanned as described above (see immunofluorescence analysis of NIS and CD31). Quantification of Ki67-positive cells (percentage of proliferating cells in the tumor) and blood vessel density (CD31-positive area in the tumor) was examined by evaluation of 4 visual fields (20x magnification) per tumor using ImageJ software (NIH).

Statistical Analysis

Results are expressed as mean ± SEM, mean-fold change ± SEM or percent. Statistical significance was generally determined by two-tailed Student's t-test.

For the therapy study, one-way ANOVA was performed for tumor volumes followed by post-hoc Tukey's Honestly Significant Difference test. Kaplan-Meier plots were used for survival curves and statistical significance was analyzed by log-rank test. *p*-values <0.05 were considered as significant (**p*<0.05; ***p*<0.01; ****p*<0.001; ns not significant).

Data Availability

The data generated in this study are available within the article.

3.5 Results

In vivo radioiodide biodistribution after MSC-mediated NIS gene transfer

To evaluate the general efficacy of MSC-mediated NIS gene delivery to GBM, functional NIS expression was determined in a syngeneic s.c. GL261 mouse model by ^{123}I-scintigraphy. Murine MSCs were administered i.v. three times in 2-day intervals followed by radioiodide injection 72 h after the last MSC application.

In vivo whole-body ^{123}I-scintigraphy showed high levels of NIS-mediated radionuclide accumulation in s.c. GL261 tumors after systemic injection of NIS-MSCs (Fig. 1A). Tumors accumulated a maximum of 8.0 ± 1.1% ID/g with an average biological half-life of 3.7 ± 0.4 h (Fig. 1B). Dosimetric calculations showed a tumor-absorbed dose of 46.5 ± 5.8 mGy/MBq for ^{131}I. In addition, ^{123}I uptake was also observed in organs that physiologically express NIS like the thyroid, salivary glands and stomach as well as the urinary bladder due to mainly renal tracer excretion. To confirm NIS-specificity of tumoral iodide uptake, the competitive NIS inhibitor perchlorate was injected to a subset of mice treated with NIS-MSCs (Fig. 1C). Perchlorate treatment resulted in a reduction of NIS-mediated tumoral radioiodide accumulation in addition to a reduction in physiological uptake by thyroid, salivary glands and stomach. Administration of Wt-MSCs as an additional control resulted in no tumoral radioiodide accumulation above background level (Fig. 1D). A second model, the s.c. U87 model, was used to demonstrate proof-of-concept in an immunocompromised background. ^{123}I-scintigraphy showed a tumoral iodide accumulation of U87 tumors after three NIS-MSC

applications of 5.1 ± 0.6 % ID/g (Fig. 1E, F). Injection of perchlorate (Fig. 1G) and Wt-MSCs (Fig. 1H) served as controls to demonstrate NIS-specificity and showed similar results as compared to the GL261 model.

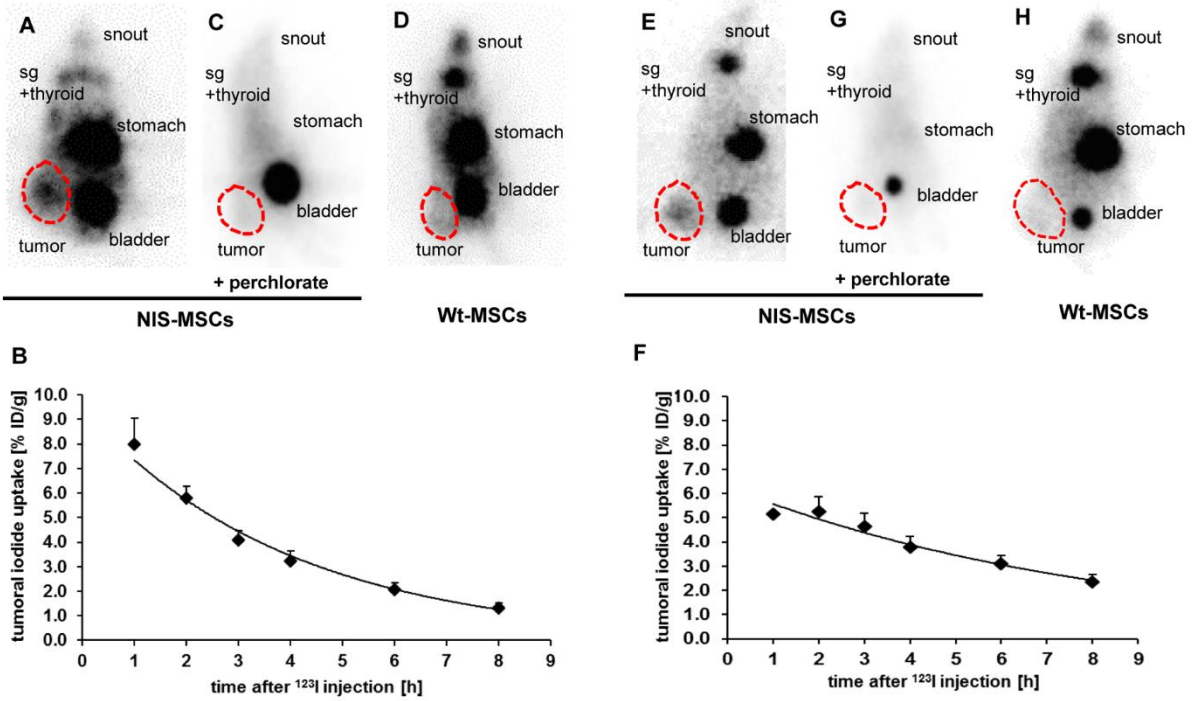

Figure 5: ^{123}I-scintigraphy revealed high tumoral radioiodide uptake after systemic NIS-MSC application in subcutaneous (s.c.) GL261 and U87 tumors. Three systemic injections of NIS-MSCs in mice harboring s.c. GL261 tumors (**A**) resulted in a maximum of 8.0 ± 1.1% of the injected dose per gram tumor (ID/g) (n=8, **B**). Iodide uptake of tumors and endogenous NIS-expressing organs was blocked upon treatment with the competitive NIS inhibitor perchlorate (n=3, **C**). Treatment with Wt-MSCs showed no tumor-specific radioiodide uptake (n=4, **D**). Tumoral iodide uptake of s.c. U87 (**E**) revealed a maximum of 5.1 ± 0.6 % ID/g (n=8, **F**) after three systemic NIS-MSC injections, which was reduced to background level using perchlorate (n=2, **G**). Injection of Wt-MSCs resulted in no tumoral ^{123}I accumulation (n=3, **H**). Physiological ^{123}I accumulation was seen in thyroid, salivary glands (sg), stomach and in the bladder due to renal excretion (**A, C, D, E, G, H**). For each group, one representative picture at 2 h after tracer application is shown. The tumor is encircled in red. Data are represented as mean values ± SEM.

This proof-of-concept study was then expanded to a clinically more relevant orthotopic GL261 model. Once mice had developed brain tumors, the same application regimen as used in the s.c. model was applied for NIS-imaging – with three cycles of MSC administration at 2-day intervals, followed by a single radionuclide injection (Fig. 2A). Functional NIS expression and, thus, MSC homing to brain tumors was monitored using three-dimensional, high resolution

small-animal ^{124}I-PET imaging (10 MBq ^{124}I, i.v.) allowing a better discrimination of exogenous and endogenous NIS-mediated signals in the head region. As determined by serial scanning, tumoral iodide uptake amounted to a maximum of 2.6 ± 0.2% ID/ml after NIS-MSC injection with an average biological half-life of 7.6 ± 2.5 h (Fig. 2G). A tumor-absorbed dose of 31.1 ± 12.2 mGy/MBq for ^{131}I was calculated. Injection of Wt-MSCs in a subset of mice resulted in an ^{124}I uptake comparable to background level showing that the tumoral iodide uptake was NIS-MSC-mediated (Fig. 2D). Analogous to ^{123}I-scintigraphy, endogenous NIS-expression by the thyroid, salivary glands and stomach as well as iodide elimination via the urinary bladder were also observed using ^{124}I-PET imaging. The thyroid gland accumulated approximately 6.3-10.9 % ID/ml of ^{124}I (Supplementary Fig. 1).

In addition, a time sparing treatment schedule that was more applicable in this rapidly growing tumor model was assessed for tumoral radioiodide uptake using PET imaging after application of a single MSC injection. MSCs were applied either 48 h or 72 h before ^{124}I injection for imaging. *In vivo* ^{124}I-PET imaging revealed high levels of NIS-mediated radionuclide accumulation in brain tumors both at 48 h or 72 h after a single NIS-MSC application (Fig. 2B, C), whereas no radionuclide accumulation above background level was detected in the tumors of mice that had received Wt-MSCs (Fig. 2E, F). When PET imaging was performed at 48 h after NIS-MSC injection, tumors of mice accumulated 3.5 ± 1.0% ID/ml of ^{124}I with an average biological half-life of 13.3 ± 2.7 h (Fig. 2G). Based on the imaging data, a tumor-absorbed dose of 60.3 ± 18.8 mGy/MBq for ^{131}I was determined. When PET imaging was conducted 72 h after a single MSC application, a tumoral ^{124}I uptake of 2.5 ± 0.2% ID/ml with an average biological half-life of 8.2 ± 2.9 h was reached. A tumor-absorbed dose of 32.7 ± 11.4 mGy/MBq for ^{131}I was calculated.

The tumoral radioiodide quantification showed no significant differences between the different application schedules of NIS-MSC treated mice. This finding implies that a single MSC application lead to sufficient radioiodide uptake of brain tumors.

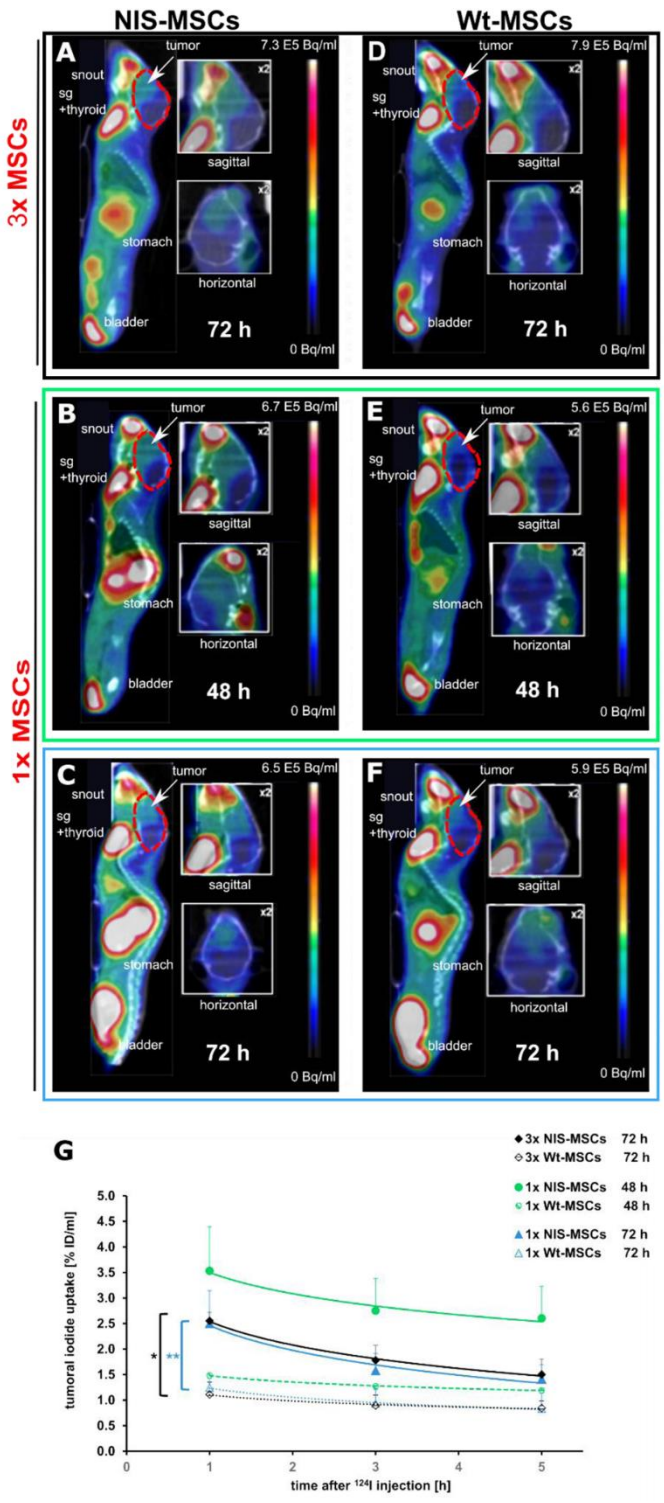

Figure 6: Enhanced tumoral radioiodide accumulation after systemic NIS-MSC injection in syngeneic orthotopic GBM tumors. (**A–F**) Exemplary whole-body ^{124}I-PET/CT scans (sagittal planes) and 2x magnification of the brain (sagittal and horizontal planes; tumor is located on the right) 3 h post ^{124}I injection are displayed. The brain areas are highlighted by red dotted lines and tumors are indicated by white arrows.^{124}I-PET imaging revealed high tumoral radioiodide uptake after three (**A,** n=6) or one (**B,** n=4**; C,** n=3) NIS-MSC applications. Treatment with Wt-MSCs did not result in tumoral radioiodide accumulation above background level (**D,** n=3**; E,** n=2**; F,** n=3). (**G**) Quantification of serial ^{124}I-PET imaging of tumoral radioiodide accumulation over 5 h used for determination of radionuclide retention time. Results are expressed as mean values ± SEM. Two-tailed Student's t-test was performed for statistical analysis of NIS-MSCs vs. Wt-MSCs of the same application schedule and was analyzed at each given time point after radionuclide injection (*p<0.05; **p<0.01); sg=salivary glands.

Ex vivo analysis of NIS expression

Hematoxylin and Eosin staining of horizontal brain sections was used to visualize the mass of GL261 tumors at the area of implantation in the right caudate putamen (Fig. 3 A). *Ex vivo* analysis of NIS protein expression showed high NIS-specific immunoreactivity throughout the tumor stroma of GL261 tumors (Fig. 3B–D) after one or three systemic NIS-MSC injections. This demonstrated efficient MSC homing to orthotopic GBM tumors and functional *NIS* transgene expression by the engineered MSCs. NIS-specific immunoreactivity was observed at the plasma membrane and in the cytoplasm of engineered MSCs, which were most abundant in perivascular regions. Normal brain tissue, non-treated tumors and brain tumors of mice that received Wt-MSCs showed no NIS protein expression above background level (Fig. 3 B, E, N). Non-target organs (liver, kidney, spleen served as controls) showed no detectable NIS protein expression (Fig. 3F–K). Only a few spots were found to be affected with a small number of MSCs in the lungs after systemic application as shown by NIS-specific immunostaining (Fig. 3L, M, N). The presence of MSCs in the lung may result from the pulmonary first-pass effect as adoptively employed MSCs move through the circulation before they reach the tumor site (63,76). Quantification of NIS immunostaining (Fig. 3N) showed results consistent with *NIS* mRNA analysis data (Fig. 3O).

To assess relative *NIS* mRNA expression after systemic MSC application, mRNA was extracted from brain tumors and controls. Significant levels of *NIS* mRNA were detected in tumors of mice after one NIS-MSC application as compared to tumors from mice treated with Wt-MSCs or untreated tumors and interestingly levels were higher as compared to mice receiving three rounds of MSCs (Fig. 3O). In addition, *Neomycin* resistance control mRNA expression (expressed for vector selection) showed the same effect in brain tumors after MSC treatment (Fig. 3P). Control organs did not show any detectable levels of *NIS* or *Neomycin* resistance mRNA expression (Supplementary Fig. 2) coherent with the NIS immunofluorescence staining.

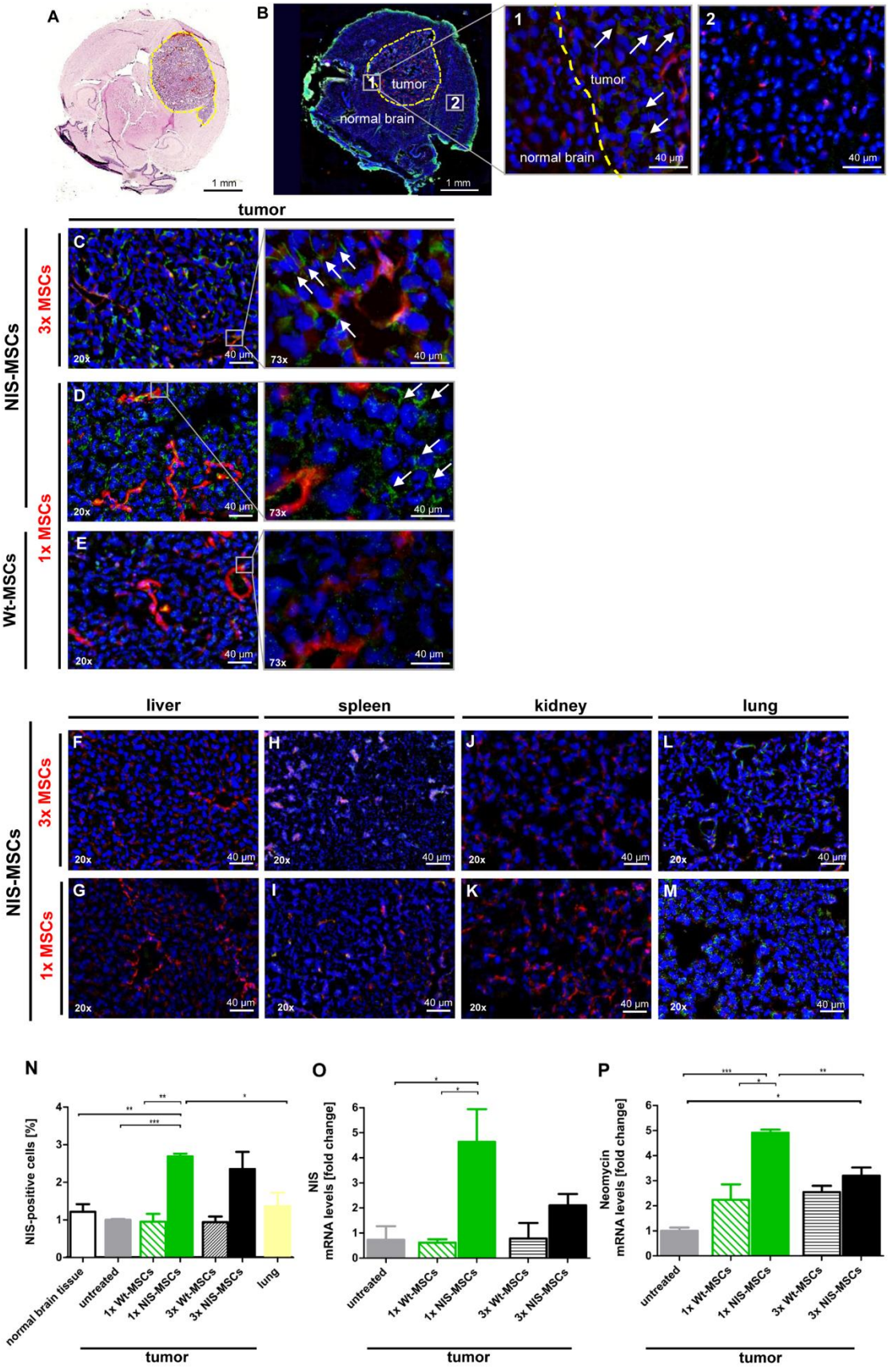
A
B
1
2
tumor
normal brain
1 mm
40 µm
tumor
NIS-MSCs
Wt-MSCs
3x MSCs
1x MSCs
C
D
E
20x
73x
liver
spleen
kidney
lung
F
G
H
I
J
K
L
M
N
O
P
NIS-positive cells [%]
NIS mRNA levels [fold change]
Neomycin mRNA levels [fold change]
normal brain tissue
untreated
1x Wt-MSCs
1x NIS-MSCs
3x Wt-MSCs
3x NIS-MSCs
lung

Figure 7: *Ex vivo* analysis of GL261 brain tumors and control organs after systemic MSC application. (**A**) Representative H&E images of horizontal sections of the brain for visualization of the tumor mass. The area of implantation in the right caudate putamen is shown and the tumor is circled in yellow. (**B–E**) NIS-specific immunofluorescence staining (green) and CD31 (red; labeling blood vessels) was performed on cryosections of brains. Nuclei are counterstained with Hoechst (blue). (**C, D**) NIS protein expression is demonstrated in tumors of NIS-MSC-treated mice by high NIS-immunoreactivity throughout the tumor stroma, which was most prominent near blood vessels and found on the cellular membrane and in the cytoplasm (white arrows). No NIS protein expression was detected in tumors after Wt-MSC injection (**E**) and in non-target organs after NIS-MSC application (**F–K**; liver, spleen, kidney). A small number of NIS-expressing MSCs was detected in the lung of mice that received three (**L**) or one (**M**) NIS-MSC application/s. One representative image is shown each; scale bar=40 µm. **(N)** Quantification of NIS-positive cells was determined of tumors and the lungs after NIS-MSC injection and tumors of mice after Wt-MSCs injection as well as of normal brain tissue as compared to untreated brain tumors showing only low background level (which was arbitrarily set to one). NIS (**O**) and Neomycin (**P**; selection marker of NIS-MSCs) mRNA expression was detected by qPCR in GL261 tumors after NIS-MSC application, while only a low background level of NIS and Neomycin mRNA expression was found in tumors of mice that had received Wt-MSCs or compared to untreated tumors (which was arbitrarily set to one; *NIS* mRNA levels of untreated ΔΔCt = 0.0003 and *Neomycin* mRNA levels of untreated ΔΔCt = 0.002). In addition, no NIS or Neomycin mRNA expression was detectable in non-target organs such as the liver, spleen, kidney and lung (see Supplementary Fig. S2). Data are represented as mean-fold change ± SEM (*p<0.05; **p<0.01; ***p<0.001).

NIS-mediated ^{131}I therapy study of GBM

The therapeutic efficacy of MSC-based NIS-mediated ^{131}I therapy was then evaluated in the syngeneic orthotopic GL261 model. Based on the NIS imaging data (Fig. 2 A–G) the therapy study was performed with three cycles of a single MSC application followed by ^{131}I administration 48 h later with a 2-day break after each cycle. This relatively short treatment regime was chosen due to the aggressive nature of tumor growth in this model. For standardized inclusion (initial tumor volume of 0.6–2.1 mm³) of the mice and tumor growth monitoring, screenings on a small animal 7T-MRI scanner were performed twice a week. A significant delay in tumor growth and reduction of the tumor burden was observed in the mice of the therapy group (NIS-MSCs + ^{131}I; Fig. 4A, E) as compared with control groups (Wt-MSCs + ^{131}I; Fig. 4B, E; NIS-MSCs + NaCl; Fig. 4C, E and NaCl + NaCl; Fig. 4D, E) determined by

MRI 10 days after therapy start. Most mice from all three controls reached humane endpoint (significant weight loss; neurological symptoms; changes in drinking, eating or cleaning behavior or signs of pain) before all treatment cycles were completed (day 11 after therapy start) (Fig. 4F). Therapy mice demonstrated significantly prolonged survival. After day 13 (therapy start), 60% of mice in the therapeutic schedule were still alive, while all control mice had already reached the pre-defined endpoint. Median survival (MS) of the therapy group was 15 days as compared to 10.5 days of NIS-MSCs + NaCl-treated and 10 days of Wt-MSCs + ^{131}I-treated mice, while the NaCl + NaCl group showed the shortest survival (MS=9 days).

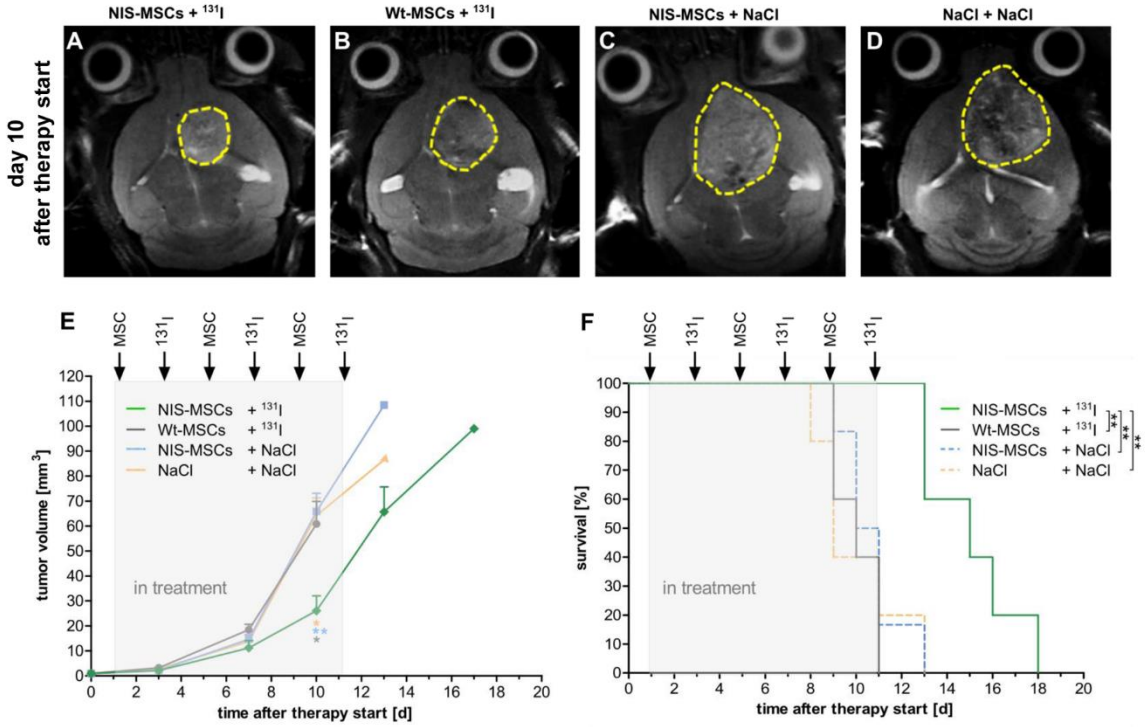

Figure 8: ^{131}I therapy study after MSC-mediated *NIS* gene transfer *in vivo*. Mice harboring orthotopic GL261 tumors were treated with three cycles of a single MSC i.v. injection followed by a single ^{131}I i.p. injection 48 h later (days 1/3, 5/7, 9/11, respectively). Tumor growth was monitored twice per week by MRI. Representative MR images of tumors 10 days after therapy start from a NIS-MSCs + ^{131}I- (**A**), a Wt-MSCs + ^{131}I- (**B**), a NIS-MSC + NaCl- (**C**) and a NaCl + NaCl-treated (**D**) mouse are shown. Tumors are circled by yellow dotted lines. (**E**) Mice treated with NIS-MSCs + ^{131}I (n=5) showed a delay in tumor growth as compared with control groups Wt-MSCs + ^{131}I (n=5; *p<0.05), NIS-MSC + NaCl (n=6; **p<0.01) and NaCl + NaCl (n=5; *p<0.05). (**F**) Treatment with NIS-MSCs + ^{131}I led to a significantly prolonged survival (**p<0.01) as compared to all control groups. Data are represented as mean ± SEM (*p<0.05; **p<0.01).

At the end of the therapy, brains were dissected and *ex vivo* immunofluorescence analysis was performed on cryopreserved tissue of tumors with similar size (Fig. 5). The intratumoral cell proliferation index (Ki67; Fig. 5A, E) of the therapeutically treated cohort was significantly lower as compared to controls (Fig. 5B–D, E). Interestingly, mice treated with saline only showed a significantly higher proliferation potential in comparison with mice treated with MSCs plus saline. Blood vessel density (CD31; Fig. 5A–D, F) analysis demonstrated a trend of reduced tumor vascularization, even though not statistically significant, in the therapeutically treated animals as compared to all controls.

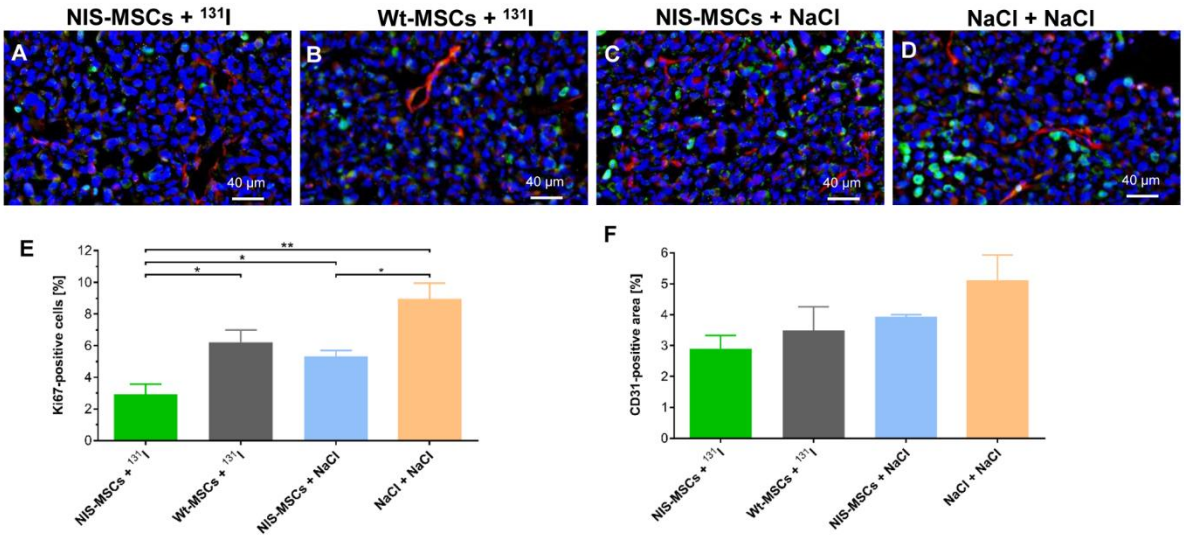

Figure 9: Ex vivo analysis of GBM brain tumors after MSC-mediated NIS gene therapy. Ki67 (proliferation index; green) and CD31 (blood vessels; red) immunofluorescence staining was performed on frozen brain tissue sections derived from mice that had received NIS-MSCs +^{131}I (**A**), Wt-MSCs + ^{131}I (**B**), NIS-MSCs + NaCl (**C**) and saline only (**D**) at the end of the therapy study. Nuclei were counterstained with Hoechst (blue). An exemplary image is shown each at 40x magnification (scale bar=40 µm). Quantification of the proliferation index (**E**) shows a significantly reduced intratumoral cell proliferation as a result of NIS-MSC + ^{131}I treatment and a non-significant decrease in blood vessel density in comparison to all control groups (**F**). Data are expressed as mean ± SEM (*p<0.05; **p<0.01).

3.6 Discussion

Glioblastoma is the most common type of primary brain tumor and shows an extremely poor prognosis with limited current treatment options. Due to its highly complex and aggressive nature, GBM is characterized by several mechanisms that help the tumor evade effective

treatment underscoring the urgent need for new therapy options (14,17,134,135). MSCs have emerged as promising cellular vectors for the delivery of therapeutic genes into the tumor microenvironment due to their robust and innate tumor homing capacity. Several studies have examined the migratory and homing capacity of MSCs to GBM including their ability to cross the BBB (98,142,144). Different routes of MSC administration have been reported to precisely and selectively target malignant brain tumors, including intracranial (141), intra-arterial (144) and i.v. delivery (155,156). Intravenous injection would be optimal for clinical translation providing broad biodistribution and easy access, while local administration routes harbor increased risk and side effects including tissue injury (157). We and others have shown the feasibility of MSCs as cellular vectors for the delivery of the theranostic *NIS* gene after systemic application in various preclinical tumor models (63,66,75,89,101). Based on this experience we sought to expand the MSC-mediated *NIS* gene therapy concept to GBM in the present study.

Monitoring the biological behavior of MSCs including migration, distribution and fate are important and highly desirable for the design of an effective MSC-mediated treatment strategy. An essential advantage of the *NIS* gene therapy concept is the application of *NIS* as a reporter gene allowing noninvasive *in vivo* imaging of NIS-MSCs e.g. using scintigraphy, SPECT or PET imaging. In a proof-of-concept study, we were able to demonstrate tumor-selective recruitment of NIS-MSCs to s.c. GL261 and s.c. U87 tumors using ^{123}I-scintigraphy. Maximal NIS-specific tumoral iodide uptakes were comparable to data obtained in previous studies using a hepatocellular cancer model which resulted in successful therapeutic application (63). Since therapeutic options for GBM are limited by the BBB and the brain tumor microenvironment, the orthotopic GL261 model, which additionally might mimic more closely the growth and immune response of human GBM, was instrumental to address these challenges. *In vivo* ^{124}I-PET imaging demonstrated (throughout all MSC application schemes) a remarkable level of MSC recruitment to brain tumors, which was quantified by ^{124}I-uptake in *NIS* transgene expressing MSCs. Conversely, Bexell *et al.* found no MSCs in gliomas 2 and 7 days following systemic intravenous MSC injection in a rat glioma model suggesting intratumoral MSC administration as the route of choice. In this context, the authors were able to show more efficient distribution of rat bone marrow-derived MSCs highly specific to tumor tissue after a single intratumoral MSC injection and substantial migration of MSCs to distant tumor microsatellites (141). However, Nakamizo *et al.* reported brain tumor-specific MSC delivery after systemic MSC injection into the carotid artery in an U87 xenograft GBM mouse model (144). In line with our findings, Shi *et al.* performed successful micro-SPECT/CT imaging using ^{125}I as radiotracer to monitor NIS functional activity to follow MSC fate after three rounds of i.v. injected bone marrow-derived GFP-NIS-MSCs in a xenograft U87 glioma model (98).

Differences in the extent of MSCs engrafted into the tumor may stem from the MSC populations used, the sources of MSCs and isolation protocols that may help explain the divergent results reported (81).

In the study reported here, a single i.v. MSC application followed by radioiodide administration 48 h later yielded the most promising results in the diagnostic imaging series. Compared with the administration of radioiodide 72 h after a single, or multiple MSC injections as determined by ^{124}I-PET imaging, the maximum radioiodide uptake was found to be higher, the efflux from the tumor setting more moderate and the average biological half-life within the tumor environment was longer resulting in an increased calculated tumor-absorbed dose for ^{131}I. *Ex vivo* analysis of NIS expression correlated with the *in vivo* data demonstrating a higher amount of NIS-positive cells 48 h after a single MSC application as compared to 72 h after receiving a total of three MSC injections. Consistent with these findings, we had reported a single MSC application to yield high tumoral radioiodide levels in an endogenous pancreatic ductal adenocarcinoma (PDAC) model as reported earlier (66). Evaluation of NIS-engineered MSCs in the PDAC tumors showed a higher number of NIS-positive cells in the group receiving only one MSC injection as compared to three rounds of MSCs using the same time points and same murine NIS-MSCs as the current study. These findings were reflected by a significant delay in tumor growth reported following ^{131}I administration (66).

In addition, the tumoral radioiodide retention time in i.c. tumors was longer as compared to the s.c. model. The situation in glioblastoma is unique in comparison to peripheral or s.c. tumors – underlying mechanisms of accurate tracer influx and clearance of the brain remain partially unknown. An interplay of different parameters such as loss of BBB integrity, aberrant perfusion, diffusion and permeability accompanied with a dysfunctional brain lympathic system, reported in rodent models as well as in patients, may contribute to an increased average biological half-life of radioiodide seen in the orthotopic brain tumors (158-161). In this circumstance, a slow brain “wash-out” is therapeutically advantageous based on potentially longer retention of radioiodide in the brain (162).

Based on our previous experience in the PDAC model, we hypothesized that the tumoral iodide uptake and calculated tumor absorbed dose for ^{131}I should be sufficient to obtain a therapeutic effect in the comparably aggressive GBM tumor model. Indeed, a significantly prolonged survival was observed in the therapy group that received NIS-MSCs + ^{131}I as compared to the three control groups conducting the therapy study with the most optimal application regime based on the imaging data. Tumor growth was significantly delayed in the therapy group most prominently after full completion of two therapy cycles (10 days after therapy start).

In accordance with former studies by our group using experimental hepatocellular carcinoma or colon carcinoma metastasis models, a significant decrease in proliferating cells was observed in tumors of the therapy group as compared with all control groups (63,64,67,75). While safety concerns for the use of MSCs have been assessed in a series of clinical trials, several central issues remain to be addressed (81). Major concerns regarding the safety or caveats for MSCs use in clinical trials include the contradictory results researchers found regarding their pro- or anti-tumorigenic effects. Pavo *et al.* reported tumor dissemination, glial invasiveness and vascular proliferation following injection of MSCs in the caudal vein – none of which were seen in mice that did not receive MSCs (163). In contrast, unmodified MSCs prolonged the survival of 9L glioma-bearing rats after intracranial administration compared to untreated rats in a further study, indicating an antitumor effect of the MSCs used (142). In the current study, no pro-tumorigenic effect was apparent, as no difference in tumor growth or survival of GBM mice was observable in the group that received MSCs + NaCl compared to the NaCl only group. However, the Ki67 proliferation index in brain tumors from MSC-treated mice (+ NaCl) was significantly reduced as compared to mice treated with NaCl only.

In addition to the lack of tumor-promoting effects by MSCs in our study, adoptively applied NIS-expressing MSCs are effectively eliminated after application of therapeutically active radioisotopes. The use of *NIS* transgene also helps address the concern of using MSCs in the context of cancer therapy, i.e. their poor persistence and retention time after transplantation (81). In our therapeutic regime, long-term survival of adoptively applied NIS-MSCs is negligible as they are eliminated by accumulation of ^{131}I and therapeutic efficacy is enhanced by a new cycle of MSC load and treatment with iodide.

When using MSCs constitutively expressing the NIS transgene, MSC migration to non-tumor tissue might be disadvantageous due to off-target toxicity (76,145). In the study presented here, *in vivo* tracking via ^{124}I-PET imaging of NIS-expressing MSCs could not demonstrate significant off-target recruitment. Relatively small numbers of NIS-expressing MSCs were detected in the lung of the mice assessed by NIS immunofluorescence staining. This general phenomenon has been observed in several studies where the presence of MSCs in lung was higher at earlier time points after injection potentially due to entrapment within the microvascular system, but was reduced by later time points (97,98).

We demonstrate here the great potential of MSCs engineered to express the theranostic *NIS* gene as an anticancer agent for the treatment of GBM. While MSC-mediated *NIS* gene therapy led to a significant prolongation of median survival up to 67 % after three treatment cycles as compared to control groups, we did not achieve a complete tumor regression. Nevertheless, this survival increase in a preclinical study is a promising result that is comparable to previous

preclinical studies made in different glioma models including GL261 (164-166). An increase of the therapeutic efficacy might be obtained through the use of the α-emitter ^{211}At as alternative isotope also transported by NIS that results in a higher dose rate based on a shorter half-life and higher energy as compared to ^{131}I (49). The syngeneic GL261 model is often used in the context of cancer immunotherapy based on the intact host immune system. While ongoing studies reveal promising preclinical results, data have to be interpreted with caution due to potential moderate immunogenicity of the GL261 model (167-170). Based on the currently available data, combination of NIS-based radionuclide therapy with immunotherapy seems to be another promising approach for future studies to increase and foster therapeutic efficacy in this still deadly disease.

The combination of MSC-mediated *NIS* gene therapy as an adjuvant for standard treatment strategies may represent a viable approach for clinical translation to enhance therapeutic efficacy. Major obstacles in the treatment of GBM include its invasive growth pattern, which means that infiltrative tumor extensions reach into the surrounding brain parenchyma leading to growth of distant tumor microsatellites. This precludes complete surgical resection and is often responsible for tumor relapse. Bexell and colleagues found that MSCs injected intratumorally in a preclinical 3000 N32 glioma model during partial resection were able to migrate efficiently within glioma remnants, even though they were not able to show long-distance engraftment of their MSCs (93). Building upon these studies the combination of NIS-MSC-based radionuclide therapy with surgical excision of the tumor may have the potential to reduce the risk of postsurgical relapse.

In addition to surgery, radiotherapy is a standard treatment for many solid tumors including GBM. An enhancement of MSC homing following irradiation pretreatment of tumors by a radiation-induced enhancement of the inflammatory response has been described after intravascular administration (96). Synergistic effects of tumor irradiation and MSC-mediated cancer treatment have been reported in hepatocellular carcinoma, breast cancer, colon cancer and glioma (90,95-98). Based on our previous studies in hepatocellular cancer and the above mentioned studies in preclinical GBM, the combination of tumor irradiation and MSC-mediated *NIS* gene therapy might be a promising approach in GBM to reduce the risk of tumor recurrence.

In conclusion, we demonstrate the potential of *ex vivo* genetically engineered MSCs as a tumor-selective vector system for *NIS* gene transfer in a syngeneic GBM model after systemic i.v. injection. *In vivo* biodistribution studies with ^{123}I-scintigraphy or ^{124}I-PET imaging showed selective MSC recruitment to s.c. and in particular to orthotopic brain tumors using *NIS* a potent and well characterized reporter gene. A critically high number of NIS-MSCs was recruited to

the tumor yielding a significantly prolonged survival and reduced tumor growth after ^{131}I treatment. *NIS* gene cancer therapy employing MSCs as a targeting vector opens the prospect of a very promising new treatment approach for newly diagnosed as well as refractory brain tumors due to the opportunity of combining conventional treatment methods with easily modifiable NIS-expressing MSCs to enhance general therapeutic efficacy.

3.7 Acknowledgements

We owe special thanks to Sybille Reder, Markus Mittelhäuser, Hannes Rolbieski and Sandra Sühnel (Department of Nuclear Medicine, School of Medicine, Klinikum rechts der Isar, Technical University of Munich, Munich) for their valuable help in performing imaging studies. We appreciate the help from Dr. Stefan Stangl and Dr. Cai Linzhi for establishing the orthotopic glioblastoma mouse model. Furthermore, we thank Prof. Dr. Julia Mayerle, Dr. Ivonne Regel and Dr. Ujjwal Mahajan for allowing us to use their lab equipment.

This work was performed as partial fulfillment of the doctoral thesis of C. Kitzberger at the faculty for Chemistry and Pharmacy of the LMU Munich.

This work was supported by grants from the Deutsche Forschungsgemeinschaft (DFG) within the Collaborative Research Center SFB 824 to C. Spitzweg (project C8), R. Glass (B2), F. Schilling (Z3), G. Multhoff (B4), M. Eiber (B11) and within the Priority Program SPP1629 to C. Spitzweg and P.J. Nelson as well as a grant from the Wilhelm-Sander-Stiftung to C. Spitzweg (2014.129.1). R.E. Kälin and R. Glass are supported by the DFG (GL691/2; SFB824), the „Wilhelm Sander-Stiftung“, the „Anni-Hofmann Stiftung“, and the „Verein zur Förderung von Wissenschaft und Forschung an der Medizinischen Fakultät der LMU München“ (WiFoMed). R. Glass acknowledges funding by DFG grant INST 409/223-1 FUGG.

3.8 Author contributions

Conception and design: C. Kitzberger, K.A. Schmohl, P.J. Nelson, C. Spitzweg

Development of methodology: C. Kitzberger, R.E. Kälin, R. Glass, G. Multhoff, P.J. Nelson, C. Spitzweg

Acquisition of data (provided animals, acquired and managed patients, provided facilities etc.): C. Kitzberger, R. Spellerberg, Y. Han, C. Stauss, F. Schilling, M. Eiber, W. A. Weber, C. Spitzweg

Analysis and interpretation of data (e.g. statistical analysis, biostatistics, computational analysis): C. Kitzberger, C. Zach, E. Wagner, P.J. Nelson, C. Spitzweg

Writing, review, and/or revision of the manuscript: C. Kitzberger, K.A. Schmohl, F.Schilling, R.E. Kälin, R. Glass, W.A. Weber, P.J. Nelson, C. Spitzweg

All authors have read and approved the final manuscript.

Administrative, technical, or material support (i.e., reporting or organizing data, constructing databases): E. Wagner, G. Multhoff, M. Eiber, F. Schilling, W.A. Weber, R. Glass, P.J. Nelson, C. Spitzweg

Study supervision: E. Wagner, P.J. Nelson, C. Spitzweg

3.9 Conflict of interests

The authors declare no potential conflicts of interest.

3.10 Abbreviations

BBB: Blood brain barrier; CMV: Cytomegalovirus; EBRT: External beam radiotherapy; GBM: Glioblastoma; H&E: Hematoxylin and Eosin; HIF-1α: Hypoxia-inducible factor -1α; HSP70B: Heat shock protein 70B; i.c.: Intracranial; i.p.: Intraperitoneal; i.v.: intravenous; L-T4: Levo-thyroxine; MRI: Magnetic resonance imaging; MSC: Mesenchymal stem cells; MS: Median survival; NaCl: Saline; NIS: Sodium iodide symporter; PBS: Phosphate-buffered saline; PDAC: Pancreatic ductal adenocarcinoma; PET: Positron emission tomography; RANTES/CCL5: Regulated on activation, normal T cell expressed and secreted/CC-chemokine ligand 5; SPECT: Single-photon emission computer tomography; subcutaneous: s.c.; TGF-β1: Transforming growth factor β1; Wt: Wild-type

3.11 Supplementary Material

Group	Uptake [% ID/ml]					
	Tumor			Thyroid		
	1 h	3 h	5 h	1 h	3 h	5 h
3x NIS-MSCs 72 h	2.6 ± 0.2	1.8 ± 0.3	1.5 ± 0.3	8.4 ± 1.2	6.6 ± 1.6	6.2 ± 1.4
3x Wt-MSCs 72 h	1.1 ± 0.3	0.9 ± 0.3	0.8 ± 0.3	8.2 ± 2.3	7.5 ± 1.1	6.3 ± 1.3
1x NIS-MSCs 48 h	3.5 ± 1.0	2.8 ± 0.7	2.6 ± 0.7	10.9 ± 1.2	9.6 ± 0.9	8.8 ± 1.6
1x Wt-MSCs 48 h	1.5 ± 0.5	1.3 ± 0.4	1.2 ± 0.4	6.3 ± 0.5	7.2 ± 0.3	6.2 ± 0.8
1x NIS-MSCs 72 h	2.5 ± 0.2	1.9 ± 0.3	1.6 ± 0.4	9.0 ± 0.5	6.1 ± 1.7	4.6 ± 1.3
1x Wt-MSCs 72 h	1.2 ± 0.1	0.9 ± 0.2	0.8 ± 0.2	6.7 ± 1.2	5.2 ± 2.0	5.6 ± 1.4

Supplementary Figure 1: Radioiodide uptake of GL261 brain tumors after systemic MSC-mediated *NIS* reporter gene delivery in comparison to thyroid as endogenous NIS-expressing organ assessed by ^{124}I PET/CT imaging. Results are expressed as mean value ± SEM.

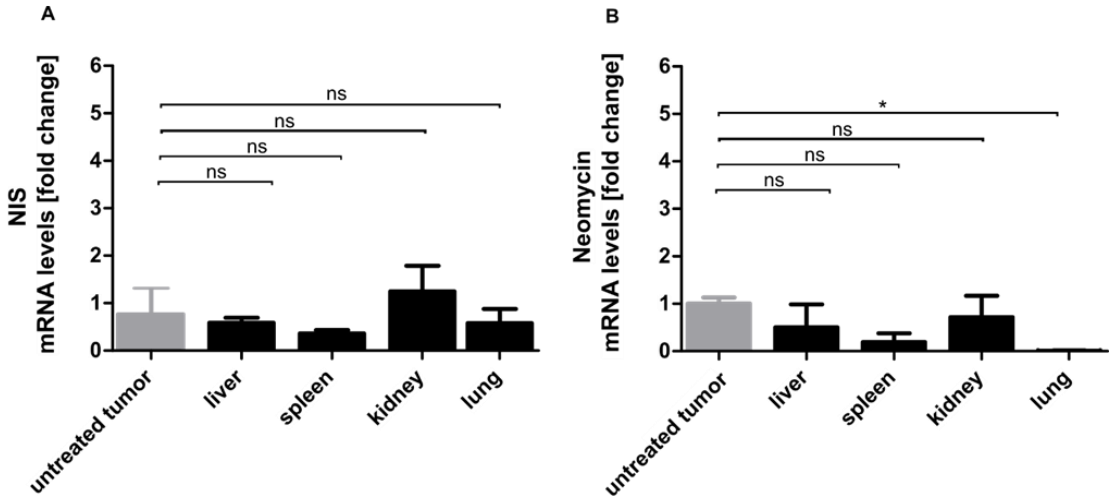

Supplementary Figure 2: ***Ex vivo*** **analysis of non-target organs after NIS-MSC gene delivery.** NIS (**A**) and Neomycin (**B**; selection marker of NIS-MSCs) mRNA expression was detected by qPCR in liver, spleen, kidney and lung after NIS-MSC application and showed no expression above the background level of untreated tumors (which was arbitrarily set to one; NIS mRNA levels of untreated ΔΔCt = 0.0003 and Neomycin mRNA levels of untreated ΔΔCt = 0.002). Data are represented as mean-fold change ± SEM (*p<0.05).

4 Chapter 3: IL-6-Controlled MSC-mediated NIS Gene Therapy of GBM

This chapter is a pre-copy-edited version of a peer-reviewed article published in Molecular Therapy – Oncolytics. 2023 Aug 15; 30:238-253 and assigned the DOI: https://doi.org/10.1016/j.omto.2023.08.004.

Interleukin-6-Controlled, Mesenchymal Stem Cell-based Sodium/Iodide Symporter Gene Therapy Improves Survival of Glioblastoma-bearing Mice

Kitzberger C [1], Shehzad K[1], Morath V [2], Spellerberg R [1], Ranke J [1], Steiger K [3], Kälin RE [4,5], Multhoff G [6,7], Eiber M [2], Schilling F [2], Glass R [4,5,8], Weber WA [2], Wagner E [9], Nelson PJ [1], Spitzweg C [1,10]

[1]Department of Internal Medicine IV, LMU University Hospital, LMU Munich, Munich, Germany

[2]Department of Nuclear Medicine, School of Medicine, Klinikum rechts der Isar, Technical University of Munich, Munich, Germany

[3]Institute of Pathology, School of Medicine, Technical University of Munich, Munich, Germany

[4]Neurosurgical Research, Department of Neurosurgery, LMU University Hospital, LMU Munich, Munich, Germany

[5]Walter Brendel Center of Experimental Medicine, Faculty of Medicine, LMU Munich, Munich, Germany

[6]Center for Translational Cancer Research (TranslaTUM), School of Medicine, Klinikum rechts der Isar, Technical University of Munich, Radiation Immuno-Oncology group, Munich, Germany

[7]Department of Radiation Oncology, School of Medicine, Klinikum rechts der Isar, Technical University of Munich, Munich Germany

[8]German Cancer Consortium (DKTK), partner site Munich, Munich and German Cancer Research Center (DKFZ), Heidelberg, Germany

[9]Pharmaceutical Biotechnology, Department of Pharmacy, Centre for System-Based Drug Research and Centre for Nanoscience, LMU Munich, Germany

[10]Division Endocrinology, Diabetes, Metabolism and Nutrition, Mayo Clinic, Rochester, MN, USA

4.1 Graphical Abstract

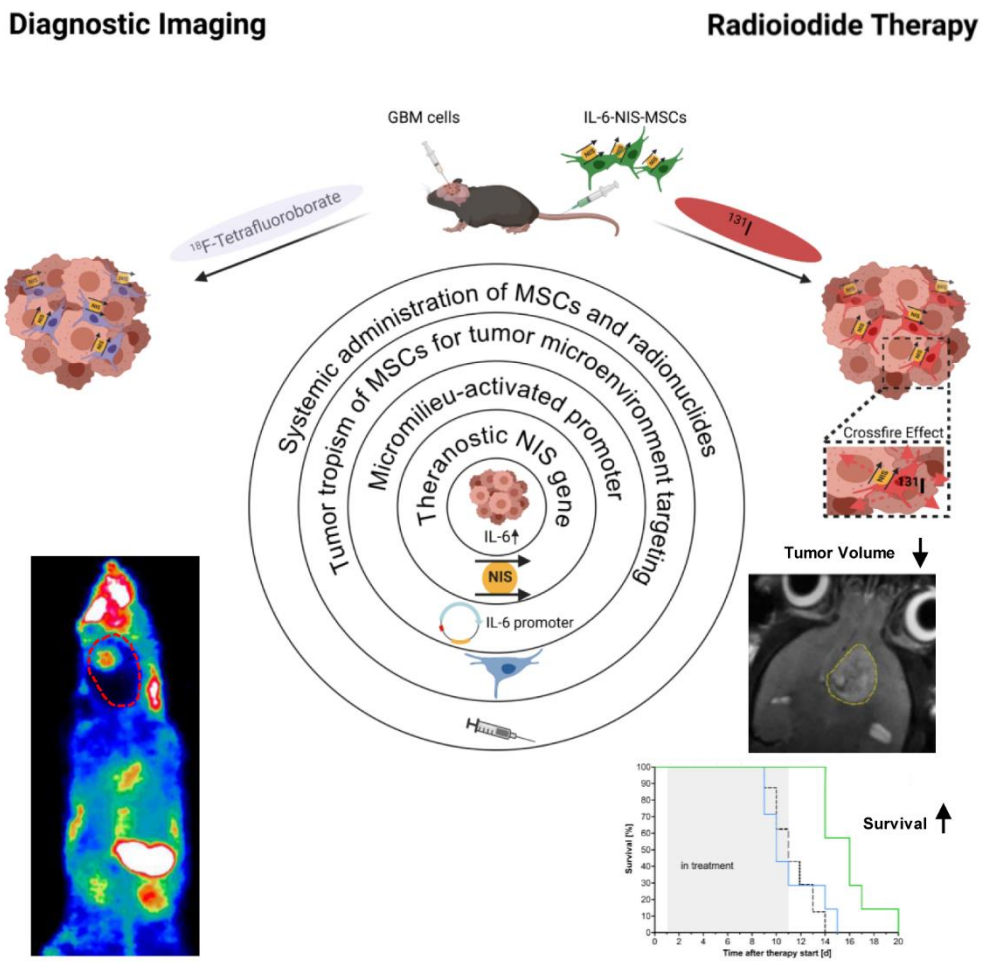

4.2 eTOC Synopsis

Spitzweg and colleagues combined the tumor-homing capacity of mesenchymal stem cells (MSCs) with tumor-specific expression of the theranostic sodium/iodide symporter (NIS) driven by the IL-6 promoter. By adding this additional layer of specificity, off-target toxicities could be reduced. Finally, IL-6-NIS-MSC-mediated radioiodide therapy led to significantly prolonged survival of glioblastoma-bearing mice.

4.3 Abstract

New treatment strategies are urgently needed for glioblastoma (GBM) – a tumor resistant to standard-of-care treatment with a high risk of recurrence and extremely poor prognosis. Based on their intrinsic tumor tropism, adoptively applied mesenchymal stem cells (MSCs) can be harnessed to deliver the theranostic sodium/iodide symporter (*NIS*) deep into the tumor microenvironment. Interleukin-6 (IL-6) is a multifunctional, highly expressed cytokine in the GBM microenvironment including recruited MSCs. MSCs engineered to drive *NIS* expression in response to IL-6 promoter activation offer the possibility of a new tumor-targeted gene therapy approach of GBM. Therefore, MSCs were stably transfected with a NIS-expressing plasmid controlled by the human IL-6 promoter (IL-6-NIS-MSCs) and systemically applied in mice carrying orthotopic GBM. Enhanced radiotracer uptake by [^{18}F]-Tetrafluoroborate-PET/MR-imaging was detected in tumors after IL-6-NIS-MSC application as compared to mice that received wildtype MSCs. *Ex vivo* analysis of tumors and non-target organs showed tumor-specific NIS protein expression. Subsequent ^{131}I-therapy after IL-6-NIS-MSC application resulted in significantly delayed tumor growth assessed by MRI and improved median survival up to 60% of GBM-bearing mice as compared to controls. In conclusion, the application of MSC-mediated *NIS* gene therapy focusing on IL-6 biology-induced NIS transgene expression represents a promising approach for GBM treatment.

4.4 Introduction

Glioblastoma (GBM) is the most aggressive and most common malignant type of primary brain tumor in adults with a median survival <2 years after diagnosis (16). Major hurdles encountered in the treatment of GBM result from multiple factors linked to the biology of this tumor including diffuse infiltrative growth, intra-and intermolecular heterogeneity and the location itself limiting complete surgical resection as well as the delivery of drugs into the tumor by the blood-brain barrier (BBB)(171). The standard treatment of newly diagnosed GBM patients includes extensive surgery followed by radiotherapy and concomitant/adjuvant chemotherapy (“Stupp Protocol”) (28,134). Therapy resistance to conventional standard-of-care as well as new treatments almost always occurs and may correlate in part with the unique genetic, epigenetic and microenvironmental features of the brain’s neural tissue (171,172).

The tumor microenvironment plays a pivotal role in tumor growth and progression of most human cancers including GBM (173). In the glioblastoma microenvironment, an increased abundance of inflammatory cytokines, chemokines and growth factors has been reported (11). One such cytokine is interleukin-6 (IL-6), a potent mediator that is omnipresent in the

inflammatory microenvironments of many solid tumors. This cytokine displays pleiotropic functions and is released by various cell types within the tumor setting.(174) The regulation of IL-6 gene expression is complex and involves numerous transcription factors and their interactions (175). Strong inducers of the IL-6 promoter are tumor necrosis factor (TNF), interleukin (IL)-1 and interferon (IFN)-γ (176). IL-6 signaling in gliomas is thought to sustain and promote tumor proliferation, tumor invasion and angiogenesis, and contribute to immune escape as well as inhibition of apoptosis of cancer cells during chemo- and radiotherapy (11,177,178). According to datasets derived from The Cancer Genome Atlas (TCGA) and the Repository of Molecular Brain Neoplasia Data (REMBRANDT), high IL-6 gene expression is associated with high grade gliomas in comparison to lower grade patient samples, and correlates with poor survival and, thus, may represent a prognostic marker in patients for a poor outcome (179-181). Due to the role of IL-6 and its signaling pathways as a driver of the malignant progression of GBM, tumor therapy which targets pathways linked to upregulation of IL-6 in MSCs represents an elegant platform for the targeted treatment of newly diagnosed as well as refractory GBM (179).

Inflammatory cytokines and chemokines that originate from the GBM micromilieu are implicated in the active recruitment of mesenchymal stem cells (MSCs) to the tumor area (145,146). MSCs have recently gained attention as a cell-based delivery system for the treatment of GBM based on their intrinsic tumor homing and migratory properties (74,146). Several studies including our own have shown that MSCs possess the ability to cross the BBB after systemic application and thus, circumvent a major limitation in the treatment of GBM often encountered in systemic drug delivery to the brain (12,93,98,136,137,141-144,147). Genetic engineering of MSCs opens the prospect of their application as shuttle vectors for the delivery of therapeutic genes, such as the sodium/iodide symporter, into the critical microenvironment of growing tumors (182).

The sodium/iodide symporter (SLC5A5; NIS) is an intrinsic plasma membrane glycoprotein with 13 putative transmembrane domains that is predominantly found in the thyroid gland. Based on its active transport function for iodide or other substrates, it represents a powerful theranostic gene that allows for radionuclide imaging and treatment that has been successfully used routinely in the treatment of thyroid cancer metastases, including brain metastases (44,47,49,50). Different isotopes are efficiently transported by NIS when used in the context of a reporter gene (e.g. ^{123}I, ^{124}I, ^{125}I, ^{99m}Tc, ^{18}F-tetrafluoroborate) using standard nuclear medicine imaging technologies such as scintigraphy, SPECT (single-photon emission computed tomography) or PET (positron emission tomography) imaging. For the monitoring of low volume tumor disease such as GBM, three-dimensional, high-resolution PET imaging is the most appropriate technique. In this context, ^{124}I or ^{18}F-TFB can be used as radiotracers for

NIS-mediated PET imaging. Both agents have been demonstrated to be delivered to the brain and allow brain tumor imaging. The use of ^{18}F-TFB further enables an improved, more accurate and less “blurred” imaging quality as compared to ^{124}I based on the radio-physicochemical properties of ^{18}F (51,61). Importantly, NIS can also be used as an effective therapy gene by the facilitated uptake of the β-emitters ^{131}I, ^{188}Re or the α-emitter ^{211}At. Because of the resultant cytotoxic effects including a significant bystander effect, treatment effectively eliminates NIS-transduced cells as well as adjacent cells in the course of therapy (49).

Cloning of the cDNA encoding *NIS* in 1996 provided the molecular platform for *NIS* gene transfer into non-thyroidal tumors and, thus, expanded its function to the treatment of extrathyroidal malignancies (48). We and others have shown the potential of *NIS* gene-based therapy using MSCs as delivery vectors for the treatment of distinct non-thyroidal tumors (63,64,66,75,89,98). Most recently, we demonstrated the potential use of *NIS* as reporter gene to track adoptively applied MSCs using NIS-MSCs constitutively expressing *NIS* driven by a CMV (cytomegalovirus)-promoter in GBM after systemic delivery followed by therapeutic application of ^{131}I, which led to a significant increase in survival and reduced tumor growth (12). In this context, MSC recruitment to non-tumor tissue due to normal tissue homeostasis along with transgene expression might lead to undesirable extratumoral toxicity.

Selective control of transgene expression allows the restriction of radiotoxicity to tumor tissue, sparing non-target tissues from potential damage. Using this additional layer of specificity, the general efficacy of MSC-based *NIS* gene therapy can be improved by the use of inducible gene promoters specifically activated in response to signaling pathways associated with factors present in the tumor environment. Our group has demonstrated the use of *ex vivo* engineered MSCs with various gene promoters to drive *NIS* transgene expression including RANTES/CCL5-, hypoxia-responsive HIF1α-, heat-inducible (HSP70B)- and a synthetic transforming growth factor β1 (TGFβ1)-inducible Smad-responsive promoter in hepatocellular carcinoma (Huh7) and metastatic colon carcinoma xenograft models (65,67,75,89).

The major goal of the present study was to make use of the factors associated with the activation of IL-6 expression in high grade gliomas to target *NIS* gene therapy to the GBM stroma in an immunocompetent setting. For this purpose, syngeneic murine bone-marrow derived MSCs were genetically modified to express *NIS* under the control of the human IL-6 gene promoter (IL-6-NIS-MSCs). *In vivo* biodistribution of IL-6-NIS-MSCs and induction of IL-6 promoter activation was monitored by NIS-mediated ^{18}F-TFB-PET imaging after systemic administration. Tumor-selective, NIS-mediated radiotracer accumulation was further examined by co-registration of PET imaging with anatomical brain MR imaging and analysis of NIS protein expression *ex vivo*. Finally, an ^{131}I therapy in GBM-bearing mice was conducted after

systemic IL-6-NIS-MSC administration and assessed by analysis of tumor volume using MRI and animal survival.

4.5 Results

In vitro stimulation of IL-6-NIS-MSCs show enhanced NIS-mediated radioiodide uptake

Murine bone-marrow derived MSCs were engineered to express NIS driven by the human IL-6 promoter (IL-6-NIS-MSC). IL-6 is induced by a variety of cell types within tumor environments in response to proinflammatory signals (173,174). To validate the inducibility of the IL-6 promoter in IL-6-NIS-MSC, the murine cytokines (IL-1 β, TNF-α and IFN-γ), that have been reported as strong activators of the IL-6 pathway (176), were used to stimulate promoter activation followed by analysis of the resulting functional NIS expression by ^{125}I uptake assay *in vitro* (Fig. 1). The NIS-specific inhibitor perchlorate was used to confirm NIS-specificity which reduced radioiodide uptake to background levels. Stimulation with murine cytokines led to a dose-dependent, significant increase of radioiodide uptake of IL-6-NIS-MSCs (Fig. 1A–C). A plateau was reached with all cytokines, IL-1 β alone (maximal level at 1 ng/ml) showed the highest increase of ^{125}I accumulation as compared to IFN-γ (maximal level at 50 ng/ml) and TNF-α (maximal level at 10 ng/ml). The combination of those factors using the concentration yielding the maximal iodide uptake level of each resulted in maximal NIS-mediated radioiodide uptake as compared to untreated IL-6-NIS-MSCs (Fig. 1D). As a basis for the *in vivo* application, incubation of IL-6-NIS-MSC with conditioned media of murine GL261 GBM cells (Fig. 1E) containing diverse tumor-derived factors resulted in significant increase of radioiodide uptake as compared to untreated cells. This stimulation could be further enhanced by adding the mixture of cytokines at their optimal concentrations. In contrast, IL-6-NIS-MSCs were additionally treated with conditioned media of mouse 4T1 breast cancer cells to determine whether this effect is also observed by cells derived from another tumor entity. Treatment with 4T1-CM alone did not induce statistically significant stimulation of iodide uptake in IL-6-NIS-MSC as compared to untreated IL-6-NIS-MSCs. But stimulation with a combination of 4T1 conditioned media and the mixture of IL-1 β, TNF-α and IFN-γ – factors produced by the tumors stromal compartment – lead to a level of iodide uptake that was comparable to that reached with GL261-CM.

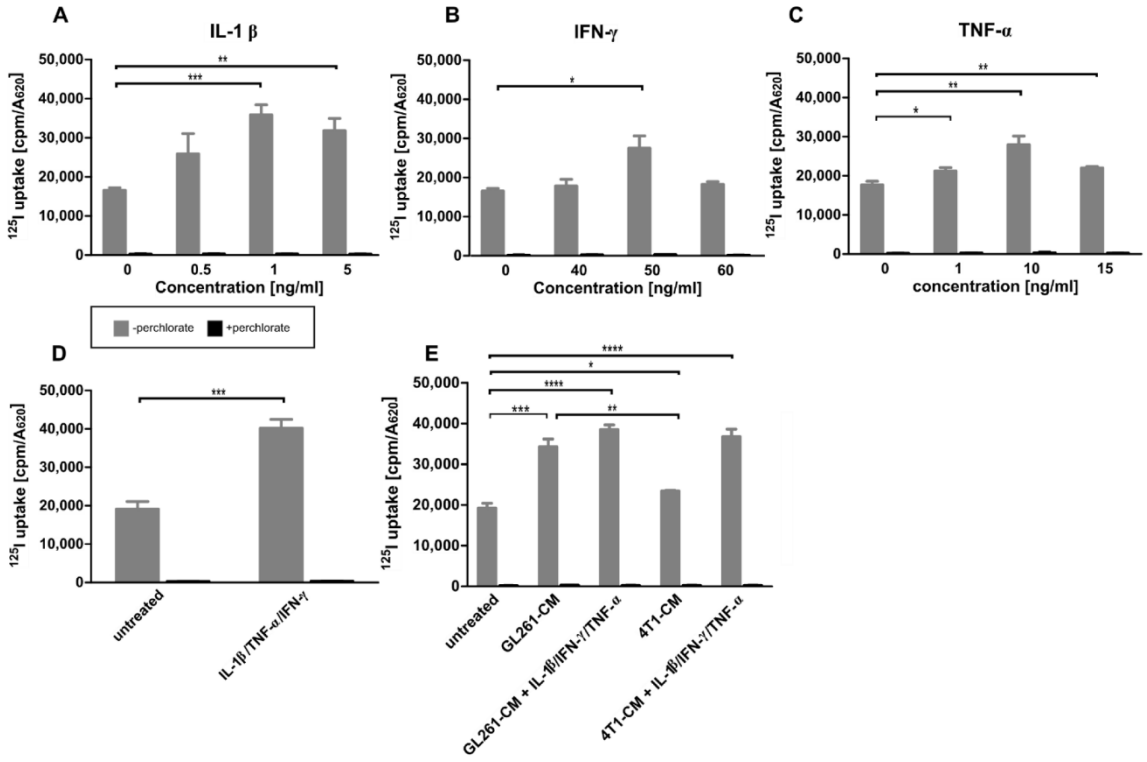

Figure 1: Establishment of mesenchymal stem cells (MSCs) stably expressing NIS regulated by an IL-6 promoter. (A–C) Stimulation with cytokines IL-1 β (0.5–5 ng/ml), IFN-γ (40–60 ng/ml) and TNF-α (1–15 ng/ml) showed NIS-specific ^{125}I-uptake which was reduced to background levels using perchlorate as NIS-specific inhibitor. **(D)** Treatment of IL-6-NIS-MSCs with IL-1 β (1 ng/ml), IFN-γ (50 ng/ml) and TNF-α (10 ng/ml) revealed an increased radioiodide uptake as compared to single stimulation studies. **(E)** Stimulation with GL261-CM led to a significant increase of radioiodide uptake as compared to unstimulated IL-6-NIS-MSCs and was further increased by combined treatment with IL-1 β (1 ng/ml), IFN-γ (50 ng/ml) and TNF-α (10 ng/ml). In contrast, stimulation with 4T1-CM was significant lower as compared to stimulation with GL261-CM, but treatment with 4T1-CM and IL-1 β (1 ng/ml), IFN-γ (50 ng/ml) and TNF-α (10 ng/ml) led to similar radioiodide uptake activity of IL-6-NIS-MSCs as treated with GL261-CM and combined factors. Results are expressed as mean ± SEM of three independent experiments (two-tailed Student's t-test *p<0.05, **p<0.01; ***p<0.001; ****p<0.0001).

IL-6-NIS-MSC migration towards GL261 tumor cell conditioned medium is increased

To evaluate the chemotactic behavior of IL-6-NIS-MSCs in response to a linear gradient of GL261-CM, a 3D migration assay using a collagen I matrix and time-lapse microscopy over a period of 24 h was performed (Fig. 2). IL-6-NIS-MSCs did not show directed chemotaxis

without the influence of a chemoattractant (yFMI = -0.0075 ± 0.0087 and yCoM = -3.7 ± 2.1 µm) used as a negative control (Fig. 2A, C). Further, when subjected to a gradient between GL261-CM and serum-free medium, IL-6-NIS-MSCs showed a strong directed chemotaxis towards the GL261-CM with significantly increased yFMI (0.0972 ± 0.0006; **p<0.01) and yCoM (56.8 ± 21.5 µm; *p<0.05) displacement along the gradient (Fig. 2B, C).

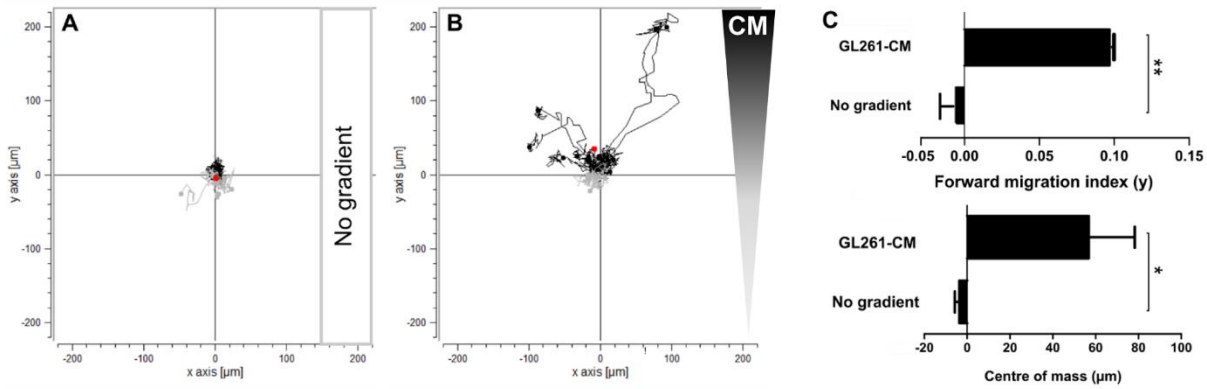

Figure 2: Impact of GL261-CM on IL-6-NIS-MSC shows a strong directed cell migratory behavior. Chemotactic behavior of MSCs subjected to a gradient of GL261-CM was evaluated using 3D live-cell imaging migration assay over a period of 24 h**. (A)** Negative control is shown without the influence of a gradient on MSCs. **(B)** Migration of IL-6-NIS-MSCs along a gradient of GL261-CM resulted in strong migration towards the GL261-CM gradient. **(C)** Quantification of the chemotaxis parameters mean forward migration index (yFMI) and centre-of-mass (yCoM, displayed by red dotes). Results are expressed as mean ± SEM from two independent experiments. Two-tailed Student's t-test was used for statistical analysis (*p<0.05; **p<0.01).

In vivo ^{18}F-TFB biodistribution studies show elevated NIS-mediated tumoral tracer accumulation after systemic IL-6-NIS-MSC administration

Once mice had developed brain tumors, the utilization of a single i.v. injection of murine IL-6-NIS-MSCs or two cycles of IL-6-NIS-MSCs in 2-days intervals followed by ^{18}F-TFB injection (10 MBq, i.v.) after 48 h was investigated to identify an optimized dosing and application schedule. *In vivo* whole-body, high-resolution ^{18}F-TFB-PET imaging was performed over a period of 2 h allowing an optimal discrimination of exogenous and endogenous NIS-mediated signals in the head region. ^{18}F-TFB-PET imaging showed high levels of NIS-mediated radionuclide accumulation in brain tumors after systemic injection of IL-6-NIS-MSCs (Fig. 3A, B). Administration of wildtype MSCs (Wt-MSCs) was used as a control, as well as non-treated GBM-bearing mice that did not receive MSCs, both resulted in a tumoral tracer accumulation comparable to background level (Fig. 3C, D). In addition, ^{18}F-TFB uptake was also observed

in organs that physiologically express NIS including the thyroid, salivary glands and stomach as well as the urinary bladder due to mainly renal elimination of the radiotracer. Tumors from mice that had received a single IL-6-NIS-MSC application accumulated a maximum of 1.9 ± 0.3% ID/ml ^{18}F-TFB 1 h post injection (Fig. 3E). When PET imaging was performed after double IL-6-NIS-MSC injections, tumoral tracer accumulation revealed a maximal level of 1.5 ± 0.1% ID/ml. The quantification of tumoral ^{18}F-TFB uptake showed no significant differences between the single-dose and two-dose application schedules of IL-6-NIS-MSC-treated mice and were measured in the same range as compared to a subset of mice injected with constitutively NIS-expressing (CMV-NIS-MSCs) MSCs (1.9 ± 0.4% ID/ml 1 h post injection; Supplementary Fig. 1). Magnification of the brain area and co-registration of anatomical i*n vivo* MR imaging of the brain with ^{18}F-TFB-PET imaging was used to facilitate delineation of areas of active tumor-selective tracer accumulation in the GBM of mice after systemic IL-6-targeted MSC-mediated *NIS* gene delivery (Fig. 3F, G), whereas tumors of mice that had received Wt-MSCs or untreated tumor-bearing mice showed no tumoral radionuclide accumulation above background level (Fig. 3H, I).

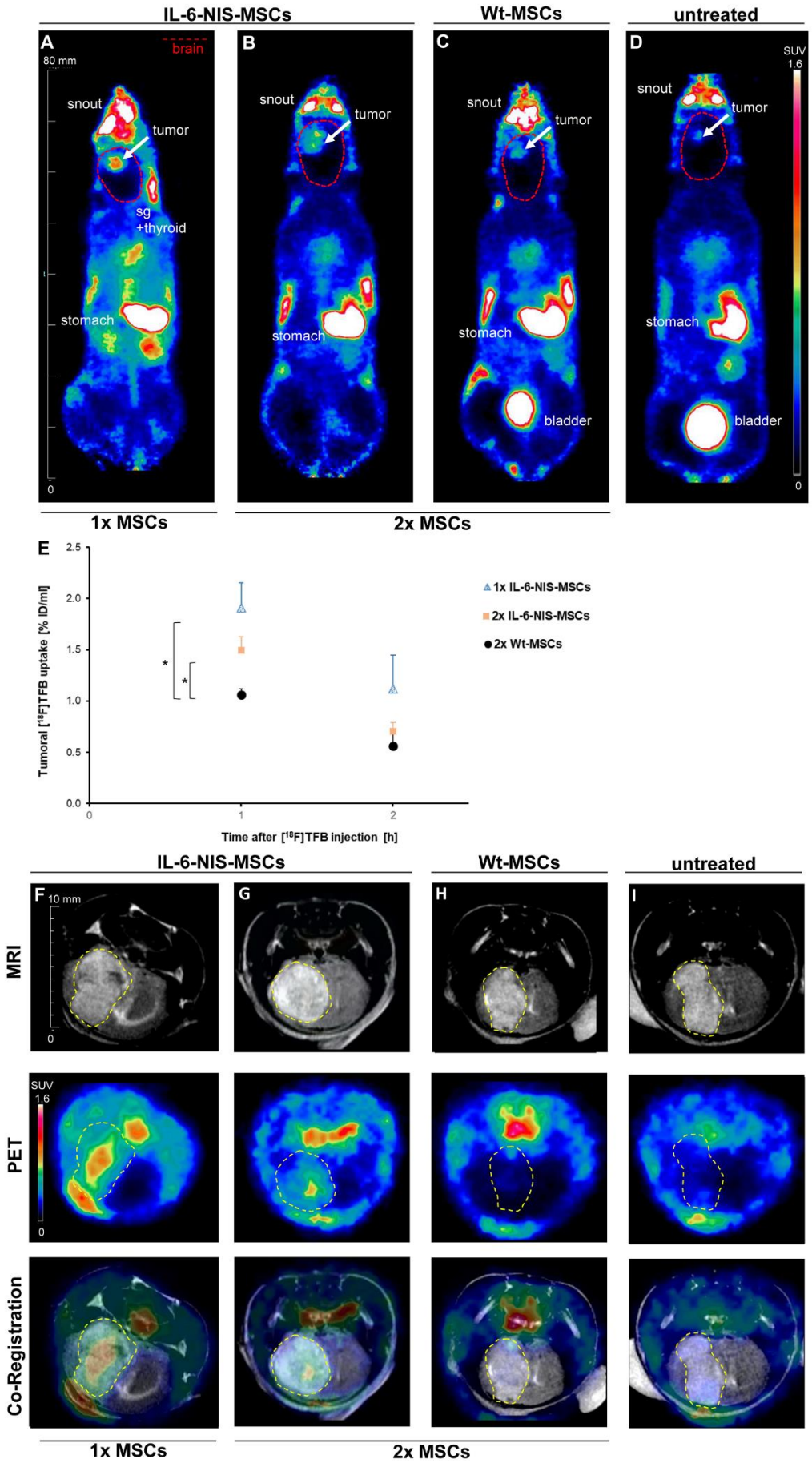
IL-6-NIS-MSCs
Wt-MSCs
untreated
A
brain
80 mm
snout
tumor
sg
+thyroid
stomach
0
B
snout
tumor
stomach
C
snout
tumor
stomach
bladder
D
SUV
1.6
snout
tumor
stomach
bladder
0
1x MSCs
2x MSCs
E
Tumoral [18F]TFB uptake [% ID/ml]
2.5
2.0
1.5
1.0
0.5
0.0
0
1
2
Time after [18F]TFB injection [h]
1x IL-6-NIS-MSCs
2x IL-6-NIS-MSCs
2x Wt-MSCs
*
*
IL-6-NIS-MSCs
Wt-MSCs
untreated
MRI
PET
Co-Registration
F
10 mm
0
G
H
I
SUV
1.6
0
1x MSCs
2x MSCs

Figure 3: ^{18}F-TFB uptake of brain tumors is elevated after systemic IL-6-NIS-MSCs delivery. Representative images of ^{18}F-TFB-PET imaging (horizontal planes; SUV_{bw} = 1.6) are shown 1 h after tracer injection of GBM-bearing mice after (**A**) single IL-6-NIS-MSC injection (n=5), (**B**) double IL-6-NIS-MSC injection (n=5), after (**C**) Wt-MSC injection (n=3) which served as a control and (**D**) no MSC injection (n=1). Brain area is encircled in red dotted lines and tumor is marked with a white arrow. (**E**) Tumoral radionuclide accumulation showed significantly higher levels after IL-6-NIS-MSC delivery as compared to Wt-MSC control mice 1 h post ^{18}F-TFB injection. (**F–I**) Exemplary images of co-registration of anatomical MRI and PET imaging of the brain of the same mice as demonstrated in panel A–D showing tumor-selective tracer accumulation. A strong tumoral ^{18}F-TFB accumulation is revealed after systemic IL-6-targeted MSC-mediated *NIS* gene transfer (**F–G**), while tumors after Wt-MSC injection did not show levels above background level (**H**) as well as compared to non-treated tumor (**I**). Tumors are encircled in yellow dotted lines. Results are expressed as % of the injected dose per ml (volume assessed by MRI) and mean ± SEM is given (Two-tailed Student's t-test at each time point; *p<0.05).

Based on this finding, a higher MSC load did not lead to an increase in tumoral tracer uptake and thus, a single MSC application that reduces stress level of mice and allows for a shortened therapy schedule was used as a basis for the following ^{131}I therapy study.

Ex vivo analysis of GL261 brain tumors and control organs demonstrate tumor-selective NIS expression

Immunohistochemistry for IL-6 protein expression was performed on formalin-fixed paraffin embedded (FFPE) GL261 tumor sections. IL-6 protein expression was observed in all tumors and its stroma (Fig. 4A). *Ex vivo* immunofluorescence staining revealed heterogenous NIS protein expression throughout the tumor stroma of GL261 tumors after systemic IL-6-NIS-MSC injection with patchy areas of high NIS immunoreactivity and areas of low NIS protein expression, while sparing non-tumor brain tissue (Fig. 4B–D). No NIS-specific immunoreactivity was detectable in brain tumors of mice that were injected with Wt-MSCs (Fig. 4E). Non-target organs such as liver, lung, kidney and spleen were analyzed for NIS-immunoreactivity that showed no detectable NIS protein expression (Fig. 4F–I). IL-6 and NIS protein expression was further analyzed by immunofluorescence co-staining of GL261 tumors in mice injected with IL-6-NIS-MSCs demonstrating nice co-localization of NIS and IL-6 protein expression (Supplementary Fig. 2).

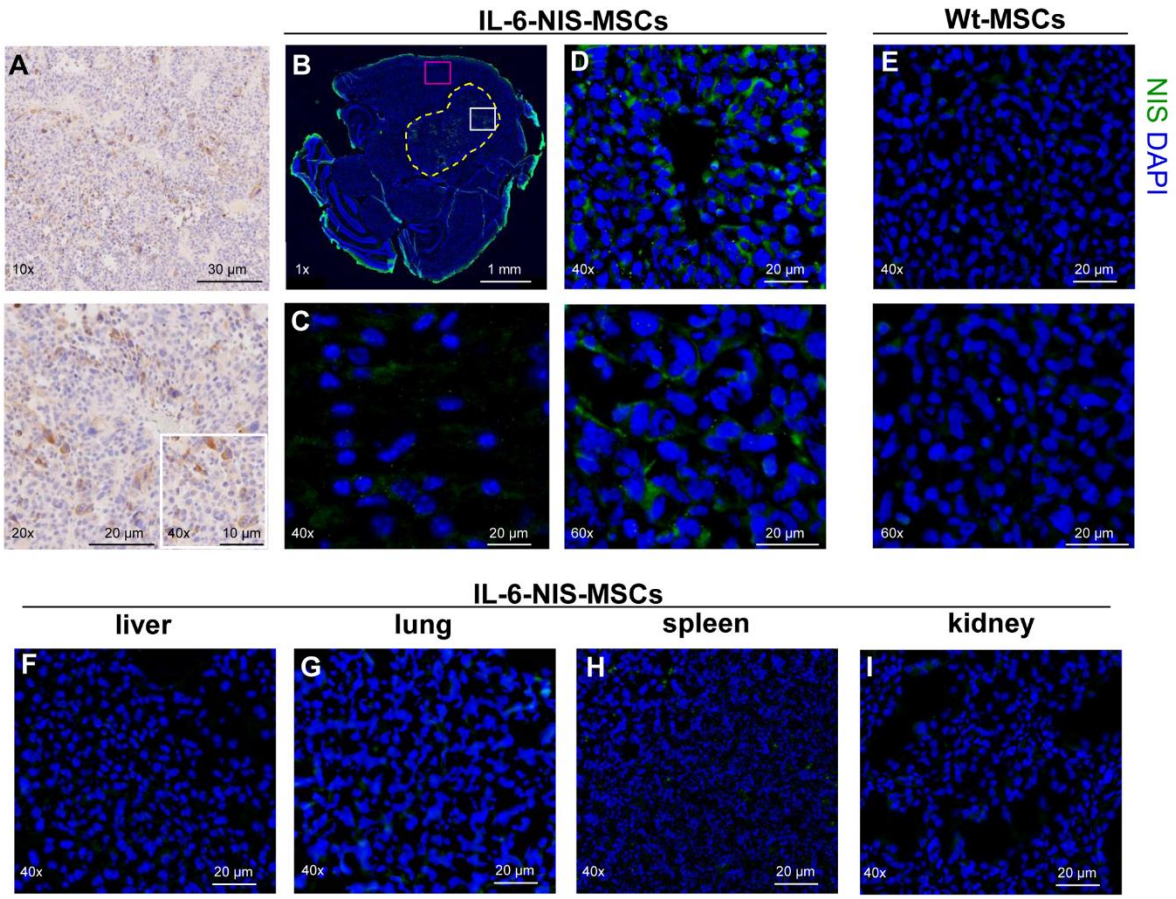

Figure 4: *Ex vivo* analysis of brain tumors and control organs show tumor-specific IL-6 and NIS protein expression. (**A**) IL-6 protein expression was confirmed in GL261 tumors and throughout the tumor stroma (DAB-positive stain is shown in brown). **(B)** NIS immunofluorescence staining is shown with 1x magnification to demonstrate tumor mass and the implantation site in the right caudate putamen. Tumor is encircled in yellow dotted lines. (**C**) No detectable NIS protein expression is observed in non-tumor brain tissue (close-up view pink window in **B**). (**D**) Close-up view (indicated by the white window in **B**) shows NIS-specific immunoreactivity within the tumor stroma, with areas of high and low NIS protein expression, after systemic application of IL-6-NIS-MSCs, while tumors of mice that had received (**E**) Wt-MSCs did not show detectable NIS expression. (**F–I**) No NIS protein expression was detected in control organs such as liver, lung, spleen and kidney after IL-6-NIS-MSC administration. A representative image is shown each.

MSC-mediated IL-6 induced *NIS* gene therapy study led to improved survival of GBM-bearing mice

Based on the results of the PET/MR imaging data and the rapidly growing nature of the GL261 model, a short therapy schedule was conducted using three cycles of a single i.v. MSC

administration (days 1/5/9) each followed by an i.p. ^{131}I injection 2 days later (days 3/7/11). Mice were included in the therapy study as soon as a tumor was clearly visible (0.6–2.1 mm³) as assessed by 7T-MRI and mice were randomly distributed to all groups. Twice a week tumor growth was monitored by MRI resulting in a significantly reduced tumor volume of mice in the therapy group (IL-6-NIS-MSCs + ^{131}I; Fig. 5A, D) as compared to control groups (IL-6-NIS-MSCs + NaCl; Fig. 5 B, D; *p<0.05 day 7 after therapy start and NaCl + NaCl; Fig. 5C, D; *p<0.05 day 7 and 10 after therapy start). Therapy mice demonstrated significantly prolonged survival (Fig. 5E) as compared to controls groups (IL-6-NIS-MSCs + NaCl; **p<0.01 and NaCl + NaCl; ***p<0.001). The median survival (MS) after therapy start was extended up to 60% as compared to controls (IL-6-NIS-MSCs + ^{131}I MS = 16 days; IL-6-NIS-MSCs + NaCl MS = 10 days; NaCl + NaCl MS = 11 days).

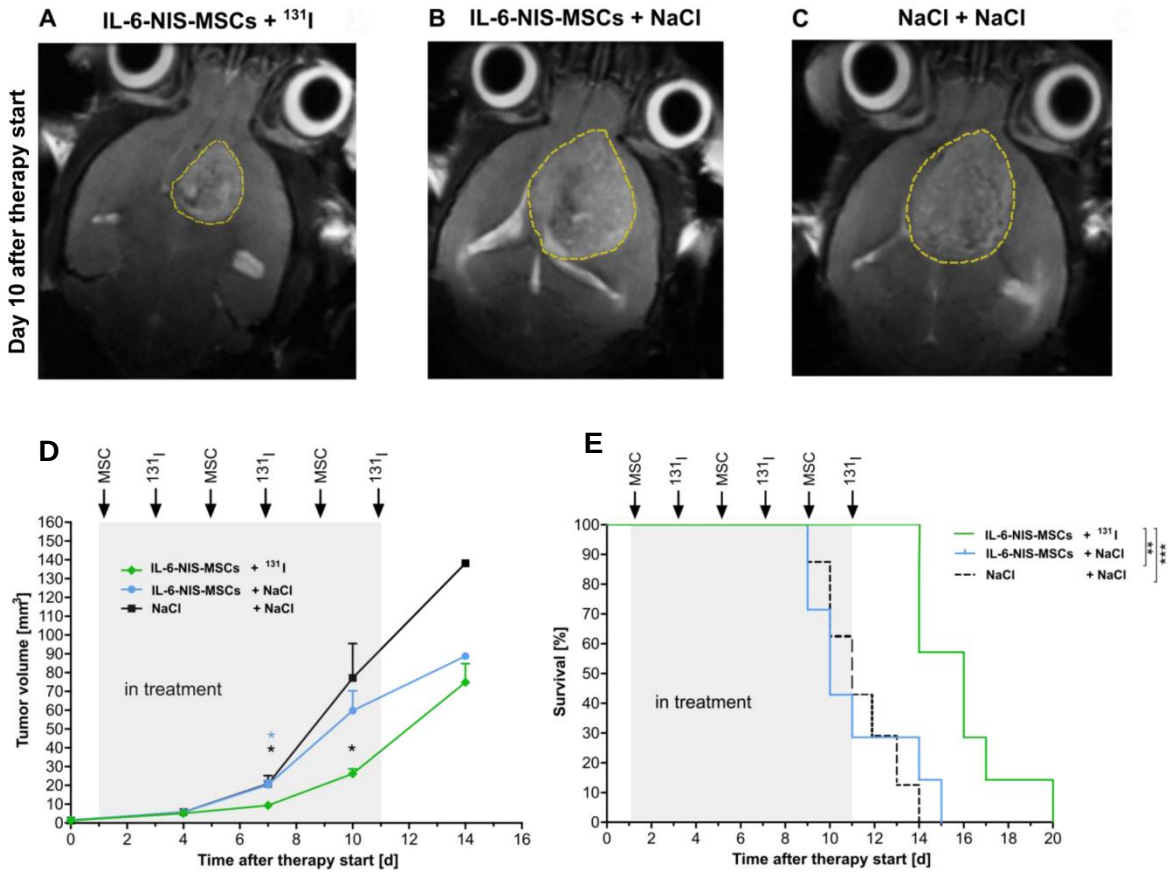

Figure 5: IL-6-targeted MSC-mediated *NIS* gene ^{131}I therapy study of GBM-bearing mice led to reduced tumor growth and improves survival. Three cycles of a single i.v. IL-6-NIS-MSC injection was applied followed by an i.p. administration of ^{131}I 48 h later (MSCs on day 1/5/9 and ^{131}I on day 3/7/11 respectively). Representative MR images 10 days after therapy start are shown after treatment with **(A)** IL-6-NIS-MSCs + ^{131}I, **(B)** IL-6-NIS-MSCs + NaCl and **(C)** NaCl + NaCl. **(D)** Tumor growth was monitored using MRI showing a significantly reduced tumor mass of IL-6-NIS-MSCs + ^{131}I as compared to controls after completion of two therapy

cycles (day 7 after treatment start, n=7 each, *p<0.05). At day 10 after therapy start, tumor growth of mice from the therapy group (n=7/7) was delayed as compared to the NaCl-only group (n=6/7, *p<0.05) and the IL-6-NIS-MSC + NaCl-treated mice (n=5/7, ns). Four-teen days after therapy start, all mice from the therapy schedule were included in the tumor measurement (n=7/7), but n=3 had to be sacrificed the same day, while in the NaCl-only group only n=1/7 and the IL-6-NIS-MSC + NaCl n=2/7 of the mice were still alive and included in the measurement. **(E)** The survival of IL-6-NIS-MSCs + ^{131}I-treated mice was significantly extended as compared to the controls treated with NaCl + NaCl (***p<0.001) and IL-6-NIS-MSCs + NaCl (**p<0.01). Tumors are encircled in yellow dotted lines and results are expressed as mean ± SEM. One-way ANOVA using Tukey's post-hoc test was performed for tumor growth analysis and log-rank test for comparison of survival curves.

At the end of therapy animals were sacrificed and brains were dissected. *Ex vivo* immunofluorescence analysis was used to analyze cell proliferation (Ki67) and blood vessel density (CD31) on cryosections of the brain to determine the effect of ^{131}I after systemic MSC-mediated *NIS* gene transfer (Fig. 6). The intratumoral cell proliferation index (Ki67; Fig. 6A–D) of the therapy group (IL-6-NIS-MSCs + ^{131}I: 2.6 ± 0.3% Ki67-positive cells) was significantly lower as compared to control groups (IL-6-NIS-MSCs + NaCl: 4.7 ± 0.9% and NaCl + NaCl: 5.1 ± 0.5% of Ki67-positive cells). Blood vessel density (CD31; Fig. 6A–C, E) analysis showed a more reduced tumor vascularization in the IL-6-NIS-MSCs + ^{131}I treated animals as compared to the IL-6-NIS-MSCs + NaCl-treated group, while no significant reduction was assessed as compared to the NaCl-only group.

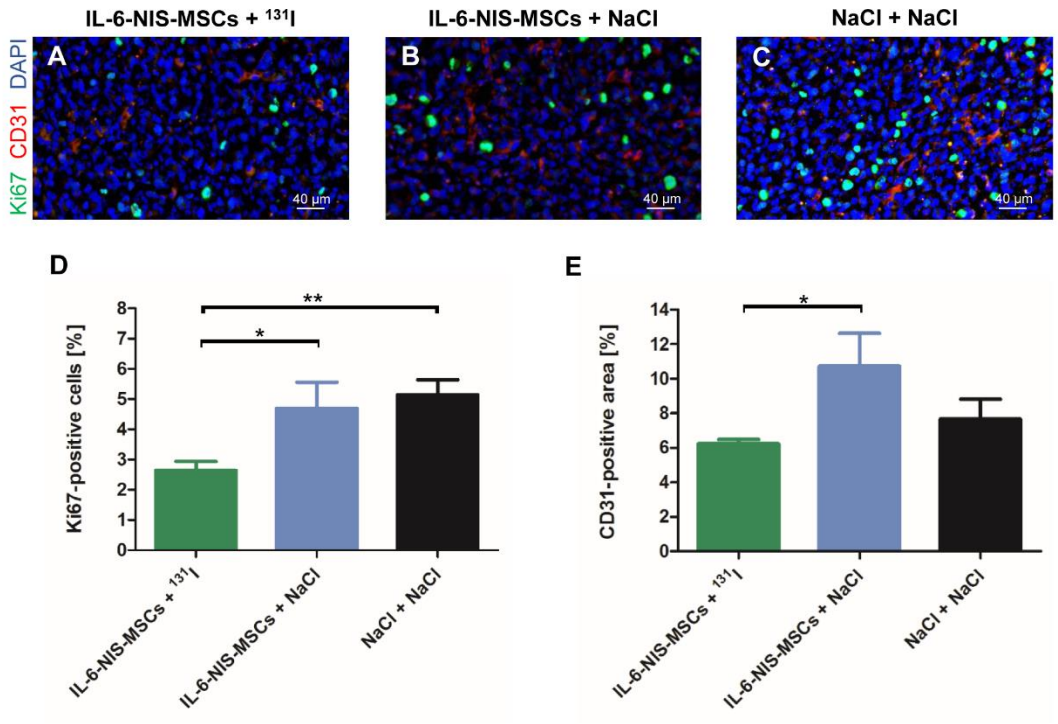

Figure 6: *Ex vivo* analysis of brain tumors after IL-6 promoter-induced MSC-mediated *NIS* gene therapy. At the end of the therapy study, frozen brain tissue sections derived from mice that were treated with IL-6-NIS-MSCs + ^{131}I (**A**), IL-6-NIS-MSCs + NaCl (**B**), and NaCl-only (**C**) were subjected to Ki67 (proliferation index; green) and CD31 (blood vessels; red) immunofluorescence staining. Nuclei were counterstained with Hoechst (blue). A representative picture is shown each at 40x magnification (scale bar = 40 µm). Quantification of the proliferation index (**D**) and blood vessel density of IL-6-NIS-MSCs + ^{131}I in comparison to both control groups (**E**). Results are expressed as mean ± SEM (Two-tailed Student's t-test *p<0.05; **p<0.01).

4.6 Discussion

Despite recent advances in the treatment of GBM, long-term treatment efficacy is poor and the disease remains incurable, thus new GBM therapeutic strategies are urgently needed. Based on their inherent tumor homing properties and abilities to overcome the BBB, MSCs represent a promising tool for the delivery of therapy genes deep into the microenvironment of GBM (12,98,142,144). MSC-mediated *NIS* gene therapy has been described in various experimental models such as hepatocellular carcinoma (63,64,75), pancreatic cancer (66), metastatic colon carcinoma (89) and glioma (98). *NIS* is a theranostic gene that allows *in vivo* tracking of NIS-transfected MSCs after systemic application and their use in cancer therapy in combination

with administration of therapeutically active radionuclides. The clinical use of radioiodide treatment in thyroid cancer patients started in 1946 and is still considered one of the most effective molecularly targeted and imaging-based radiation treatments in cancer with a well-understood safety profile (183,184). The application of *ex vivo* engineered MSCs using *NIS* in the context of solid tumor treatment is currently being examined in early-phase human clinical trials. One study explores the safety and tolerability of MSCs engineered with an oncolytic measles virus encoding NIS (MV-NIS) in recurrent ovarian cancer (NTC02068794).

Previous work by the authors has made use of engineered versions of syngeneic MSCs constitutively expressing NIS driven by a CMV-promoter (CMV-NIS-MSCs). Successful tumor tropism was shown after systemic application by *in vivo* imaging using *NIS* as reporter gene followed by effective therapeutic trials in several tumor models, including most recently in experimental GBM demonstrating selective MSC recruitment and homing to GBM tumors by overcoming the BBB (12,63,66). While the application of CMV-NIS-MSCs showed strong tumor tropism, a portion of exogenously applied MSCs might potentially be recruited to non-target organs in the process of normal tissue homeostasis or by entrapment in vascular organs after intravenous injection (12,63,76,157). The use of MSCs genetically engineered with gene promoters activated by factors in the tumor micromilieu to drive NIS expression in the tumor stroma can reduce the risk of potential off-target effects to non-tumor tissue.

As seen in other solid tumors, the GBM microenvironment is composed of non-malignant stromal cells such as endothelial cells, pericytes, cancer-associated fibroblasts (CAFs) and immune cells [e.g. brain-resident microglia and infiltrating macrophages (GAMs)] and the tumor cells themselves (185). Further, endogenous MSCs are recruited from different origins in the body into the tumor as part of its stromal compartment. In addition to the cellular constitutes, glioblastomas are also surrounded by a pool of pro-inflammatory cytokines, chemokines and growth factors such as TNF-α, TGF-β, IL-6, IL-10, IL-8, CCL2/MCP-1 and RANTES/CCL5 (152,186).

In the present study, *NIS* transgene expression was linked to activation of the promoter for the human IL-6 gene in MSCs. The IL-6 gene is upregulated in response to various pro-inflammatory factors present in solid tumor environments and the protein is associated with important aspects of tumor biology.(173) IL-6 regulates a variety of biological functions including acute phase response, leucocyte maturation and infiltration at sites of inflammation and endothelial cell properties.(25) In the GBM environment, IL-6 is produced by resident MSCs, GAMs, tumor-associated endothelial cells, glioma stem cells (GSCs), a small cellular subpopulation with potent tumorigenic and stem cell like properties that have been implicated

to play a crucial role in GBM maintenance and recurrence as well as by the tumor cells themselves (180,187,188).

Reports have demonstrated the impact of IL-6 on the tumorigenicity of GBM using transgenic mice, where genetic IL-6 depletion blocked GBM formation (189). Furthermore, a study by Lamano *et al*. reported increased IL-6 plasma levels of mice orthotopically implanted with GL261 cells as compared to sham-operated mice 14 days post-injection and mice implanted with CRISPR/Cas9 IL-6 knock-out (KO) GL261 cells showed significantly smaller tumors and an overall increased survival of 77% as compared to unmodified GL261 cells (190). GBM cells producing IL-6 are associated with an enhanced chemo-and radioresistant phenotype (191-193). In addition, IL-6 signaling exerts immunosuppressive effects in GBM via stimulation of GAMs and suppresses T cell functions (181). Tumors often modify their stromal compartment to favor its progression. In this context, indirect crosstalk of MSCs (or other cell types) with tumor cells via growth factors, chemokines and cytokines function in a bidirectional way and lead to functional changes of both cell types through activation of intracellular signaling. The MSC-mediated release of IL-6 has been found in various preclinical tumor models such as ovarian cancer (194), nasopharyngeal carcinoma (195), breast cancer (196) and glioma (197) and is often associated with their differentiation into CAFs, endothelial cells, smooth muscle cells and pericytes, where IL-6 produced by MSCs (or cell types they differentiated to) helps promote tumor growth, resistance to drugs and tumor vascularization (198). Besides its well-known role as critical driver of cancer formation, IL-6 plays a dual role in the TME by its additional contribution to anti-tumor immunity through mobilizing anti-tumor T cell immune responses (199). Increasing evidence points to IL-6 as a key player in the activation, proliferation and survival of lymphocytes as well as T cell trafficking, thereby boosting immune surveillance (199,200). While the exact mechanisms regulating the balance between the anti-tumor and pro-tumor effects of IL-6 are not fully understood, there is clear evidence of robust expression of IL-6 within GBM tissues highlighting the potential of using TME-expressed factors for activation of the IL-6 promoter and subsequent therapeutic transgene expression by MSCs.

In the present study, syngeneic murine bone-marrow derived MSCs were stably transfected with the IL-6 gene promoter driving NIS expression (IL-6-NIS-MSCs) that enabled NIS-mediated *in vivo* tracking of MSC homing to the tumor as well as therapeutic ^{131}I application in response to activation of the IL-6 gene promoter signaling. The upregulation of IL-6 pathway inducers like TNF-α has been reported in GBM patient samples (201) as well as in the experimental GBM used in this study (202). *In vitro* characterization of IL-6-NIS-MSCs demonstrated their ability to significantly concentrate ^{125}I in a dose-dependent manner after stimulation with the pro-inflammatory cytokines IL-1 β, TNF-α and IFN-γ previously shown to

stimulate increased IL-6 biosynthesis (181,203-205). The iodine uptake was perchlorate-sensitive demonstrating NIS-dependent radionuclide accumulation of these MSCs. Treatment with tumor cell-conditioned media (CM) derived from GL261 glioma cells led to a significant accumulation of radioiodide in IL-6-NIS-MSCs that was further enhanced by combination with a mixture of IL-1 β, TNF-α and IFN-γ. Stimulation with GL261-CM alone showed a significantly higher NIS-mediated iodide uptake ability as compared to the breast cancer 4T1-CM demonstrating a stronger IL-6 promoter induction when using GL261 supernatants.

Further, *in vitro* analysis of IL-6-NIS-MSCs migration towards GL261-CM, which represents a mix of diverse factors, demonstrated a strong directed chemotaxis as compared to random basal chemotactic behavior of those MSCs lacking the influence of a gradient as seen in several other tumor models suggesting that the tumor produces factors that can enhance the selective recruitment of MSCs (94,206). The mechanisms underlying MSC tropism to the tumor have not been fully elucidated, but are thought to parallel the mechanisms used by leucocytes in the course of inflammation where recruitment is driven by the presence of inflammatory chemokines and cytokines such as TGF-β, TNF-α, interleukins (e.g. IL-1, IL-6, IL-8, IL-10), interferons and chemokines secreted by the tumor and the tumor stroma and the associated receptors on MSCs (79,146).

In the *in vivo* imaging studies, small-animal PET/MR imaging after administration of IL-6-NIS-MSCs in GBM-bearing mice showed significant tumoral ^{18}F-TFB accumulation after a single or double MSC injection as compared to mice that received Wt-MSCs or no MSCs that showed only background levels. Co-registration with MRI demonstrated tumor-selective tracer accumulation with spots of higher and lower tracer concentration which may be due to a combination of heterogeneous MSC recruitment and/or pro-inflammatory factor expression resulting in heterogeneous IL-6 promoter-driven *NIS* transgene expression. No off-target NIS protein expression was observed in the current study using tumor-stroma selective IL-6 gene promoter: *Ex vivo* NIS protein immunofluorescence of IL-6-NIS-MSC-treated mice exhibited NIS expression largely restricted to tumors, while no NIS protein expression was detected in healthy brain tissue and non-target organs, and thus may avoid severe off-target damage e.g. in the lungs when therapeutic doses are employed. These findings are consistent with our previous study in the same GBM model using constitutively NIS-expressing CMV-NIS-MSCs that showed MSC homing with NIS protein expression restricted to the tumor areas (12). In contrast to the current study using IL-6-NIS-MSCs, in the previous study a small number of CMV-NIS-MSCs were detected in the lungs of mice probably due to entrapment in the microvascular system (12), thereby demonstrating enhanced tumor selectivity of NIS transgene expression by the use of TME-inducible gene promoters.

Although ^{18}F-TFB is a poorer NIS substrate in comparison to ^{124}I used as traditional tracer for NIS PET imaging, and the short physical half-life of ^{18}F precludes its use for dosimetric studies for the required therapeutic dose of ^{131}I in context of personalized cancer treatment, the physical properties of ^{18}F are much better suited for PET imaging in small animals (51). In the current study a subset of mice received CMV-NIS-MSCs as a standard application and showed approximately the same level of ^{18}F-TFB accumulation in the GBM tumors as compared to levels of mice that were injected with IL-6-NIS-MSCs. Based on these comparative studies (66) and our previous experience in the same tumor model using CMV-NIS-MSCs followed by ^{124}I-PET imaging including dosimetric calculations and therapy studies (12), we hypothesized that the tumoral tracer uptake after IL-6-NIS-MSC application in the present study should be sufficient to obtain a therapeutic effect. In the current study, the survival of GBM mice was significantly extended after systemic IL-6-NIS-MSCs administration followed by ^{131}I and a significant reduction of the tumor volume as compared to control groups was observed. The median survival after therapy start was improved up to 60% as compared to the controls. In line with earlier studies by our group using various tumor models, the number of proliferating cells was significantly decreased in tumors of the therapy group as compared to control groups (63,64,67,75). MSC recruitment to the GBM tumor microenvironment with activation of the IL-6 pathway followed by IL-6-targeted NIS transduction is suggested to lead to cell death of NIS-expressing MSCs through particle decay of accumulated ^{131}I and the neighboring tissue (e.g. tumor cells or GSCs) through bystander effects based on the path length in tissue of up to 2.4 mm of the decaying particles. Potential problems encountered by the use of MSCs such as tumor-promoting effects or their long-term retention time(81) may be reduced by the inclusion of suicide genes that allow the efficient elimination of the applied cells at the conclusion of therapy (207).

A potential clinical implementation of the IL-6-directed MSC-mediated *NIS* gene concept would be as an adjuvant treatment to enhance the therapeutic effect of established conventional treatments such as surgery or radiotherapy(90) or novel targeted treatments. Current challenges for the treatment of GBM include the extreme heterogeneity, infiltrative growth including microsatellites, aberrant vascularization, intrinsic resistance to the conventional treatments and delivery problems to the brain. Many of these issues may be effectively addressed through the use of MSCs-based therapy vehicles. GBM is a highly vascularized tumor (27), anti-angiogenic treatments such as bevacizumab, a monoclonal antibody that blocks vascular endothelial growth factor (VEGF) approved by the FDA for the treatment of GBM has not lead to an improvement of patient survival as a monotherapy and the tumor often develops resistance to treatment within months of starting therapy (164). Targeting IL-6 signaling in combination with a VEGF-signaling blockade has been reported as a promising

treatment strategy to reduce tumor invasiveness and growth in experimental GBM (208). Immunotherapy for GBM treatment is currently being evaluated in human clinical phase II/III trials (209). Combination of anti-IL-6 treatment and anti-PD-L1 (programmed death-ligand 1) treatment has been reported to have additive beneficial effects in terms of animal survival in preclinical GL261 that was not observed with either monotherapy (190).

The essential role of IL-6 in tumor biology makes the IL-6 signaling pathway an attractive candidate to potentially control NIS expression within the tumor microenvironment. Genetically engineered MSCs were employed to target NIS expression to the GBM environment and mediate transgene induction through IL-6 signaling to reduce potential side-effects associated with MSC recruitment to non-target tissue and use synergistic effects in terms of enhanced MSC recruitment and promoter activation during ^{131}I therapy. An improvement of the therapeutic effect may be based on a possible self-energizing effect: A potential increased inflammatory response and enhanced vascular permeability due to tissue damage following radioiodide treatment may enhance MSC recruitment to the tumor stroma and increase IL-6 signaling that in turn stimulates promoter activation. Repeated cycles of this treatment regime may lead to an amplification of the therapeutic effect (90).

Effective MSC recruitment and robust, tumor-selective NIS expression and induction of NIS-mediated radionuclide accumulation in GBM tumors driven by the inflammatory micromilieu in GBM was visualized by ^{18}F-TFB-PET/MR imaging *in vivo* and *ex vivo* staining using the function of *NIS* as reporter gene. ^{131}I treatment was employed to IL-6-NIS-MSCs-treated mice resulting in a reduction of GBM growth and significantly extended median survival of GBM-bearing mice. In conclusion, the flexibility of the MSC-based *NIS* gene therapy concept may help address many of the major hurdles associated with the treatment of GBM and offers the opportunity for more individualized and optimized treatment concepts especially when combined with conventional treatment approaches adjustable to the patient's situation.

4.7 Material and Methods

Cell culture

The murine glioma cell line GL261 was purchased and authenticated from the National Cancer Institute (NCI, Frederick, MD, USA). Cells were grown in DMEM low glucose (Sigma-Aldrich, St. Louis, Missouri, USA) containing 10% (v/v) fetal bovine serum (FBS Superior, Sigma-Aldrich), 1% (v/v) MEM non-essential amino acid solution (Thermo Fisher Scientific, Waltham, MA, USA) and 1% (v/v) penicillin/streptomycin (Sigma-Aldrich).

The murine breast cancer cell line 4T1 was purchased from the ATCC and cultured in RPMI-1640 (Sigma-Aldrich) supplemented with 10% (v/v) FBS and 1% (v/v) penicillin/streptomycin.

Murine bone marrow-derived MSCs (Wt-MSCs) were isolated from C57Bl/6 $p53^{-/-}$ mice as described and characterized previously.(66,76) MSCs were grown in RPMI (Sigma-Aldrich) supplemented with 10% (v/v) FBS and 1% (v/v) penicillin/streptomycin.

Cells were maintained in an incubator in a humidified atmosphere at 37 °C with 5% CO_2. For *in vivo* experiments, cells were tested for mycoplasma and viruses according to the FELASA guidelines by Charles River Research Animal Diagnostic Services (CR RADS, Wilmington, MA, USA; Mouse essential panel).

Plasmid construct

To establish the pcDNA6-2LITRHygro-IL-6-Promoter-NIS plasmid construct, the Multisite Gateway Pro Plus Kit (Invitrogen Thermo Fisher Scientific, Waltham, Massachusetts, USA) was used following the manufacturer's recommendations and the plasmids produced as previously described (65,210). The pcDNA6-2LITRHygro-IL-6-Promoter-NIS plasmid contains the full-length human *NIS* gene (NIS cDNA kindly provided by SM Jhiang, Ohio State University, Columbus, Ohio, USA) driven by the human IL-6-promoter, two sleeping beauty transposition sites and a hygromycin resistance gene.

Stable transfection of MSCs

IL-6-NIS-MSCs were produced by stable transfection of Wt-MSCs with the two plasmids pcDNA6-2ITRHygro-IL-6-Promoter-NIS (pSB.H.IL6.hNIS), pCMV (CAT)T7-SB100X (provided from Z Ivics, Max Delbrück Center for Molecular Medicine, Berlin, Germany) which contains the sleeping beauty transposase system (210). 1x 10^6 Wt-MSCs were electroporated with 500 ng of each plasmid at 800 V, 30 ms and 2 pulses using the Neon Nucleofection system (Invitrogen). From t=24 h on, cells were cultivated in selection medium containing RPMI (Sigma-Aldrich) supplemented with 10% (v/v) FBS, 1% (v/v) Penicillin/Streptomycin), 100 µg/ml hygromycin (Invivogen, San Diego, CA, USA) and 50 µg/ml geneticin (Sigma-Aldrich).

Single clones of stably transfected MSCs were isolated and tested for functional NIS expression using ^{125}I uptake assay (see below). About 35 clones were screened over 2-3 passages and the sub-cell line with the highest NIS-mediated radioiodide uptake activity was used for further experiments and referred to as IL-6-NIS-MSC in the following.

Tumor cell conditioned medium

GL261 and 4T1 cells ($1x10^6$ cells) were seeded on a 100 mm^3 surface cell culture plate and cultured for 24 h. Afterwards, cells were starved for 12 h in serum free medium. Supernatant was removed after 48 h and GL261- and 4T1-conditioned medium (GL261-CM and 4T1-CM) was centrifuged and stored at -80 °C. Tumor cell conditioned media was used for migration assay and *in vitro* iodide uptake experiments.

^{125}I uptake assay *in vitro*

IL-6-NIS-MSCs (1.5×10^5 cells/well) were seeded on a 6-well cell culture plate and after 48 h starved for 12 h. Cells were stimulated for 24 h with the murine cytokines IL-1 β (0.5-5 ng/ml; Peprotech, Cranbury, NJ, USA; Catalog #211-11B), TNF-α (1-15 ng/ml; Peprotech; Catalog #315-01A), or IFN-γ (40-60 ng/ml; Peprotech; Catalog #315-05), the combination of the three cytokines at given concentrations, tumor cell-conditioned medium (GL261-CM/4T1-CM) or a combination of GL261-CM/4T1-CM plus the mixture of the three cytokines. ^{125}I uptake was performed as previously described(67) and normalized to cell viability. Cell viability was measured using commercially available MTT reagent (Sigma-Aldrich) according to the manufacturer's instructions. Absorbance was measured at 620 nm with a Sunrise Microplate Absorbance Reader (Tecan). Results were expressed as counts per minute normalized to cell viability (cpm/A_{260}).

3D Migration assay

The migratory capacity of IL-6-NIS-MSCs was investigated using the µ-slide Chemotaxis system^{3D} (Ibidi, Martinsried, Germany) according to the manufacturer's protocol. IL-6-NIS-MSC ($2x10^6$ cells/ml) were seeded in collagen I (bovine, Gibco, Carlsbad, CA, USA; Catalog #A1064401) and a gradient was established between serum-free unconditioned medium and GL261-CM to monitor MSC migration. Time-lapse live cell imaging was performed over 24 h on a Leica DMI6000B microscope equipped with a Leica DFC365 FX camera and Leica MM AF software (Leica Microsystems GmbH, Wetzlar, Germany) and pictures were taken in 15-min intervals. Randomly selected cells (n = 20) were manually tracked with the Manual tracking ImageJ (NIH, Bethesda, MD, USA) plug-in. The Chemotaxis and Migration Tool software (Ibidi) was used for the analysis of the migratory behavior by the centre-of-mass (CoM) localization which is determined by the averaged point of all cell endpoints and forward migration index (FMI) which is a measure of the efficiency of forward migration of the MSCs in relation to the chemoattractant (GL261-CM).

Animals

Female (7-week-old) C57Bl/6 mice were purchased from Charles River (Sulzfeld, Germany). Mice were housed under specific pathogen-free conditions with access to chow and water *ad libitum.*

To establish orthotopic brain tumors, 8-9-week-old mice were anesthetized with ketamine/xylazine and GL261 ($1x10^5$ cells/1 µl) tumor cells were stereotactically inoculated 1 mm anterior, 1.5 mm to the right of the *bregma* and 4 mm deep using a blunt Hamilton syringe (22G, Hamilton, Reno, Nevada, USA) as previously described (12).

Ten days prior to the PET imaging and during ^{131}I therapy experiments, mouse chow was changed to an iodide-deficient diet (ssniff Spezialdiäten GmbH, Soest, Germany) and mice were treated with 5 mg/ml levothyroxine (L-T4, Sigma-Aldrich) in 0.01% (v/v) bovine serum albumin (BSA, Sigma Aldrich) supplemented to the drinking water to reduce the inherent tracer accumulation of the thyroid gland.

Animal experiments were performed in compliance with the German animal welfare laws and the approval of the local animal care committee of the Government of Upper Bavaria (Regierung von Oberbayern) under the license ROB-55.2-2532.Vet_02-17-133. According to the animal protocol, mice were sacrificed at defined presymptomatic time points or at a defined humane endpoint during survival studies (significant weight loss; neurological symptoms; changes in drinking, eating or cleaning behavior; signs of pain).

[^{18}F]Tetrafluoroborate (TFB) tracer synthesis

[^{18}F]tetrafluoroborate radiotracer for NIS-based PET-imaging was produced in-house on a Modular-Lab Standard synthesis module (Eckert & Ziegler, Berlin, Germany) using the protocol previously described by Koshnevisan *et al* (124). In brief, [^{18}F]F^- was eluted from a Sep-Pak QMA Carbonate Plus Light cartridge (Waters, Milford, MA) using 500 µl saline (NaCl, B.Braun, Melsungen, Germany), dried twice at 95°C by addition of 550 µl acetonitrile (MeCN for DNA synthesis; Merck) and reaction was started by addition of boron trifluoride diethyl etherate (BF_3OEt; 1 µl; Sigma-Aldrich) and 15-Crown-5 (24 mg; Sigma-Aldrich) in 1 ml acetonitrile (Merck). Fluorination reaction was carried out for 10 min at 80°C and subsequently the product solution was diluted by 10 ml of H_2O and passed through a Sep-Pak Plus Alumina N cartridge (Waters) to remove free fluorine and a QMA Carbonate Plus Light cartridge in tandem. The resulting product was eluted from the QMA cartridge with 500 µl NaCl (B. Braun). Quality control was performed by radio thin-layer chromatography (radio-TLC) using a neutral alumina stationary phase (10x80 mm, Polygram ALOX N/UV_{254}, Macherey-Nagel, Düren, Germany)

with methanol as a mobile phase. Plates were scanned using a radio-TLC scanner (Mini-Scan, Bioscan Inc, Washington DC, USA). This radio-TLC resulted in a separation of free [^{18}F]F$^-$ that reacts with the aluminum (R_f = 0) and mobile [^{18}F]TFB (R_f = 0.6).(124) Reactions were started with 5-6 GBq and resulted in a decay-corrected radiochemical yield of 15% and radiochemical purity of > 97.5%.

Radionuclide biodistribution studies *in vivo* in orthotopic GBM tumors using ^{18}F-TFB-PET imaging

IL-6-NIS- or Wt-MSCs (5x10^5 cells/injection) were systemically applied via the tail vein 2–2.5 weeks after intracranial (i.c.) tumor cell implantation and three-dimensional serial PET imaging was performed. MSCs were applied twice in 2-day intervals or in a shortened application regime using only one MSC injection, followed by ^{18}F-TFB PET imaging 48 h after the last MSC administration. Mice received 10 MBq of in-house synthesized ^{18}F-TFB intravenously and serial acquisition was conducted 1 h and 2 h post injection using a preclinical nanoScan PET/MRI system (Mediso Medical Imaging Solutions, Budapest, Hungary). PET images were reconstructed with Monte Carlo-based Tera-Tomo 3D PET reconstruction (Mediso). All PET datasets were analyzed using Nucline acquisition software (Mediso) and volumes of interests of the whole tumor (VOIs) were drawn and stated as fraction of the initially injected ^{18}F-TFB dose (% ID/ml). Tumor volume was assessed by MRI and only mice with tumors >30 mm³ were taken into consideration for the quantification (average tumor volume = 57.6 ± 4.5 mm³ at the day of the imaging).

Mouse brain tissue preparation

Mice were transcardially perfused by manual infusion of PBS (Sigma-Aldrich) followed by 4% formaldehyde solution (Pharmacy, University Hospital LMU Munich, Munich, Germany). Brains were removed and incubated in 4% formaldehyde for 24 h at room temperature. Subsequently, brains were either transferred into 30% sucrose solution at 4 °C until the brain sank to the bottom of the tube and embedded in Tissue-Tek OCT compound (Sakura Finetek, Torrance, CA, USA) or directly paraffin embedded following formalin-fixation (FFPE). Horizontal sections were cut (10 µm thick slices of cryopreserved tissue or 3 µm thick slices of FFPE tissue) and subjected to immunostaining.

IL-6 immunohistochemistry

Immunohistochemical staining for mouse IL-6 of FFPE brain sections was performed on a Bond RXm autostainer (Leica Biosystems, Nussloch, Germany) using primary rabbit anti-mouse IL-6 (ab290735, abcam, Cambridge, UK; 1:50 dilution) antibody and polymer refine detection kit (Leica Biosystems). After deparaffinization, slides were pretreated with EDTA buffer (pH 6) for 30 min at 100 °C for antigen retrieval. Primary antibody diluted in antibody diluent was incubated for 15 min after blocking of endogenous peroxidase for 5 min. Antibody binding was detected with diaminobenzidine (DAB) as chromogen for 10 min and hematoxylin for 5 min was used for counterstaining. Slides were digitalized using an automated slide scanner (Leica Biosystems; AT-2) and representative images were taken with Aperio Imagescope software (version 12.3; Leica Biosystems).

Immunofluorescence analysis of NIS

Immunofluorescence staining of frozen sections of brain tumors and sections of control organs (liver, lung, kidney, spleen) were stained for NIS using rabbit anti-NIS (EUD4101, Origene, Rockville, MD, USA; 1:1000) primary antibody and an anti-rabbit Alexa Fluor 488-conjugated secondary antibody (Jackson ImmunoResearch, West Groove, Pennsylvania, USA). Hoechst bisbenzimide (5 µg/ml) was used to counterstain nuclei and sections were mounted with fluorescence mounting medium (Dako, Hamburg, Germany).

Sections were scanned using a Panoramic MIDI II slide scanner and pictures were taken with CaseViewer (version 2.4, 3DHISTECH, Budapest, Hungary).

Immunofluorescence analysis of NIS and IL-6 co-expression

Immunofluorescence staining of frozen sections of brain tumors after imaging experiments were stained using the primary antibodies mouse anti-NIS (antibody MAB3564, clone FP5A, Merck Millipore; 1:650 dilution) and rabbit anti-IL-6 (ab290735, abcam, Cambridge, UK; 1:50 dilution), followed by the secondary antibodies anti-mouse Alexa Fluor 488-conjugated (Jackson ImmunoResearch, West Groove, Pennsylvania, USA) and anti-rabbit Alexa Fluor Cy3-conjugated (Jackson ImmunoResearch, West Groove, Pennsylvania, USA), respectively. Hoechst bisbenzimide (5 µg/ml) was used to counterstain nuclei and sections were mounted with fluorescence mounting medium (Dako, Hamburg, Germany).

Radioiodide therapy studies *in vivo*

Five-to-six days post i.c. tumor inoculation an initial MRI scan was performed to assess tumor onset using a preclinical small animal 7T-MRI scanner (Agilent & GE healthcare MR Discovery 901 with Bruker AVANCE III HD electronics) with a volume resonator and a dedicated two-channel brain coil (RAPID Biomedical, Rimpar, Germany). Mice were randomly assigned to the treatment groups as soon as a tumor volume of 0.6–2.1 mm^3 was detected (day 0) to start with a therapeutic trial. An application schedule with a single i.v. MSC application (day 1) followed by i.p. injection of ^{131}I (55.5 MBq; Rotop Pharmaka, Dresden, Germany) 48 h later was conducted and this therapy cycle was repeated after 2 days for a total of 3 times (MSCs on days 1/5/9 +^{131}I injection on days 3/7/11). Three treatment cohorts were investigated: IL-6-NIS-MSCs + ^{131}I (referred to as therapy group) and the control groups IL-6-NIS-MSCs + saline (NaCl) or NaCl only (n = 7 respectively).

MRI screenings to assess tumor volume and to monitor tumor growth were performed twice a week. Tumor volume was determined as previously described (61).

Indirect immunofluorescence analysis of CD31/Ki67

Following ^{131}I therapy, immunofluorescence staining for Ki67 (ab16667, abcam, Cambridge, UK; 1:200) and CD31 (blood vessel density; BD Pharmingen; 1:100) was performed on frozen brain tumor sections as described previously.(12) Six visual fields (20x magnification) per tumor were examined for Ki67-positive cells (fraction of proliferating cells) and blood vessel density (CD31-positive area) using ImageJ (NIH).

Statistical Analysis

Results are expressed as mean ± SEM. Statistical significance of *in vitro* experiments and *in vivo* imaging experiment was determined by two-tailed Student's t-test.

Statistical analysis of the *in vivo* therapy study was performed by one-way ANOVA for tumor volumes followed by post-hoc Tukey's Honestly Significant Difference test. Survival plots were analyzed by log-rank test. *p*-values <0.05 were considered as significant (**p*<0.05; ***p*<0.01; ****p*<0.001; *****p*<0.0001; ns not significant).

4.8 Acknowledgements

This work was supported by grants from the Deutsche Forschungsgemeinschaft (DFG) within the Collaborative Research Center SFB 824 to C. Spitzweg (project C8), F. Schilling (Z3), G. Multhoff (B4), M. Eiber (B11), K. Steiger (Z2) and within the Priority Program SPP1629 to C. Spitzweg and P.J. Nelson as well as a grant from the Wilhelm-Sander-Stiftung to C. Spitzweg (2021.094.1). R.E. Kälin and R. Glass are supported by the DFG (GL691/2; SFB824), the „Wilhelm-Sander-Stiftung“, the „Anni-Hofmann Stiftung“, and the „Verein zur Förderung von Wissenschaft und Forschung an der Medizinischen Fakultät der LMU München“ (WiFoMed). R. Glass acknowledges funding by DFG grant INST 409/223-1 FUGG.

We are grateful to Sybille Reder, Markus Mittelhäuser, Sandra Sühnel and Nadine Setzer (Department of Nuclear Medicine, School of Medicine, Klinikum rechts der Isar, Technical University of Munich) for their valuable help in performing the animal studies. We appreciate the help from Olga Seelbach, Ulrike Mühlthaler, Annett Hering and Marion Mielke (CEP, Comparative Experimental Pathology, Institute of Pathology, School of Medicine, Technical University of Munich) with immunohistochemical staining. Furthermore, we thank Prof. Dr. Julia Mayerle, Dr. Ivonne Regel and Dr. Ujjwal Mahajan for providing us their lab equipment.

This work was performed as partial fulfillment of the doctoral thesis of C. Kitzberger at the faculty for Chemistry and Pharmacy of the LMU Munich.

4.9 Author contributions

Conception and design: C.K., P.J.N., C.S.; **Development of methodology:** C.K., K.S., V.M., R.E. K, R.G., G.M., K.S., J.R. P.J.N, C.S.; **Acquisition of data (provided animals, acquired and managed patients, provided facilities etc.):** C.K., K.S., K.S, R.S., F.S., W.A.W., C.S.; **Analysis and interpretation of data (e.g. statistical analysis, biostatistics, computational analysis):** C.K., K.S., M.E., P.J.N., C.S.; **Writing, review, and/or revision of the manuscript:** C.K., V.M., K.S., G.M., F.S., R.E.K., E.W., R.G., W.A.W., P.J.N., C.S.; All authors have read and approved the final manuscript. **Administrative, technical, or material support (i.e., reporting or organizing data, constructing databases):** G.M., M.E., F.S., W.A.W., R.G., P.J.N., C.S.; Study supervision: E.W., P.J.N., C.S.

4.10 Declaration of Interests

The authors declare no potential conflicts of interest.

4.11 Keywords

Interleukin-6 promoter, glioblastoma; gene therapy; mesenchymal stem cells; sodium/iodide symporter (NIS); PET imaging

4.12 Data Availability Statement

Data generated in this study are available upon request from the corresponding author.

4.13 Supplementary Material

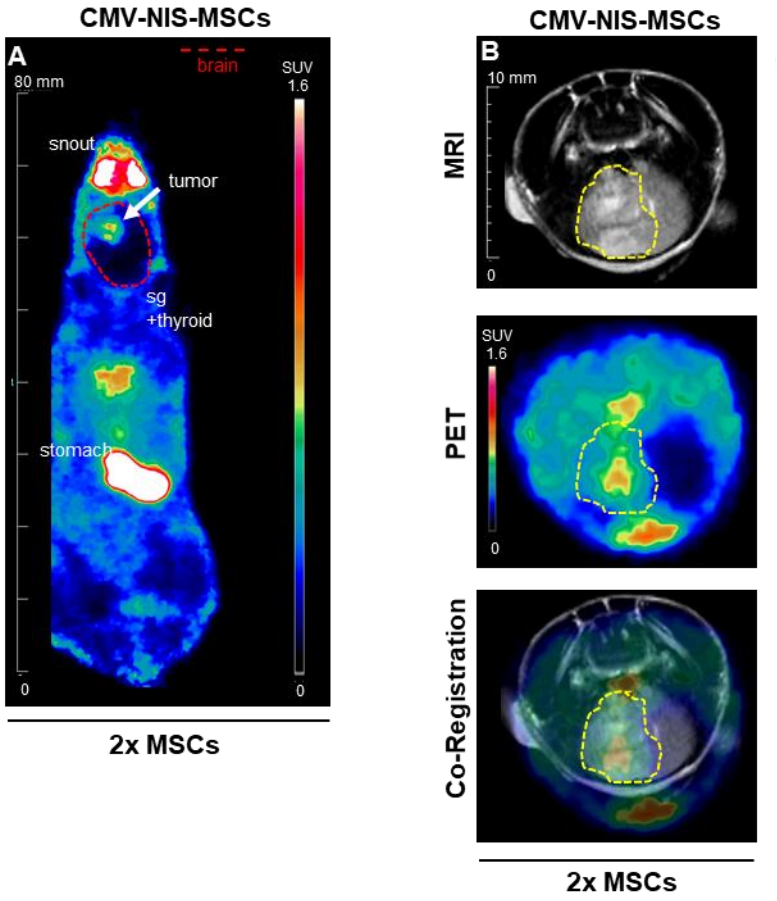

Figure S1: ^{18}F-TFB uptake of brain tumors is elevated after systemic CMV-NIS-MSCs delivery. (A) Representative images of ^{18}F-TFB PET imaging (horizontal planes; SUV_{bw} = 1.6) are shown 1 h after tracer injection of GBM-bearing mice (n=3). Brain area is encircled in red dotted lines and tumor is marked with a white arrow. **(B)** Exemplary images of co-registration of anatomical MRI and PET imaging of the brain showing tumor-selective tracer accumulation. Tumors are encircled in yellow dotted lines.

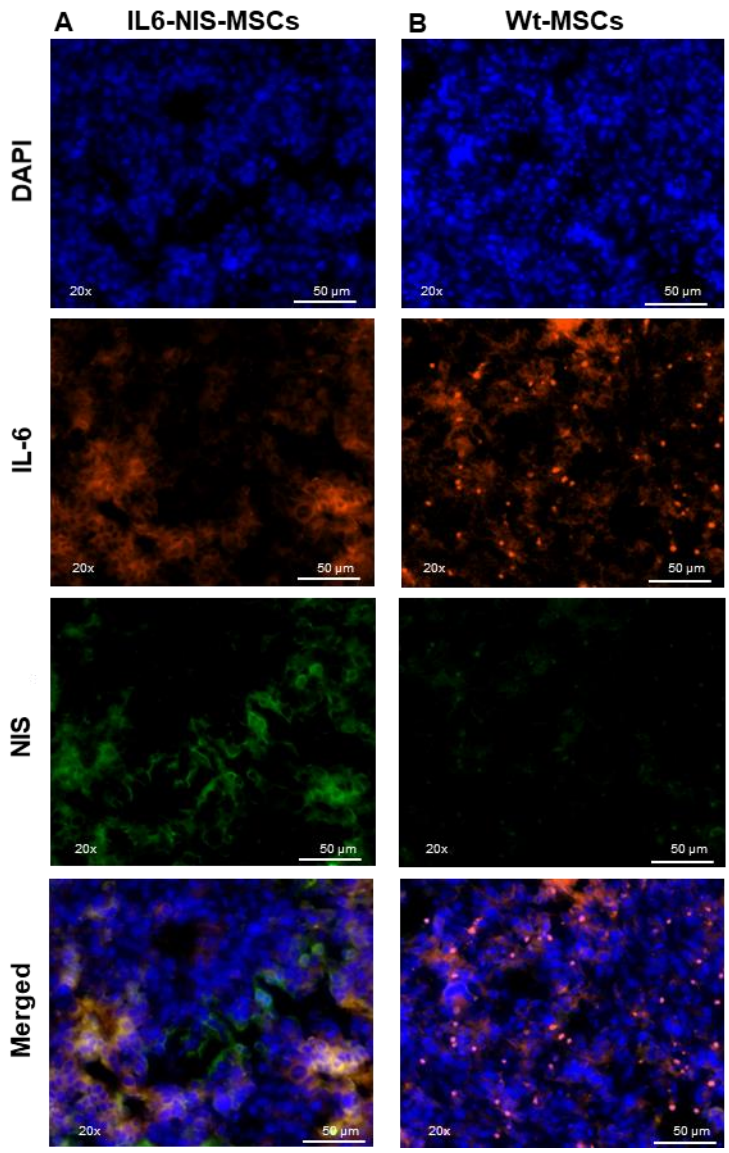

Figure S2*: Ex vivo* immunofluorescence analysis of GL261 tumors. (A) Representative images of co-localization of IL-6 (red) and NIS (green) protein expression in brain tumors after IL-6-NIS-MSC application. Tumors of Wt-MSC mice (**B**) showed no NIS protein expression despite IL-6 protein expression.

5 Summary

Glioblastoma (GBM) is a highly aggressive malignancy of the brain with a poor prognosis. Despite extensive research evaluating new therapies, no significant improvement in survival was achieved in the last decade. The main challenges for effective GBM therapy are the tumor location hampering complete resection within critical brain areas, heterogeneity of GBM limiting the efficacy of targeted therapies and, the blood-brain barrier (BBB) hampering drug delivery. To overcome these limitations, a mesenchymal stem cell (MSC)-based gene therapy approach targeting the GBM microenvironment (TME) was investigated within this doctoral thesis. Based on their inherent tumor-homing capabilities, MSCs are promising delivery vectors for anti-cancer therapy. MSCs were armed with the sodium iodide symporter (*NIS*) gene as an effector mechanism. *NIS* represents the oldest and well-characterized theranostic gene transporting iodide or other ions from the blood into NIS-expressing cells. NIS allows for *in vivo* monitoring of NIS-expressing MSCs and their fate in the body using nuclear medicine imaging techniques such as scintigraphy, SPECT, and PET after injection of suitable radiotracers (^{123}I, ^{124}I, ^{125}I, ^{18}F-TFB). In addition, the uptake of therapeutic radionuclides (e.g., ^{131}I, ^{188}Re, ^{211}At) by NIS-expressing MSCs recruited to the tumor site induce a therapy effect in neighboring cancer cells (bystander effect), while the MSCs themselves are eliminated (intrinsic suicide gene). In Chapters 1 and 2 of this thesis, requirements needed for a successful MSC-mediated *NIS* gene therapy in GBM have been investigated preclinically: i) delivery of NIS-MSCs across the BBB after intravenous injection, ii) optimal MSC dosing regimens, iii) BBB penetration of diagnostic and therapeutic NIS-radiotracers, iv) visualization of small volume tumor disease by high-resolution imaging techniques.

In GBM, high-resolution PET is the most appropriate technique to visualize low-volume disease. In Chapter 1, the two NIS PET tracers ^{124}I and ^{18}F-TFB were evaluated in terms of tumor accumulation and obtained resolution. The automated in-house synthesis of ^{18}F-TFB was established on an Eckert & Ziegler synthesis module within this thesis. For biological evaluation, a NIS-expressing human U87 glioblastoma cell line (U87-NIS) was generated and characterized *in vitro*. Mice harboring subcutaneous and intracranial U87-NIS xenografts were subjected to PET imaging following i.v. ^{124}I and ^{18}F-TFB application. A strong NIS-specific tumoral tracer uptake of ^{124}I (6.6 ± 2.1% ID/ml) and ^{18}F-TFB (6.8 ± 1.6% ID/ml) in the intracranial setting was observed. These experiments using U87-NIS xenografts represent an ideal case scenario with 100% NIS-positive cells with maximal tracer accumulation. To our knowledge, we were the first to show an improved image quality using NIS-based PET in preclinical glioma imaging.

While the study mentioned above used stably NIS-transfected GBM cells, we next systemically applied TME-homing NIS-MSCs and used the tested PET radiotracers to monitor their *in vivo* biodistribution in different GBM models. In Chapter 2, bone marrow-derived MSCs constitutively expressing NIS under the control of the CMV promoter were evaluated in subcutaneous GBM models, GL261 and U87, to demonstrate tumor homing of these MSCs. We observed a higher NIS-specific maximal uptake of ^{123}I following CMV-NIS-MSC administration in GL261 as compared to U87 tumors by scintigraphy. Based on these results, *in vivo* studies with more relevant orthotopically implanted GL261 cells were conducted as a next step. All used dosing regimens achieved a sufficiently high MSC recruitment to brain tumors, enabling their monitoring by ^{124}I PET and were confirmed by various *ex vivo* analysis methods. Based on the encouraging pre-therapy data and dosimetry from ^{124}I for ^{131}I, a subsequent therapy of GBM-bearing mice was conducted. Due to the aggressive growth of this model, a relatively fast and frequent treatment regimen was selected. Therapy mice (CMV-NIS-MSCs + ^{131}I) showed a reduction of tumor volume as analyzed by MRI and significantly extended survival as compared to control groups.

In Chapter 3, MSCs expressing the *NIS* gene under the control of a TME-inducible promoter were generated and characterized *in vitro*. Interleukin (IL)-6 is a multifunctional inflammatory cytokine that is highly abundant in the GBM TME. These IL-6-NIS-MSCs were investigated in the same orthotopic GL261 model and demonstrated NIS-specific ^{18}F-TFB uptake assessed by PET/MR imaging and an increased tumor-selective NIS expression analyzed *ex vivo* as compared to mice injected with CMV-NIS-MSCs. Unspecific detainment and/or off-target recruitment of MSCs to non-tumor tissue, which was observed to a low extent in the previous study using CMV-NIS-MSCs, was reduced. In GBM-bearing mice, IL-6-NIS-MSCs + ^{131}I increased the median survival up to 60%, CMV-NIS-MSC + ^{131}I led to a 67% extension of median survival, as compared to control groups. Although comparable treatment efficacy, we postulate that TME-inducible gene promoters driving NIS expression constitutes an elegant tool to add an additional layer of specificity.

Taken together, many challenges associated with GBM treatment could be effectively addressed by using MSC-based *NIS* gene therapy. As a future step, also towards clinical translation, the MSC-mediated *NIS* gene therapy allows for combination with other cancer therapies that could finally result in beneficial synergistic or additive effects.

6 Publications

6.1 Original Articles

Kitzberger C, Shehzad K, Morath V, Spellerberg R, Ranke J, Steiger K, Kälin RE, Multhoff G, Eiber M, Schilling F, Glass R, Weber WA, Wagner E, Nelson PJ, Spitzweg C. Interleukin-6-Controlled, Mesenchymal Stem Cell-based Sodium/Iodide Symporter Gene Therapy Improves Survival of Glioblastoma-bearing Mice. Mol Ther Oncolytics. 2023 Aug 15;30:238-253

Kitzberger C, Spellerberg R, Han Y, Schmohl KA, Stauss C, Zach C, Kälin RE, Multhoff G, Eiber M, Schilling F, Glass R, Weber WA, Wagner E, Nelson PJ, Spitzweg C. Mesenchymal Stem Cell-mediated Image-guided Sodium Iodide Symporter (NIS) Gene Therapy Improves Survival of Glioblastoma-bearing Mice. Clin Cancer Res. 2023 Mar 1;29(5):930-942

Spellerberg R, Benli-Hoppe T, **Kitzberger C**, Hageneier M, Schwenk N, Öztürk Ö, Steiger K, Multhoff G, Eiber M, Schilling F, Weber WA, Kälin RE, Glass R, Nelson PJ, Wagner E, Spitzweg C. Dual EGFR- and TfR-targeted gene transfer for sodium iodide symporter gene therapy of glioblastoma. Mol Ther Oncolytics. 2022 Nov 3;27:272-287

Kitzberger C, Spellerberg R, Morath V, Schwenk N, Schmohl KA, Schug C, Urnauer S, Tutter M, Eiber M, Schilling F, Weber WA, Ziegler S, Bartenstein P, Wagner E, Nelson PJ, Spitzweg C. The sodium iodide symporter (NIS) as theranostic gene: its emerging role in new imaging modalities and non-viral gene therapy. EJNMMI Res. 2022 May 3;12(1):25

Spellerberg R, Benli-Hoppe T, **Kitzberger C**, Berger S, Schmohl KA, Schwenk N, Yen HY, Zach C, Schilling F, Weber WA, Kälin RE, Glass R, Nelson PJ, Wagner E, Spitzweg C. Selective sodium iodide symporter (NIS) gene therapy of glioblastoma mediated by EGFR-targeted lipopolyplexes. Mol Ther Oncolytics. 2021 Oct 30;23:432-446

Koehler VF, Keller P, Waldmann E, Schwenk N, **Kitzberger C**, Schmohl KA, Knösel T, Stief CG, Spitzweg C. An unusual case of struma ovarii. Endocrinol Diabetes Metab Case Rep. 2021 Mar 5; 2021:20-0142

Tutter M, Schug C, Schmohl KA, Urnauer S, **Kitzberger C**, Schwenk N, Petrini M, Zach C, Ziegler S, Bartenstein P, Weber WA, Multhoff G, Wagner E, Lindner LH, Nelson PJ, Spitzweg C. Regional Hyperthermia Enhances Mesenchymal Stem Cell Recruitment to Tumor Stroma: Implications for Mesenchymal Stem Cell-Based Tumor Therapy. Mol Ther. 2021 Feb 3;29(2):788-803.

Schug C, **Kitzberger C**, Sievert W, Spellerberg R, Tutter M, Schmohl KA, Schwenk N, Zach C, Schwaiger M, Multhoff G, Wagner E, Nelson PJ and Spitzweg C. Radiation-induced Amplification of TGFB1-induced Mesenchymal Stem Cell-mediated NIS Gene 131I Therapy. Clin Cancer Res. 2019 Oct 1;25(19):5997-6008

6.2 Manuscripts in preparation

Kitzberger C*, Grashei M**, Sühnel S, Spellerberg R, Reder S, Steiger K, Kälin RE, Glass R, Weber WA, Nelson PJ, Schilling F#, Spitzweg C#. Hypoxia imaging-guided, mesenchymal stem cell-mediated sodium iodide symporter gene delivery in glioblastoma.

*, # Authors contributed equally

Han Y*, Koehler VF*, Nagarajah J, Schmohl KA, Stauss C, Schwenk N, Spellerberg R, **Kitzberger C**, Zach C, Steiger K, Morris JC, Weber WA, Bartenstein P, Ziegler SI, Nelson PJ, Spitzweg C. Using TGF-β1 Biology in Radioiodine Refractory Differentiated Thyroid Cancer to Re-establish Sodium Iodide Symporter Expression Using Engineered Mesenchymal Stem Cells as Therapy Vehicles.

* Authors contributed equally

6.3 Oral Presentations

91st Annual Meeting of the American Thyroid Association, Montreal, Canada, October 2022. **Kitzberger C**, Shehzad K, Morath V, Spellerberg R, Kälin KE, Glass R, Multhoff G, Eiber M, Schilling F, Weber WA, Wagner E, Nelson PJ, Spitzweg C. Tumor-Selective Interleukin-6-Targeted Mesenchymal Stem Cell-Mediated Sodium Iodide Symporter (NIS) Gene Therapy in Glioblastoma. S*hort presentation.*

23rd Annual Meeting of the Young Active Research in Endocrinology, Herrsching am Ammersee, Germany, September 2022. **Kitzberger C**. Mesenchymal Stem Cell-Mediated Sodium Iodide Symporter (NIS) Gene Therapy in Glioblastoma. *Invited speaker.*

65th Annual Meeting of the German Society of Endocrinology, virtual conference, Germany, March 2022. **Kitzberger C**, Grashei M, Sühnel S, Reder S, Spellerberg R, Steiger K, Glaß R, Weber WA, Nelson PJ, Schilling F, Spitzweg C. Hypoxia imaging-guided systemic mesenchymal stem cell-mediated sodium iodide symporter (NIS) gene delivery in glioblastoma.

90th Annual Meeting of the American Thyroid Association, virtual conference, October 2021. **Kitzberger C**, Spellerberg R, Sühnel S, Han Y, Schmoh KA, Kälin KE, Glaß R, Schilling F, Weber WA, Nelson PJ, Spitzweg C. Mesenchymal stem cell-mediated sodium iodide symporter (NIS) gene therapy in glioblastoma. *Highlighted oral session*.

European Molecular Imaging Meeting, Göttingen, August 2021. **Kitzberger C**, Grashei M, Spellerberg R, Steiger K, Sarker RSJ, Glaß R, Weber WA, Nelson PJ, Schilling F, Spitzweg C. Hypoxia imaging-guided systemic mesenchymal stem cell-mediated sodium iodide symporter (NIS) gene delivery in glioblastoma. *Study group „Image-Guided Drug Delivery "– short presentation.*

64th Annual Meeting of the German Society of Endocrinology, virtual conference, Germany, March 2021. **Kitzberger C**, Grashei M, Steiger K, Glaß R, Weber WA, Nelson PJ, Schilling F, Spitzweg C. Hypoxia-targeted imaging of glioblastoma after systemic mesenchymal stem cell-mediated sodium iodide symporter (NIS) reporter gene delivery.

42nd Annual Meeting of the European Thyroid Association, Budapest, Hungary, September 2019. **Kitzberger C**, Schmohl KA, Spellerberg R, Schug C, Tutter M, Schwenk N, Kälin RE, Glass R, Nelson PJ, Spitzweg C. Mesenchymal stem cell-mediated sodium iodide symporter (NIS) reporter gene delivery in glioblastoma

62nd Annual Meeting of the German Society of Endocrinology, Göttingen, Germany, March 2019. **Kitzberger C**, Schmohl KA, Spellerberg R, Tutter M, Schwenk N, Kälin RE, Glass R,

Nelson PJ, Spitzweg C. Mesenchymal stem cell-mediated sodium iodide symporter (NIS) reporter gene delivery in glioblastoma

18th Symposium Gentianum, Klausurtagung der Medizinischen Klinik und Poliklinik IV, Frauenchiemsee, Germany, Februar 2019. **Kitzberger C**, Spellerberg R Non-viral sodium iodide symporter (NIS) gene transfer in glioblastoma

6.4 Poster Presentations

91st Annual Meeting of the American Thyroid Association, Montreal, Canada, October 2022. **Kitzberger C**, Shehzad K, Morath V, Spellerberg R, Kälin KE, Glass R, Multhoff G, Eiber M, Schilling F, Weber WA, Wagner E, Nelson PJ, Spitzweg C. Tumor-Selective Interleukin-6-Targeted Mesenchymal Stem Cell-Mediated Sodium Iodide Symporter (NIS) Gene Therapy in Glioblastoma. *Highlighted Poster.*

European Molecular Imaging Meeting, Göttingen, August 2021. **Kitzberger C**, Grashei M, Spellerberg R, Steiger K, Sarker RSJ, Glaß R, Weber WA, Nelson PJ, Schilling F, Spitzweg C. Hypoxia imaging-guided systemic mesenchymal stem cell-mediated sodium iodide symporter (NIS) gene delivery in glioblastoma.

6.5 Awards and Grants

Travel grant, German Society of Endocrinology

91st Annual Meeting of the American Thyroid Association, Montreal, Canada, October 2022.

Poster award category “Radiotheranostics”

European Molecular Imaging Meeting, Göttingen, August 2021. **Kitzberger C**, Grashei M, Spellerberg R, Steiger K, Sarker RSJ, Glaß R, Weber WA, Nelson PJ, Schilling F, Spitzweg C. Hypoxia imaging-guided systemic mesenchymal stem cell-mediated sodium iodide symporter (NIS) gene delivery in glioblastoma.

Travel grant, German Society of Endocrinology

42nd Annual Meeting of the European Thyroid Association, Budapest, Hungary, September 2019.

7 References

1. Weinberg RA. The Biology of Cancer (2nd ed.). Garland Science, Taylor & Francis Group, LLC; 2013.
2. Hanahan D, Weinberg RA. Hallmarks of cancer: the next generation. *Cell* 2011;**144**(5):646-74.
3. Hanahan D, Weinberg RA. The Hallmarks of Cancer. *Cell* 2000;**100**(1):57-70.
4. Hanahan D. Hallmarks of Cancer: New Dimensions. *Cancer Discov* 2022;**12**(1):31-46.
5. Ostrom QT, Gittleman H, Truitt G, Boscia A, Kruchko C, Barnholtz-Sloan JS. CBTRUS Statistical Report: Primary Brain and Other Central Nervous System Tumors Diagnosed in the United States in 2011-2015. *Neuro Oncol* 2018;**20**(suppl_4):iv1-iv86.
6. Aldape K, Zadeh G, Mansouri S, Reifenberger G, von Deimling A. Glioblastoma: pathology, molecular mechanisms and markers. *Acta Neuropathol* 2015;**129**(6):829-48.
7. Canoll P, Goldman JE. The interface between glial progenitors and gliomas. *Acta Neuropathol* 2008;**116**(5):465-77.
8. Krebs in Deutschland für 2017/2018. Berlin, 2021: Robert Koch-Institut (Hrsg.) und die Gesellschaft der epidemiologischen Krebsregister in Deutschland e.V. (Hrsg.).
9. Davis ME. Glioblastoma: Overview of Disease and Treatment. *Clin J Oncol Nurs* 2016;**20**(5 Suppl):S2-8.
10. Solanki C, Sadana D, Arimappamagan A, Rao K, Rajeswaran J, Subbakrishna DK*, et al.* Impairments in Quality of Life and Cognitive Functions in Long-term Survivors of Glioblastoma. *J Neurosci Rural Pract* 2017;**8**(2):228-35.
11. Olar A, Aldape KD. Using the molecular classification of glioblastoma to inform personalized treatment. *The Journal of Pathology* 2014;**232**(2):165-77.
12. Kitzberger C, Spellerberg R, Han Y, Schmohl KA, Stauss C, Zach C*, et al.* Mesenchymal Stem Cell-mediated Image-guided Sodium Iodide Symporter (NIS) Gene Therapy Improves Survival of Glioblastoma-bearing Mice. *Clinical Cancer Research* 2022.
13. Louis DN, Perry A, Reifenberger G, von Deimling A, Figarella-Branger D, Cavenee WK*, et al.* The 2016 World Health Organization Classification of Tumors of the Central Nervous System: a summary. *Acta Neuropathol* 2016;**131**(6):803-20.
14. Verhaak RGW, Hoadley KA, Purdom E, Wang V, Qi Y, Wilkerson MD*, et al.* Integrated genomic analysis identifies clinically relevant subtypes of glioblastoma characterized by abnormalities in PDGFRA, IDH1, EGFR, and NF1. *Cancer Cell* 2010;**17**(1):98-110.
15. Wang H, Xu T, Jiang Y, Xu H, Yan Y, Fu D*, et al.* The Challenges and the Promise of Molecular Targeted Therapy in Malignant Gliomas. *Neoplasia* 2015;**17**(3):239-55.

16. Tan AC, Ashley DM, Lopez GY, Malinzak M, Friedman HS, Khasraw M. Management of glioblastoma: State of the art and future directions. *CA Cancer J Clin* 2020;**70**(4):299-312.

17. Aldape K, Brindle KM, Chesler L, Chopra R, Gajjar A, Gilbert MR*, et al.* Challenges to curing primary brain tumours. *Nature Reviews Clinical Oncology* 2019;**16**(8):509-20.

18. Daneman R, Prat A. The blood-brain barrier. *Cold Spring Harb Perspect Biol* 2015;**7**(1):a020412.

19. Pardridge WM, Boado RJ, Patrick DJ, Ka-Wai Hui E, Lu JZ. Blood-Brain Barrier Transport, Plasma Pharmacokinetics, and Neuropathology Following Chronic Treatment of the Rhesus Monkey with a Brain Penetrating Humanized Monoclonal Antibody Against the Human Transferrin Receptor. *Mol Pharm* 2018;**15**(11):5207-16.

20. Perrin SL, Samuel MS, Koszyca B, Brown MP, Ebert LM, Oksdath M*, et al.* Glioblastoma heterogeneity and the tumour microenvironment: implications for preclinical research and development of new treatments. *Biochem Soc Trans* 2019;**47**(2):625-38.

21. Mazilu L, Suceveanu A-I, Stanculeanu D-L, Gheorghe A-D, Fricatel G, Negru S-M. Tumor microenvironment is not an 'innocent bystander' in the resistance to treatment of head and neck cancers (Review). *Exp Ther Med* 2021;**22**(4):1128.

22. Anderson NM, Simon MC. The tumor microenvironment. *Curr Biol* 2020;**30**(16):R921-R5.

23. Yang L, Lin C, Wang L, Guo H, Wang X. Hypoxia and hypoxia-inducible factors in glioblastoma multiforme progression and therapeutic implications. *Exp Cell Res* 2012;**318**(19):2417-26.

24. Balkwill FR, Capasso M, Hagemann T. The tumor microenvironment at a glance. *Journal of Cell Science* 2012;**125**(23):5591-6.

25. Yeo ECF, Brown MP, Gargett T, Ebert LM. The Role of Cytokines and Chemokines in Shaping the Immune Microenvironment of Glioblastoma: Implications for Immunotherapy. *Cells* 2021;**10**(3).

26. Ebert LM, Yu W, Gargett T, Toubia J, Kollis PM, Tea MN*, et al.* Endothelial, pericyte and tumor cell expression in glioblastoma identifies fibroblast activation protein (FAP) as an excellent target for immunotherapy. *Clin Transl Immunology* 2020;**9**(10):e1191.

27. Brem S, Cotran R, Folkman J. Tumor Angiogenesis: A Quantitative Method for Histologic Grading2. *JNCI: Journal of the National Cancer Institute* 1972;**48**(2):347-56.

28. Stupp R, Mason WP, van den Bent MJ, Weller M, Fisher B, Taphoorn MJ*, et al.* Radiotherapy plus concomitant and adjuvant temozolomide for glioblastoma. *N Engl J Med* 2005;**352**(10):987-96.

29. Wilson TA, Karajannis MA, Harter DH. Glioblastoma multiforme: State of the art and future therapeutics. *Surg Neurol Int* 2014;**5**:64.

30. Batash R, Asna N, Schaffer P, Francis N, Schaffer M. Glioblastoma Multiforme, Diagnosis and Treatment; Recent Literature Review. *Curr Med Chem* 2017;**24**(27):3002-9.

31. Fabian D, Guillermo Prieto Eibl MDP, Alnahhas I, Sebastian N, Giglio P, Puduvalli V*, et al.* Treatment of Glioblastoma (GBM) with the Addition of Tumor-Treating Fields (TTF): A Review. *Cancers (Basel)* 2019;**11**(2).

32. Kirson ED, Dbalý V, Tovarys F, Vymazal J, Soustiel JF, Itzhaki A*, et al.* Alternating electric fields arrest cell proliferation in animal tumor models and human brain tumors. *Proc Natl Acad Sci U S A* 2007;**104**(24):10152-7.

33. Stupp R, Taillibert S, Kanner AA, Kesari S, Steinberg DM, Toms SA*, et al.* Maintenance Therapy With Tumor-Treating Fields Plus Temozolomide vs Temozolomide Alone for Glioblastoma: A Randomized Clinical Trial. *Jama* 2015;**314**(23):2535-43.

34. Fisher JP, Adamson DC. Current FDA-Approved Therapies for High-Grade Malignant Gliomas. *Biomedicines* 2021;**9**(3).

35. Fulci G, Chiocca EA. The status of gene therapy for brain tumors. *Expert Opin Biol Ther* 2007;**7**(2):197-208.

36. Hager S, Wagner E. Bioresponsive polyplexes - chemically programmed for nucleic acid delivery. *Expert Opin Drug Deliv* 2018;**15**(11):1067-83.

37. Ginn SL, Amaya AK, Alexander IE, Edelstein M, Abedi MR. Gene therapy clinical trials worldwide to 2017: An update. *The Journal of Gene Medicine* 2018;**20**(5):e3015.

38. Tobias A, Ahmed A, Moon KS, Lesniak MS. The art of gene therapy for glioma: a review of the challenging road to the bedside. *J Neurol Neurosurg Psychiatry* 2013;**84**(2):213-22.

39. Dai G, Levy O, Carrasco N. Cloning and characterization of the thyroid iodide transporter. *Nature* 1996;**379**(6564):458-60.

40. Smanik PA, Liu Q, Furminger TL, Ryu K, Xing S, Mazzaferri EL*, et al.* Cloning of the human sodium lodide symporter. *Biochem Biophys Res Commun* 1996;**226**(2):339-45.

41. Dohán O, De la Vieja A, Paroder V, Riedel C, Artani M, Reed M*, et al.* The sodium/iodide Symporter (NIS): characterization, regulation, and medical significance. *Endocr Rev* 2003;**24**(1):48-77.

42. Spitzweg C, Joba W, Schriever K, Goellner JR, Morris JC, Heufelder AE. Analysis of human sodium iodide symporter immunoreactivity in human exocrine glands. *J Clin Endocrinol Metab* 1999;**84**(11):4178-84.

43. Ravera S, Nicola JP, Salazar-De Simone G, Sigworth FJ, Karakas E, Amzel LM*, et al.* Structural insights into the mechanism of the sodium/iodide symporter. *Nature* 2022;**612**(7941):795-801.

44. Hingorani M, Spitzweg C, Vassaux G, Newbold K, Melcher A, Pandha H*, et al.* The biology of the sodium iodide symporter and its potential for targeted gene delivery. *Curr Cancer Drug Targets* 2010;**10**(2):242-67.

45. Llorente-Esteban A, Manville RW, Reyna-Neyra A, Abbott GW, Amzel LM, Carrasco N. Allosteric regulation of mammalian Na(+)/I(-) symporter activity by perchlorate. *Nat Struct Mol Biol* 2020;**27**(6):533-9.

46. Seidlin SM, Marinelli LD, Oshry E. Radioactive iodine therapy; effect on functioning metastases of adenocarcinoma of the thyroid. *J Am Med Assoc* 1946;**132**(14):838-47.

47. Hjiyiannakis P, Jefferies S, Harmer CL. Brain metastases in patients with differentiated thyroid carcinoma. *Clin Oncol (R Coll Radiol)* 1996;**8**(5):327-30.

48. Ravera S, Reyna-Neyra A, Ferrandino G, Amzel LM, Carrasco N. The Sodium/Iodide Symporter (NIS): Molecular Physiology and Preclinical and Clinical Applications. *Annu Rev Physiol* 2017;**79**:261-89.

49. Spitzweg C, Nelson PJ, Wagner E, Bartenstein P, Weber WA, Schwaiger M*, et al.* The sodium iodide symporter (NIS): novel applications for radionuclide imaging and treatment. *Endocr Relat Cancer* 2021;**28**(10):T193-T213.

50. Penheiter AR, Russell SJ, Carlson SK. The sodium iodide symporter (NIS) as an imaging reporter for gene, viral, and cell-based therapies. *Curr Gene Ther* 2012;**12**(1):33-47.

51. Kitzberger C, Spellerberg R, Morath V, Schwenk N, Schmohl KA, Schug C*, et al.* The sodium iodide symporter (NIS) as theranostic gene: its emerging role in new imaging modalities and non-viral gene therapy. *EJNMMI Res* 2022;**12**(1):25.

52. Cho JY, Shen DH, Yang W, Williams B, Buckwalter TL, La Perle KM*, et al.* In vivo imaging and radioiodine therapy following sodium iodide symporter gene transfer in animal model of intracerebral gliomas. *Gene Ther* 2002;**9**(17):1139-45.

53. Guo R, Xi Y, Zhang M, Miao Y, Zhang M, Li B. Human sodium iodide transporter gene-mediated imaging and therapy of mouse glioma, comparison between (188)Re and (131)I. *Oncol Lett* 2018;**15**(3):3911-7.

54. Opyrchal M, Allen C, Iankov I, Aderca I, Schroeder M, Sarkaria J*, et al.* Effective radiovirotherapy for malignant gliomas by using oncolytic measles virus strains encoding the sodium iodide symporter (MV-NIS). *Hum Gene Ther* 2012;**23**(4):419-27.

55. Lachelt U, Wagner E. Nucleic Acid Therapeutics Using Polyplexes: A Journey of 50 Years (and Beyond). *Chem Rev* 2015;**115**(19):11043-78.

56. Schmohl KA, Dolp P, Schug C, Knoop K, Klutz K, Schwenk N*, et al.* Reintroducing the Sodium-Iodide Symporter to Anaplastic Thyroid Carcinoma. *Thyroid* 2017;**27**(12):1534-43.

57. Urnauer S, Muller AM, Schug C, Schmohl KA, Tutter M, Schwenk N*, et al.* EGFR-targeted nonviral NIS gene transfer for bioimaging and therapy of disseminated colon cancer metastases. *Oncotarget* 2017;**8**(54):92195-208.

58. Klutz K, Schaffert D, Willhauck MJ, Grunwald GK, Haase R, Wunderlich N*, et al.* Epidermal growth factor receptor-targeted (131)I-therapy of liver cancer following systemic delivery of the sodium iodide symporter gene. *Mol Ther* 2011;**19**(4):676-85.

59. Schmohl KA, Gupta A, Grunwald GK, Trajkovic-Arsic M, Klutz K, Braren R*, et al.* Imaging and targeted therapy of pancreatic ductal adenocarcinoma using the theranostic sodium iodide symporter (NIS) gene. *Oncotarget* 2017;**8**(20):33393-404.

60. Klein PM, Kern S, Lee DJ, Schmaus J, Höhn M, Gorges J*, et al.* Folate receptor-directed orthogonal click-functionalization of siRNA lipopolyplexes for tumor cell killing in vivo. *Biomaterials* 2018;**178**:630-42.

61. Spellerberg R, Benli-Hoppe T, Kitzberger C, Berger S, Schmohl KA, Schwenk N*, et al.* Selective sodium iodide symporter (NIS) genetherapy of glioblastoma mediatedby EGFR-targeted lipopolyplexes. *Molecular Therapy - Oncolytics* 2021;**23**:432-46.

62. Spellerberg R, Benli-Hoppe T, Kitzberger C, Hageneier M, Schwenk N, Öztürk Ö*, et al.* Dual EGFR- and TfR-targeted gene transfer for sodium iodide symporter gene therapy of glioblastoma. *Mol Ther Oncolytics* 2022;**27**:272-87.

63. Knoop K, Kolokythas M, Klutz K, Willhauck MJ, Wunderlich N, Draganovici D*, et al.* Image-guided, tumor stroma-targeted 131I therapy of hepatocellular cancer after systemic mesenchymal stem cell-mediated NIS gene delivery. *Mol Ther* 2011;**19**(9):1704-13.

64. Muller AM, Schmohl KA, Knoop K, Schug C, Urnauer S, Hagenhoff A*, et al.* Hypoxia-targeted 131I therapy of hepatocellular cancer after systemic mesenchymal stem cell-mediated sodium iodide symporter gene delivery. *Oncotarget* 2016;**7**(34):54795-810.

65. Schug C, Urnauer S, Jaeckel C, Schmohl KA, Tutter M, Steiger K*, et al.* TGFB1-driven mesenchymal stem cell-mediated NIS gene transfer. *Endocr Relat Cancer* 2019;**26**(1):89-101.

66. Schug C, Gupta A, Urnauer S, Steiger K, Cheung PF, Neander C*, et al.* A Novel Approach for Image-Guided (131)I Therapy of Pancreatic Ductal Adenocarcinoma Using Mesenchymal Stem Cell-Mediated NIS Gene Delivery. *Mol Cancer Res* 2019;**17**(1):310-20.

67. Tutter M, Schug C, Schmohl KA, Urnauer S, Schwenk N, Petrini M*, et al.* Effective control of tumor growth through spatial and temporal control of theranostic sodium iodide symporter (NIS) gene expression using a heat-inducible gene promoter in engineered mesenchymal stem cells. *Theranostics* 2020;**10**(10):4490-506.

68. Sakemura R, Bansal A, Siegler EL, Hefazi M, Yang N, Khadka RH*, et al.* Development of a Clinically Relevant Reporter for Chimeric Antigen Receptor T-cell Expansion, Trafficking, and Toxicity. *Cancer Immunol Res* 2021;**9**(9):1035-46.

69. Volpe A, Lang C, Lim L, Man F, Kurtys E, Ashmore-Harris C*, et al.* Spatiotemporal PET Imaging Reveals Differences in CAR-T Tumor Retention in Triple-Negative Breast Cancer Models. *Mol Ther* 2020;**28**(10):2271-85.

70. Pittenger MF, Mackay AM, Beck SC, Jaiswal RK, Douglas R, Mosca JD*, et al.* Multilineage potential of adult human mesenchymal stem cells. *Science* 1999;**284**(5411):143-7.

71. Friedenstein AJ, Chailakhjan RK, Lalykina KS. The development of fibroblast colonies in monolayer cultures of guinea-pig bone marrow and spleen cells. *Cell Tissue Kinet* 1970;**3**(4):393-403.

72. Friedenstein AJ, Deriglasova UF, Kulagina NN, Panasuk AF, Rudakowa SF, Luria EA*, et al.* Precursors for fibroblasts in different populations of hematopoietic cells as detected by the in vitro colony assay method. *Exp Hematol* 1974;**2**(2):83-92.

73. Viswanathan S, Shi Y, Galipeau J, Krampera M, Leblanc K, Martin I*, et al.* Mesenchymal stem versus stromal cells: International Society for Cell & Gene Therapy (ISCT(R)) Mesenchymal Stromal Cell committee position statement on nomenclature. *Cytotherapy* 2019;**21**(10):1019-24.

74. Hagenhoff A, Bruns CJ, Zhao Y, von Luttichau I, Niess H, Spitzweg C*, et al.* Harnessing mesenchymal stem cell homing as an anticancer therapy. *Expert Opin Biol Ther* 2016;**16**(9):1079-92.

75. Knoop K, Schwenk N, Dolp P, Willhauck MJ, Zischek C, Zach C*, et al.* Stromal targeting of sodium iodide symporter using mesenchymal stem cells allows enhanced imaging and therapy of hepatocellular carcinoma. *Hum Gene Ther* 2013;**24**(3):306-16.

76. Zischek C, Niess H, Ischenko I, Conrad C, Huss R, Jauch KW*, et al.* Targeting tumor stroma using engineered mesenchymal stem cells reduces the growth of pancreatic carcinoma. *Ann Surg* 2009;**250**(5):747-53.

77. Mohr A, Lyons M, Deedigan L, Harte T, Shaw G, Howard L*, et al.* Mesenchymal stem cells expressing TRAIL lead to tumour growth inhibition in an experimental lung cancer model. *J Cell Mol Med* 2008;**12**(6b):2628-43.

78. Grisendi G, Bussolari R, Cafarelli L, Petak I, Rasini V, Veronesi E*, et al.* Adipose-derived mesenchymal stem cells as stable source of tumor necrosis factor-related apoptosis-inducing ligand delivery for cancer therapy. *Cancer research* 2010;**70**(9):3718-29.

79. Dvorak HF. Tumors: wounds that do not heal. Similarities between tumor stroma generation and wound healing. *N Engl J Med* 1986;**315**(26):1650-9.

80. Musial-Wysocka A, Kot M, Majka M. The Pros and Cons of Mesenchymal Stem Cell-Based Therapies. *Cell Transplant* 2019;**28**(7):801-12.

81. Nowak B, Rogujski P, Janowski M, Lukomska B, Andrzejewska A. Mesenchymal stem cells in glioblastoma therapy and progression: How one cell does it all. *Biochim Biophys Acta Rev Cancer* 2021;**1876**(1):188582.

82. Studeny M, Marini FC, Dembinski JL, Zompetta C, Cabreira-Hansen M, Bekele BN*, et al.* Mesenchymal stem cells: potential precursors for tumor stroma and targeted-delivery vehicles for anticancer agents. *J Natl Cancer Inst* 2004;**96**(21):1593-603.

83. Katakowski M, Buller B, Zheng X, Lu Y, Rogers T, Osobamiro O*, et al.* Exosomes from marrow stromal cells expressing miR-146b inhibit glioma growth. *Cancer Lett* 2013;**335**(1):201-4.

84. Miletic H, Fischer Y, Litwak S, Giroglou T, Waerzeggers Y, Winkeler A*, et al.* Bystander killing of malignant glioma by bone marrow-derived tumor-infiltrating progenitor cells expressing a suicide gene. *Mol Ther* 2007;**15**(7):1373-81.

85. Chang DY, Yoo SW, Hong Y, Kim S, Kim SJ, Yoon SH*, et al.* The growth of brain tumors can be suppressed by multiple transplantation of mesenchymal stem cells expressing cytosine deaminase. *Int J Cancer* 2010;**127**(8):1975-83.

86. Ahmed AU, Tyler MA, Thaci B, Alexiades NG, Han Y, Ulasov IV*, et al.* A comparative study of neural and mesenchymal stem cell-based carriers for oncolytic adenovirus in a model of malignant glioma. *Mol Pharm* 2011;**8**(5):1559-72.

87. Mangraviti A, Tzeng SY, Gullotti D, Kozielski KL, Kim JE, Seng M*, et al.* Non-virally engineered human adipose mesenchymal stem cells produce BMP4, target brain tumors, and extend survival. *Biomaterials* 2016;**100**:53-66.

88. Cao B, Yang M, Zhu Y, Qu X, Mao C. Stem cells loaded with nanoparticles as a drug carrier for in vivo breast cancer therapy. *Adv Mater* 2014;**26**(27):4627-31.

89. Knoop K, Schwenk N, Schmohl K, Muller A, Zach C, Cyran C*, et al.* Mesenchymal stem cell-mediated, tumor stroma-targeted radioiodine therapy of metastatic colon cancer using the sodium iodide symporter as theranostic gene. *J Nucl Med* 2015;**56**(4):600-6.

90. Schug C, Kitzberger C, Sievert W, Spellerberg R, Tutter M, Schmohl KA*, et al.* Radiation-Induced Amplification of TGFB1-Induced Mesenchymal Stem Cell-Mediated Sodium Iodide Symporter (NIS) Gene (131)I Therapy. *Clin Cancer Res* 2019;**25**(19):5997-6008.

91. Schmohl KA, Mueller AM, Dohmann M, Spellerberg R, Urnauer S, Schwenk N*, et al.* Integrin alphavbeta3-Mediated Effects of Thyroid Hormones on Mesenchymal Stem Cells in Tumor Angiogenesis. *Thyroid* 2019;**29**(12):1843-57.

92. Albertsson P, Bäck T, Bergmark K, Hallqvist A, Johansson M, Aneheim E*, et al.* Astatine-211 based radionuclide therapy: Current clinical trial landscape. *Front Med (Lausanne)* 2022;**9**:1076210.

93. Bexell D, Gunnarsson S, Svensson A, Tormin A, Henriques-Oliveira C, Siesjo P*, et al.* Rat multipotent mesenchymal stromal cells lack long-distance tropism to 3 different rat glioma models. *Neurosurgery* 2012;**70**(3):731-9.

94. Schug C, Sievert W, Urnauer S, Muller AM, Schmohl KA, Wechselberger A*, et al.* External Beam Radiation Therapy Enhances Mesenchymal Stem Cell-Mediated Sodium-Iodide Symporter Gene Delivery. *Hum Gene Ther* 2018;**29**(11):1287-300.

95. Thomas JG, Parker Kerrigan BC, Hossain A, Gumin J, Shinojima N, Nwajei F*, et al.* Ionizing radiation augments glioma tropism of mesenchymal stem cells. *J Neurosurg* 2018;**128**(1):287-95.

96. Klopp AH, Spaeth EL, Dembinski JL, Woodward WA, Munshi A, Meyn RE*, et al.* Tumor irradiation increases the recruitment of circulating mesenchymal stem cells into the tumor microenvironment. *Cancer Res* 2007;**67**(24):11687-95.

97. Zielske SP, Livant DL, Lawrence TS. Radiation increases invasion of gene-modified mesenchymal stem cells into tumors. *Int J Radiat Oncol Biol Phys* 2009;**75**(3):843-53.

98. Shi S, Zhang M, Guo R, Miao Y, Li B. Bone Marrow-Derived Mesenchymal Stem Cell-Mediated Dual-Gene Therapy for Glioblastoma. *Hum Gene Ther* 2019;**30**(1):106-17.

99. François S, Bensidhoum M, Mouiseddine M, Mazurier C, Allenet B, Semont A*, et al.* Local irradiation not only induces homing of human mesenchymal stem cells at exposed sites but promotes their widespread engraftment to multiple organs: a study of their quantitative distribution after irradiation damage. *Stem Cells* 2006;**24**(4):1020-9.

100. Friedman JE. Immune Modulation by Ionizing Radiation and its Implications for Cancer Immunotherapy. *Current Pharmaceutical Design* 2002;**8**(19):1765-80.

101. Tutter M, Schug C, Schmohl KA, Urnauer S, Kitzberger C, Schwenk N*, et al.* Regional Hyperthermia Enhances Mesenchymal Stem Cell Recruitment to Tumor Stroma: Implications for Mesenchymal Stem Cell-Based Tumor Therapy. *Mol Ther* 2021;**29**(2):788-803.

102. De La Vieja A, Dohan O, Levy O, Carrasco N. Molecular analysis of the sodium/iodide symporter: impact on thyroid and extrathyroid pathophysiology. *Physiol Rev* 2000;**80**(3):1083-105.

103. Spitzweg C, Bible KC, Hofbauer LC, Morris JC. Advanced radioiodine-refractory differentiated thyroid cancer: the sodium iodide symporter and other emerging therapeutic targets. *Lancet Diabetes Endocrinol* 2014;**2**(10):830-42.

104. Willhauck MJ, Sharif Samani BR, Gildehaus FJ, Wolf I, Senekowitsch-Schmidtke R, Stark HJ*, et al.* Application of 188rhenium as an alternative radionuclide for treatment of prostate cancer after tumor-specific sodium iodide symporter gene expression. *J Clin Endocrinol Metab* 2007;**92**(11):4451-8.

105. Willhauck MJ, Samani BR, Wolf I, Senekowitsch-Schmidtke R, Stark HJ, Meyer GJ*, et al.* The potential of 211Astatine for NIS-mediated radionuclide therapy in prostate cancer. *Eur J Nucl Med Mol Imaging* 2008;**35**(7):1272-81.

106. Dadachova E, Bouzahzah B, Zuckier LS, Pestell RG. Rhenium-188 as an alternative to Iodine-131 for treatment of breast tumors expressing the sodium/iodide symporter (NIS). *Nucl Med Biol* 2002;**29**(1):13-8.

107. Shimura H, Haraguchi K, Miyazaki A, Endo T, Onaya T. Iodide uptake and experimental 131I therapy in transplanted undifferentiated thyroid cancer cells expressing the Na+/I- symporter gene. *Endocrinology* 1997;**138**(10):4493-6.

108. Schafer A, Pahnke A, Schaffert D, van Weerden WM, de Ridder CM, Rodl W*, et al.* Disconnecting the yin and yang relation of epidermal growth factor receptor (EGFR)-mediated delivery: a fully synthetic, EGFR-targeted gene transfer system avoiding receptor activation. *Hum Gene Ther* 2011;**22**(12):1463-73.

109. He D, Wagner E. Defined polymeric materials for gene delivery. *Macromol Biosci* 2015;**15**(5):600-12.

110. Kos P, Lachelt U, Herrmann A, Mickler FM, Doblinger M, He D*, et al.* Histidine-rich stabilized polyplexes for cMet-directed tumor-targeted gene transfer. *Nanoscale* 2015;**7**(12):5350-62.

111. Urnauer S, Morys S, Krhac Levacic A, Muller AM, Schug C, Schmohl KA*, et al.* Sequence-defined cMET/HGFR-targeted Polymers as Gene Delivery Vehicles for the Theranostic Sodium Iodide Symporter (NIS) Gene. *Mol Ther* 2016;**24**(8):1395-404.

112. Urnauer S, Schmohl KA, Tutter M, Schug C, Schwenk N, Morys S, *et al.* Dual-targeted NIS polyplexes-a theranostic strategy toward tumors with heterogeneous receptor expression. *Gene Ther* 2019;**26**(3-4):93-108.

113. Melzer C, Yang Y, Hass R. Interaction of MSC with tumor cells. *Cell Commun Signal* 2016;**14**(1):20.

114. Schmohl KA, Müller AM, Wechselberger A, Rühland S, Salb N, Schwenk N, *et al.* Thyroid hormones and tetrac: new regulators of tumour stroma formation via integrin αvβ3. *Endocrine-related cancer* 2015;**22**(6):941-52.

115. Droujinine IA, Eckert MA, Zhao W. To grab the stroma by the horns: from biology to cancer therapy with mesenchymal stem cells. *Oncotarget* 2013;**4**(5):651-64.

116. Birnbaum T, Roider J, Schankin CJ, Padovan CS, Schichor C, Goldbrunner R, *et al.* Malignant gliomas actively recruit bone marrow stromal cells by secreting angiogenic cytokines. *J Neurooncol* 2007;**83**(3):241-7.

117. Niess H, von Einem JC, Thomas MN, Michl M, Angele MK, Huss R, *et al.* Treatment of advanced gastrointestinal tumors with genetically modified autologous mesenchymal stromal cells (TREAT-ME1): study protocol of a phase I/II clinical trial. *BMC Cancer* 2015;**15**:237.

118. Spitzweg C. Gene therapy in thyroid cancer. *Horm Metab Res* 2009;**41**(6):500-9.

119. Jiang H, DeGrado TR. [(18)F]Tetrafluoroborate ([(18)F]TFB) and its analogs for PET imaging of the sodium/iodide symporter. *Theranostics* 2018;**8**(14):3918-31.

120. Samnick S, Al-Momani E, Schmid JS, Mottok A, Buck AK, Lapa C. Initial Clinical Investigation of [18F]Tetrafluoroborate PET/CT in Comparison to [124I]Iodine PET/CT for Imaging Thyroid Cancer. *Clin Nucl Med* 2018;**43**(3):162-7.

121. Portulano C, Paroder-Belenitsky M, Carrasco N. The Na+/I- symporter (NIS): mechanism and medical impact. *Endocr Rev* 2014;**35**(1):106-49.

122. Dittmann M, Gonzalez Carvalho JM, Rahbar K, Schafers M, Claesener M, Riemann B, *et al.* Incremental diagnostic value of [(18)F]tetrafluoroborate PET-CT compared to [(131)I]iodine scintigraphy in recurrent differentiated thyroid cancer. *Eur J Nucl Med Mol Imaging* 2020;**47**(11):2639-46.

123. Jauregui-Osoro M, Sunassee K, Weeks AJ, Berry DJ, Paul RL, Cleij M, *et al.* Synthesis and biological evaluation of [(18)F]tetrafluoroborate: a PET imaging agent for thyroid disease and reporter gene imaging of the sodium/iodide symporter. *Eur J Nucl Med Mol Imaging* 2010;**37**(11):2108-16.

124. Khoshnevisan A, Jauregui-Osoro M, Shaw K, Torres JB, Young JD, Ramakrishnan NK, *et al.* [(18)F]tetrafluoroborate as a PET tracer for the sodium/iodide symporter: the importance of specific activity. *EJNMMI Res* 2016;**6**(1):34.

125. O'Doherty J, Jauregui-Osoro M, Brothwood T, Szyszko T, Marsden PK, O'Doherty MJ, *et al.* (18)F-Tetrafluoroborate, a PET Probe for Imaging Sodium/Iodide Symporter Expression: Whole-Body Biodistribution, Safety, and Radiation Dosimetry in Thyroid Cancer Patients. *J Nucl Med* 2017;**58**(10):1666-71.

126. Jiang H, Schmit NR, Koenen AR, Bansal A, Pandey MK, Glynn RB, *et al.* Safety, pharmacokinetics, metabolism and radiation dosimetry of (18)F-

tetrafluoroborate ((18)F-TFB) in healthy human subjects. *EJNMMI Res* 2017;**7**(1):90.

127. Jiang H, Bansal A, Pandey MK, Peng KW, Suksanpaisan L, Russell SJ*, et al.* Synthesis of 18F-Tetrafluoroborate via Radiofluorination of Boron Trifluoride and Evaluation in a Murine C6-Glioma Tumor Model. *J Nucl Med* 2016;**57**(9):1454-9.

128. Nagarajah J, Le M, Knauf JA, Ferrandino G, Montero-Conde C, Pillarsetty N*, et al.* Sustained ERK inhibition maximizes responses of BrafV600E thyroid cancers to radioiodine. *J Clin Invest* 2016;**126**(11):4119-24.

129. Diocou S, Volpe A, Jauregui-Osoro M, Boudjemeline M, Chuamsaamarkkee K, Man F*, et al.* [(18)F]tetrafluoroborate-PET/CT enables sensitive tumor and metastasis in vivo imaging in a sodium iodide symporter-expressing tumor model. *Sci Rep* 2017;**7**(1):946.

130. Verburg FA, Giovanella L, Hoffmann M, Iakovou I, Mihailovic J, Ovcaricek PP*, et al.* New! F-18-based PET/CT for sodium-iodine-symporter-targeted imaging! *Eur J Nucl Med Mol Imaging* 2020;**47**(11):2484-6.

131. Ho AL, Grewal RK, Leboeuf R, Sherman EJ, Pfister DG, Deandreis D*, et al.* Selumetinib-enhanced radioiodine uptake in advanced thyroid cancer. *N Engl J Med* 2013;**368**(7):623-32.

132. Jentzen W, Hoppenbrouwers J, van Leeuwen P, van der Velden D, van de Kolk R, Poeppel TD*, et al.* Assessment of lesion response in the initial radioiodine treatment of differentiated thyroid cancer using 124I PET imaging. *J Nucl Med* 2014;**55**(11):1759-65.

133. Castillo-Rivera F, Ondo-Mendez A, Guglielmi J, Guigonis JM, Jing L, Lindenthal S*, et al.* Tumor microenvironment affects exogenous sodium/iodide symporter expression. *Transl Oncol* 2021;**14**(1):100937.

134. Weller M, van den Bent M, Preusser M, Le Rhun E, Tonn JC, Minniti G*, et al.* EANO guidelines on the diagnosis and treatment of diffuse gliomas of adulthood. *Nature Reviews Clinical Oncology* 2021;**18**(3):170-86.

135. Birzu C, French P, Caccese M, Cerretti G, Idbaih A, Zagonel V*, et al.* Recurrent Glioblastoma: From Molecular Landscape to New Treatment Perspectives. *Cancers* 2021;**13**(1):47.

136. Terstappen GC, Meyer AH, Bell RD, Zhang W. Strategies for delivering therapeutics across the blood-brain barrier. *Nat Rev Drug Discov* 2021;**20**(5):362-83.

137. Sarkaria JN, Hu LS, Parney IF, Pafundi DH, Brinkmann DH, Laack NN*, et al.* Is the blood-brain barrier really disrupted in all glioblastomas? A critical assessment of existing clinical data. *Neuro Oncol* 2018;**20**(2):184-91.

138. Bonavia R, Inda MM, Cavenee WK, Furnari FB. Heterogeneity maintenance in glioblastoma: a social network. *Cancer Res* 2011;**71**(12):4055-60.

139. Charles NA, Holland EC, Gilbertson R, Glass R, Kettenmann H. The brain tumor microenvironment. *Glia* 2012;**60**(3):502-14.

140. Stefani FR, Eberstål S, Vergani S, Kristiansen TA, Bengzon J. Low-dose irradiated mesenchymal stromal cells break tumor defensive properties in vivo. *Int J Cancer* 2018;**143**(9):2200-12.

141. Bexell D, Gunnarsson S, Tormin A, Darabi A, Gisselsson D, Roybon L*, et al.* Bone marrow multipotent mesenchymal stroma cells act as pericyte-like migratory vehicles in experimental gliomas. *Mol Ther* 2009;**17**(1):183-90.

142. Nakamura K, Ito Y, Kawano Y, Kurozumi K, Kobune M, Tsuda H*, et al.* Antitumor effect of genetically engineered mesenchymal stem cells in a rat glioma model. *Gene Ther* 2004;**11**(14):1155-64.

143. Aboody KS, Brown A, Rainov NG, Bower KA, Liu S, Yang W*, et al.* Neural stem cells display extensive tropism for pathology in adult brain: evidence from intracranial gliomas. *Proc Natl Acad Sci U S A* 2000;**97**(23):12846-51.

144. Nakamizo A, Marini F, Amano T, Khan A, Studeny M, Gumin J*, et al.* Human bone marrow-derived mesenchymal stem cells in the treatment of gliomas. *Cancer Res* 2005;**65**(8):3307-18.

145. Al-Kharboosh R, ReFaey K, Lara-Velazquez M, Grewal SS, Imitola J, Quinones-Hinojosa A. Inflammatory Mediators in Glioma Microenvironment Play a Dual Role in Gliomagenesis and Mesenchymal Stem Cell Homing: Implication for Cellular Therapy. *Mayo Clin Proc Innov Qual Outcomes* 2020;**4**(4):443-59.

146. Spaeth E, Klopp A, Dembinski J, Andreeff M, Marini F. Inflammation and tumor microenvironments: defining the migratory itinerary of mesenchymal stem cells. *Gene Ther* 2008;**15**(10):730-8.

147. Liu L, Eckert MA, Riazifar H, Kang DK, Agalliu D, Zhao W. From blood to the brain: can systemically transplanted mesenchymal stem cells cross the blood-brain barrier? *Stem Cells Int* 2013;**2013**:435093.

148. Choi SA, Hwang SK, Wang KC, Cho BK, Phi JH, Lee JY*, et al.* Therapeutic efficacy and safety of TRAIL-producing human adipose tissue-derived mesenchymal stem cells against experimental brainstem glioma. *Neuro Oncol* 2011;**13**(1):61-9.

149. Chiu AC, Delpassand ES, Sherman SI. Prognosis and treatment of brain metastases in thyroid carcinoma. *J Clin Endocrinol Metab* 1997;**82**(11):3637-42.

150. Vrachimis A, Schmid KW, Jurgens H, Schober O, Weckesser M, Riemann B. Cerebral metastases from thyroid carcinoma: complete remission following radioiodine treatment. *Dtsch Arztebl Int* 2013;**110**(50):861-6.

151. Oh T, Fakurnejad S, Sayegh ET, Clark AJ, Ivan ME, Sun MZ*, et al.* Immunocompetent murine models for the study of glioblastoma immunotherapy. *J Transl Med* 2014;**12**:107.

152. Niess H, Bao Q, Conrad C, Zischek C, Notohamiprodjo M, Schwab F*, et al.* Selective targeting of genetically engineered mesenchymal stem cells to tumor stroma microenvironments using tissue-specific suicide gene expression suppresses growth of hepatocellular carcinoma. *Ann Surg* 2011;**254**(5):767-74; discussion 74-5.

153. Franklin KBJPG. Paxino's and Franklin's the Mouse Brain in Stereotaxic Coordinates : Compact 5th Edition. 2019.

154. Zhao D, Zhang H, Uyar R, Hossain JA, Miletic H, Tonn JC*, et al.* Comparing Tumor Cell Invasion and Myeloid Cell Composition in Compatible Primary and Relapsing Glioblastoma. *Cancers (Basel)* 2021;**13**(14).

155. Pacioni S, D'Alessandris QG, Giannetti S, Morgante L, Cocce V, Bonomi A*, et al.* Human mesenchymal stromal cells inhibit tumor growth in orthotopic glioblastoma xenografts. *Stem Cell Res Ther* 2017;**8**(1):53.

156. Wu X, Hu J, Zhou L, Mao Y, Yang B, Gao L*, et al.* In vivo tracking of superparamagnetic iron oxide nanoparticle-labeled mesenchymal stem cell tropism to malignant gliomas using magnetic resonance imaging. Laboratory investigation. *J Neurosurg* 2008;**108**(2):320-9.

157. Fischer UM, Harting MT, Jimenez F, Monzon-Posadas WO, Xue H, Savitz SI*, et al.* Pulmonary passage is a major obstacle for intravenous stem cell delivery: the pulmonary first-pass effect. *Stem Cells Dev* 2009;**18**(5):683-92.

158. Ma Q, Schlegel F, Bachmann SB, Schneider H, Decker Y, Rudin M*, et al.* Lymphatic outflow of cerebrospinal fluid is reduced in glioma. *Sci Rep* 2019;**9**(1):14815.

159. Toh CH, Siow TY. Factors Associated With Dysfunction of Glymphatic System in Patients With Glioma. *Front Oncol* 2021;**11**:744318.

160. Cserr HF, Berman BJ. Iodide and thiocyanate efflux from brain following injection into rat caudate nucleus. *Am J Physiol* 1978;**235**(4):F331-7.

161. Davson H, Hollingsworth JR. Active transport of 131-I across the blood-brain barrier. *J Physiol* 1973;**233**(2):327-47.

162. Mogensen FL, Delle C, Nedergaard M. The Glymphatic System (En)during Inflammation. *Int J Mol Sci* 2021;**22**(14).

163. Pavon LF, Sibov TT, de Souza AV, da Cruz EF, Malheiros SMF, Cabral FR*, et al.* Tropism of mesenchymal stem cell toward CD133(+) stem cell of glioblastoma in vitro and promote tumor proliferation in vivo. *Stem Cell Res Ther* 2018;**9**(1):310.

164. Mastrella G, Hou M, Li M, Stoecklein VM, Zdouc N, Volmar MNM*, et al.* Targeting APLN/APLNR Improves Antiangiogenic Efficiency and Blunts Proinvasive Side Effects of VEGFA/VEGFR2 Blockade in Glioblastoma. *Cancer Res* 2019;**79**(9):2298-313.

165. Pitter KL, Tamagno I, Alikhanyan K, Hosni-Ahmed A, Pattwell SS, Donnola S*, et al.* Corticosteroids compromise survival in glioblastoma. *Brain* 2016;**139**(Pt 5):1458-71.

166. Stock K, Kumar J, Synowitz M, Petrosino S, Imperatore R, Smith ESJ*, et al.* Neural precursor cells induce cell death of high-grade astrocytomas through stimulation of TRPV1. *Nature Medicine* 2012;**18**(8):1232-8.

167. Mohme M, Maire CL, Geumann U, Schliffke S, Dührsen L, Fita K*, et al.* Local Intracerebral Immunomodulation Using Interleukin-Expressing Mesenchymal Stem Cells in Glioblastoma. *Clinical Cancer Research* 2020;**26**(11):2626-39.

168. Reardon DA, Gokhale PC, Klein SR, Ligon KL, Rodig SJ, Ramkissoon SH*, et al.* Glioblastoma Eradication Following Immune Checkpoint Blockade in an Orthotopic, Immunocompetent Model. *Cancer Immunol Res* 2016;**4**(2):124-35.

169. Wu S, Calero-Perez P, Arus C, Candiota AP. Anti-PD-1 Immunotherapy in Preclinical GL261 Glioblastoma: Influence of Therapeutic Parameters and Non-Invasive Response Biomarker Assessment with MRSI-Based Approaches. *Int J Mol Sci* 2020;**21**(22).

170. Szatmari T, Lumniczky K, Desaknai S, Trajcevski S, Hidvegi EJ, Hamada H*, et al.* Detailed characterization of the mouse glioma 261 tumor model for experimental glioblastoma therapy. *Cancer Sci* 2006;**97**(6):546-53.

171. Aldape K, Brindle KM, Chesler L, Chopra R, Gajjar A, Gilbert MR*, et al.* Challenges to curing primary brain tumours. *Nat Rev Clin Oncol* 2019;**16**(8):509-20.

172. Kiyokawa J, Kawamura Y, Ghouse SM, Acar S, Barcin E, Martinez-Quintanilla J*, et al.* Modification of Extracellular Matrix Enhances Oncolytic Adenovirus Immunotherapy in Glioblastoma. *Clin Cancer Res* 2021;**27**(3):889-902.

173. West AJ, Tsui V, Stylli SS, Nguyen HPT, Morokoff AP, Kaye AH*, et al.* The role of interleukin-6-STAT3 signalling in glioblastoma. *Oncol Lett* 2018;**16**(4):4095-104.

174. Van Meir EG. Cytokines and tumors of the central nervous system. *Glia* 1995;**15**(3):264-88.

175. Faggioli L, Costanzo C, Donadelli M, Palmieri M. Activation of the Interleukin-6 promoter by a dominant negative mutant of c-Jun. *Biochim Biophys Acta* 2004;**1692**(1):17-24.

176. Luo Y, Zheng SG. Hall of Fame among Pro-inflammatory Cytokines: Interleukin-6 Gene and Its Transcriptional Regulation Mechanisms. *Front Immunol* 2016;**7**:604.

177. Sasaki A, Ishiuchi S, Kanda T, Hasegawa M, Nakazato Y. Analysis of interleukin-6 gene expression in primary human gliomas, glioblastoma xenografts, and glioblastoma cell lines. *Brain Tumor Pathol* 2001;**18**(1):13-21.

178. Liu Q, Li G, Li R, Shen J, He Q, Deng L*, et al.* IL-6 promotion of glioblastoma cell invasion and angiogenesis in U251 and T98G cell lines. *J Neurooncol* 2010;**100**(2):165-76.

179. Tchirkov A, Khalil T, Chautard E, Mokhtari K, Veronese L, Irthum B*, et al.* Interleukin-6 gene amplification and shortened survival in glioblastoma patients. *Br J Cancer* 2007;**96**(3):474-6.

180. Hori T, Sasayama T, Tanaka K, Koma YI, Nishihara M, Tanaka H*, et al.* Tumor-associated macrophage related interleukin-6 in cerebrospinal fluid as a prognostic marker for glioblastoma. *J Clin Neurosci* 2019;**68**:281-9.

181. Wang Q, He Z, Huang M, Liu T, Wang Y, Xu H*, et al.* Vascular niche IL-6 induces alternative macrophage activation in glioblastoma through HIF-2α. *Nat Commun* 2018;**9**(1):559.

182. Conrad C, Gupta R, Mohan H, Niess H, Bruns CJ, Kopp R*, et al.* Genetically engineered stem cells for therapeutic gene delivery. *Curr Gene Ther* 2007;**7**(4):249-60.

183. Hertz S, Roberts A. Radioactive iodine in the study of thyroid physiology; the use of radioactive iodine therapy in hyperthyroidism. *J Am Med Assoc* 1946;**131**:81-6.

184. Riesco-Eizaguirre G, Santisteban P, De la Vieja A. The complex regulation of NIS expression and activity in thyroid and extrathyroidal tissues. *Endocr Relat Cancer* 2021;**28**(10):T141-T65.

185. Grisendi G, Spano C, Rossignoli F, N DS, Golinelli G, Fiori A*, et al.* Tumor Stroma Manipulation By MSC. *Curr Drug Targets* 2016;**17**(10):1111-26.

186. Yeung YT, McDonald KL, Grewal T, Munoz L. Interleukins in glioblastoma pathophysiology: implications for therapy. *Br J Pharmacol* 2013;**168**(3):591-606.

187. Chang CY, Li MC, Liao SL, Huang YL, Shen CC, Pan HC. Prognostic and clinical implication of IL-6 expression in glioblastoma multiforme. *J Clin Neurosci* 2005;**12**(8):930-3.

188. Wang H, Lathia JD, Wu Q, Wang J, Li Z, Heddleston JM*, et al.* Targeting interleukin 6 signaling suppresses glioma stem cell survival and tumor growth. *Stem Cells* 2009;**27**(10):2393-404.

189. Weissenberger J, Loeffler S, Kappeler A, Kopf M, Lukes A, Afanasieva TA*, et al.* IL-6 is required for glioma development in a mouse model. *Oncogene* 2004;**23**(19):3308-16.

190. Lamano JB, Lamano JB, Li YD, DiDomenico JD, Choy W, Veliceasa D*, et al.* Glioblastoma-Derived IL6 Induces Immunosuppressive Peripheral Myeloid Cell PD-L1 and Promotes Tumor Growth. *Clin Cancer Res* 2019;**25**(12):3643-57.

191. Dubost J-J, Rolhion C, Tchirkov A, Bertrand S, Chassagne J, Dosgilbert A*, et al.* Interleukin-6-producing Cells in a Human Glioblastoma Cell Line are not Affected by Ionizing Radiation. *Journal of Neuro-Oncology* 2002;**56**(1):29-34.

192. Pasi F, Facoetti A, Nano R. IL-8 and IL-6 bystander signalling in human glioblastoma cells exposed to gamma radiation. *Anticancer Res* 2010;**30**(7):2769-72.

193. Chen HY, Lin LT, Wang ML, Lee SH, Tsai ML, Tsai CC*, et al.* Musashi-1 regulates AKT-derived IL-6 autocrinal/paracrinal malignancy and chemoresistance in glioblastoma. *Oncotarget* 2016;**7**(27):42485-501.

194. Ding DC, Liu HW, Chu TY. Interleukin-6 from Ovarian Mesenchymal Stem Cells Promotes Proliferation, Sphere and Colony Formation and Tumorigenesis of an Ovarian Cancer Cell Line SKOV3. *J Cancer* 2016;**7**(13):1815-23.

195. Zeng J, Chen S, Li C, Ye Z, Lin B, Liang Y*, et al.* Mesenchymal stem/stromal cells-derived IL-6 promotes nasopharyngeal carcinoma growth and resistance to cisplatin via upregulating CD73 expression. *J Cancer* 2020;**11**(8):2068-79.

196. Karnoub AE, Dash AB, Vo AP, Sullivan A, Brooks MW, Bell GW*, et al.* Mesenchymal stem cells within tumour stroma promote breast cancer metastasis. *Nature* 2007;**449**(7162):557-63.

197. Tumangelova-Yuzeir K, Naydenov E, Ivanova-Todorova E, Krasimirova E, Vasilev G, Nachev S*, et al.* Mesenchymal Stem Cells Derived and Cultured from Glioblastoma Multiforme Increase Tregs, Downregulate Th17, and Induce the Tolerogenic Phenotype of Monocyte-Derived Cells. *Stem Cells Int* 2019;**2019**:6904638.

198. Liang W, Chen X, Zhang S, Fang J, Chen M, Xu Y*, et al.* Mesenchymal stem cells as a double-edged sword in tumor growth: focusing on MSC-derived cytokines. *Cell Mol Biol Lett* 2021;**26**(1):3.

199. Fisher DT, Appenheimer MM, Evans SS. The two faces of IL-6 in the tumor microenvironment. *Semin Immunol* 2014;**26**(1):38-47.

200. Liu Q, Yu S, Li A, Xu H, Han X, Wu K. Targeting interlukin-6 to relieve immunosuppression in tumor microenvironment. *Tumour Biol* 2017;**39**(6):1010428317712445.

201. Wang Q-W, Lin W-W, Zhu Y-J. Comprehensive analysis of a TNF family based-signature in diffuse gliomas with regard to prognosis and immune significance. *Cell Communication and Signaling* 2022;**20**(1):6.

202. Sanchez VE, Lynes JP, Walbridge S, Wang X, Edwards NA, Nwankwo AK*, et al.* GL261 luciferase-expressing cells elicit an anti-tumor immune response: an evaluation of murine glioma models. *Sci Rep* 2020;**10**(1):11003.

203. Tanabe K, Matsushima-Nishiwaki R, Yamaguchi S, Iida H, Dohi S, Kozawa O. Mechanisms of tumor necrosis factor-alpha-induced interleukin-6 synthesis in glioma cells. *J Neuroinflammation* 2010;**7**:16.

204. Spooren A, Mestdagh P, Rondou P, Kolmus K, Haegeman G, Gerlo S. IL-1beta potently stabilizes IL-6 mRNA in human astrocytes. *Biochem Pharmacol* 2011;**81**(8):1004-15.

205. Yeung YT, Bryce NS, Adams S, Braidy N, Konayagi M, McDonald KL*, et al.* p38 MAPK inhibitors attenuate pro-inflammatory cytokine production and the invasiveness of human U251 glioblastoma cells. *J Neurooncol* 2012;**109**(1):35-44.

206. Schmohl KA, Muller AM, Wechselberger A, Ruhland S, Salb N, Schwenk N*, et al.* Thyroid hormones and tetrac: new regulators of tumour stroma formation via integrin alphavbeta3. *Endocr Relat Cancer* 2015;**22**(6):941-52.

207. Brandt LJB, Barnkob MB, Michaels YS, Heiselberg J, Barington T. Emerging Approaches for Regulation and Control of CAR T Cells: A Mini Review. *Front Immunol* 2020;**11**:326.

208. Saidi A, Hagedorn M, Allain N, Verpelli C, Sala C, Bello L*, et al.* Combined targeting of interleukin-6 and vascular endothelial growth factor potently inhibits glioma growth and invasiveness. *Int J Cancer* 2009;**125**(5):1054-64.

209. McKelvey KJ, Hudson AL, Prasanna Kumar R, Wilmott JS, Attrill GH, Long GV*, et al.* Temporal and spatial modulation of the tumor and systemic immune response in the murine Gl261 glioma model. *PLoS One* 2020;**15**(4):e0226444.

210. Jäckel C, Nogueira MS, Ehni N, Kraus C, Ranke J, Dohmann M*, et al.* A vector platform for the rapid and efficient engineering of stable complex transgenes. *Sci Rep* 2016;**6**:34365.

8 Acknowledgements

I would like to appreciate the help and support of many people, professionally and personally, who have helped make this thesis happen over the past few years.

Foremost, I would like to express my sincere gratitude to Prof. Christine Spitzweg for the opportunity to perform my doctoral thesis in her laboratory and her supervision over five intense years. I highly appreciated the chance to work on exciting projects in this fruitful, interdisciplinary, and collaborative research environment within the *Sonderforschungsbereich 824* (SFB824). Thank you, Christine, for your continuous scientific support and guidance throughout my thesis, for the encouragement to manage my projects with self-responsibility, the chance to grow and surpass myself. I am very grateful for the opportunity to participate in national and international scientific conferences in Europe and the US and for all the cheerful stories on the phone.

Furthermore, I am very thankful to Prof. Ernst Wagner for accepting me as an external PhD student. Thank you for the helpful advice and broad scientific discussions within the work-in-progress seminar.

I am very grateful to Prof. Peter Nelson, for his persistent help and scientific input whenever needed, and proofreading of my manuscripts. Further, I also thank all his lab members for their outstanding support and collaboration.

Many thanks to all the colleagues of the Spitzweg lab for supporting me all these years and for the time we spent together. I enjoyed our nearly endless coffee breaks and never-ending discussions about every possible topic and sharing many laughs. Thank you, Nathalie, for your constant support from the very beginning until the end of my thesis and for being our (lab) shopping queen. I am very thankful to Katy for many extended tea breaks with scientific exchange and for being the best pre-submission reviewer of manuscripts and abstracts ever. Special thanks to Rebekka for being my seat-neighbor, glioma and rechts der Isar partner for all these years. Many thanks to Christina for your valuable “Küken” supervision at rechts der Isar during the first months of my thesis and for the joyful atmosphere. Thanks to Mariella for the long imaging nights and for sharing your expertise for the best restaurants and Christmas

markets in town. Furthermore, I would like to thank Yang for dealing with a girls' lab and Viktoria for the nice talks and for being my conference partner in Montreal. I am grateful to Ujjwal, Yvonne, and all their lab members for their continuous support and input for fluorescence imaging and for always allowing us to use all their lab equipment.

I want to thank all collaborators within the SFB824 who contributed to my projects, for the great working atmosphere, and the inspiring scientific and joyful get-togethers:

I am very grateful to Prof. Rainer Glass and Dr. Roland Kälin for their tremendous input with GBM models, insightful scientific discussions, and revision of my manuscripts.

Many thanks to the CeP (Comparative experimental pathology) team, especially PD Katja Steiger, Olga, Ulrike, Simone, and Petra, for their valuable help with tissue processing and staining.

Furthermore, I would like to thank all the people of the Nuclear Medicine Department at the Klinikum rechts der Isar (Director Prof. Wolfgang Weber), especially Franz, Sybille, Markus, Sandra, and Birgit for their great support and technical assistance during our imaging and therapy studies. My warmest appreciation goes to Volker and Martin for their persistent scientific and personal support. Further, I also would like to thank the radiation protection team, Jakob, Simone & Maxi, for their support at any time and for making our experiments happen.

Finally, I want to express my deepest thankfulness to my family for always supporting me and for their trust. I also would like to thank all my friends for encouraging me, cheering me up, and always having an “open ear” in this intense time of my life. Thank you all for always believing in me and for accepting only short-notice free time & travel plans.